UNIVERSITY OF CALIFORNIA, DAVIS

DOCTORAL THESIS

Feed Forward Wind Turbine Control Using Upwind Turbines as Sensors

Author:
Eric William Anderson

Supervisor:
Dr. Case van Dam

A thesis submitted in fulfilment of the requirements
for the degree of Doctor of Philosophy

in the

Applied Aerodynamics Research Group
Department of Mechanical and Aerospace Engineering

April 2017

Declaration of Authorship

I, Eric William Anderson, declare that this thesis titled, 'Feed Forward Wind Turbine Control Using Upwind Turbines as Sensors' and the work presented in it are my own. I confirm that:

- This work was done wholly or mainly while in candidature for a research degree at this University.

- Where any part of this thesis has previously been submitted for a degree or any other qualification at this University or any other institution, this has been clearly stated.

- Where I have consulted the published work of others, this is always clearly attributed.

- Where I have quoted from the work of others, the source is always given. With the exception of such quotations, this thesis is entirely my own work.

- I have acknowledged all main sources of help.

- Where the thesis is based on work done by myself jointly with others, I have made clear exactly what was done by others and what I have contributed myself.

Signed:

_____

Date:

_____

"Thanks to my solid academic training, today I can write hundreds of words on virtually any topic without possessing a shred of information, which is how I got a good job in journalism."

Dave Barry

UNIVERSITY OF CALIFORNIA, DAVIS

Abstract

Dr. Case van Dam

Department of Mechanical and Aerospace Engineering

Doctor of Philosophy

Feed Forward Wind Turbine Control Using Upwind Turbines as Sensors

by Eric William Anderson

The Thesis Abstract is written here (and usually kept to just this page). The page is kept centered vertically so can expand into the blank space above the title too. . .

Acknowledgements

The acknowledgements and the people to thank go here, don't forget to include your project advisor...

Contents

List of Figures

List of Tables

Abbreviations

COE	**C**ost **O**f **E**nergy
NREL	**N**ational **R**enewable **E**nergy **L**aboratory
NWTC	**N**ational **W**ind **T**echnology **C**enter
FAST	**F**atigue, **A**erodynamics, **S**tructures, and **T**urbulence
SOWFA	**S**imulator f**O**r **W**ind **F**arm **A**pplications
DEL	**D**amage **E**quivalent **L**oad

Physical Constants

Speed of Light $\quad c \quad = \quad 2.997\ 924\ 58 \times 10^8$ ms^{-S} (exact)

Symbols

U	incoming wind speed at the turbine rotor	m·s^{-1}
R	rotor radius	m
C_p	coefficient of power	-
D	downwind distance between turbines	m
U_{conv}	convection speed	m·s^{-1}
U_{mean}	local mean wind speed	m·s^{-1}
U_{turb}	wind speed fluctuations due to turbulence	m·s^{-1}
U_{ff}	feed forward wind speed estimate supplied by upwind turbine	m·s^{-1}
θ	collective blade pitch angle of the turbine	°
Ω_{Rotor}	rotational speed of the rotor	rad·s^{-1}
T_{Gen}	torque supplied by the generator	$N \cdot m$
$I_{Drivetrain}$	Low speed shaft equivalent inertia	kg·m^2
T_{Aero}	aerodynamic torque on the rotor due to the wind	$N \cdot m$
N_{Gear}	gear box ratio	-
ρ	air density	kg·m^{-3}
R	rotor radius	m
λ	tip speed ratio	-
t_D	time required for a gust to pass from the upwind to downwind turbine	s
θ_{ff}	pitch command issued by the feed forward controller	°
θ_c	pitch command issued by the closed loop controller	°
T_{ff}	torque command issued by the feed forward controller	$N \cdot m$
ξ	damping ratio of the pitch actuator	-
ω_o	undamped natural frequency of the pitch actuator	rad·s^{-1}
θ_{ss}	steady state pitch function	°
U_{ffd}	dynamic feed forward velocity	m/s

Ω_{Gen}	rotational speed of the generator	rad$\cdot s^{-1}$
$\Omega_{GenFilt}$	low pass filtered rotational speed of the generator	rad$\cdot s^{-1}$
$D_{fatigue}$	total damage due to cyclic loading	-
$N_{fatigue,i}$	number of cycles to failure for the ith loading cycle	-
$L_{ultimate}$	ultimate design load	-
L_{mean}	mean load over a components load history	-
$L_{range,i}$	range of a cyclic load	-
$N_{equivalent}$	number of cycles to failure for the damage equivalent load	-
m	Wöhler exponent	

For/Dedicated to/To my. . .

Chapter 1

Introduction and Background

1.1 Wind Power

Wind power is the fastest growing energy source in the world. From 2000 to 2012, global wind power capacity grew from 17,400MW to 1282,587MW, with an average increase of 24% per year (Figure 1.1). In the United States, installed wind capacity grew from approximately 2500MW in the year 2000 to 60,007MW in 2012 [7]. Though wind power only represents a small fraction of total global power generation, it is an important source of clean renewable energy and its importance will increase in the future.
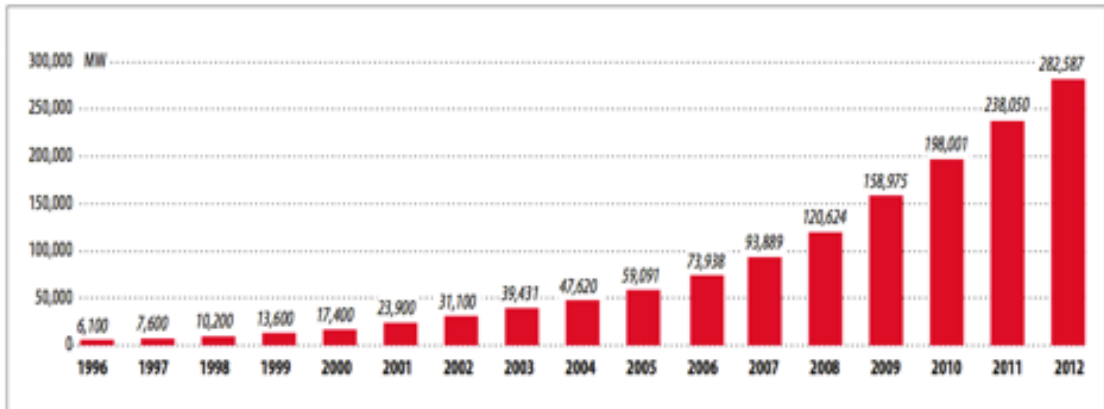
FIGURE 1.1: Global wind power capacity. [1]

Much of wind power's success is due to two factors: the widespread availability of wind resources and the relatively low Cost of Energy (COE) when compared to other renewable energy sources. For example, utility scale wind energy typically costs 5-12 cents per KW-hr while utility scale solar-PV typically costs 15-30 cents per KW-hr [8]. Though some renewable energy sources such as geothermal plants or large hydro plants

can produce energy at lower COE than wind farms, the natural resources needed for those plants are much more limited.

The cost of wind power has been steadily decreasing. The decreases in wind power COE have gone hand in hand with increases in both the size and complexity of wind turbines. As the turbines have grown in size and complexity, more sophisticated methods for controlling those turbines have been required.

1.2   Wind Turbine Control

A control system typically consists of sensors, actuators, and a controller. A modern wind turbine might include sensors such as: an anemometer, a wind vane, at least one rotor speed sensor, an electric power sensor, accelerometers, load sensors, pitch position sensors, various limit switches, vibration sensors, temperature and oil level indicators, hydraulic pressure sensors, operator switches, and push buttons. Actuators might include: hydraulic or electric pitch actuators, an electric generator that can actively control generator torque, generator contacts, switches for activating shaft brakes, and yaw motors. The controller collects information from sensors, processes that data, the issues commands to actuators. For a wind turbine, the controller typically consists of a computer based controller used for normal operation, and a highly reliable hard wired safety system that overrides the computer based controller and brings the turbine to a safe state if a serious problem occurs.[9]

The control system performs a variety of functions, but this research is primarily concerned with the closed loop control system that optimizes turbine performance during power production. The majority of utility scale turbines built today use variable speed and collective pitch to feather control. In this control scheme both the rotational speed of the turbine and the collective pitch of the turbine's three blades are controlled. At low and medium wind speeds the pitch is held constant while the turbine speed is varied. At high wind speeds both the turbine speed and the blade pitch can be varied.

At low and medium wind speeds, the rotational speed of the rotor is manipulated to maximize aerodynamic efficiency and maximize energy capture. The variations in rotational speed are achieved by torque control, which is implemented by using a pre-determined generator torque vs. generator speed curve like the one shown in Figure 1.2. The torque controller receives measurements from a generator speed sensor, looks up the appropriate generator torque on the speed-torque curve and commands the generator to produce that torque. The blue line in Figure 1.2 shows the torque vs. speed curve for the torque controller on the NREL 5-MW reference turbine. The black line shows

the torque-speed curve corresponding to maximum aerodynamic efficiency of the turbine. Figure 1.3 shows the relationship between generator speed and generated power. In region 1 the generator produces no torque and no power, in region 2 the generator tracks optimum aerodynamic efficiency, and in region 3 the generator tracks constant power output. Regions 1.5 and 2.5 simply serve as smooth transitions between the other regions.
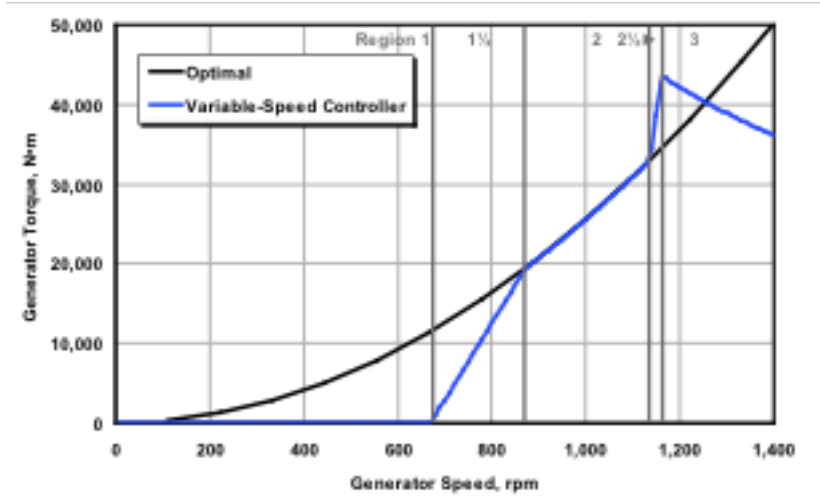
FIGURE 1.2: Torque-speed curve for NREL 5-MW turbine.[2]
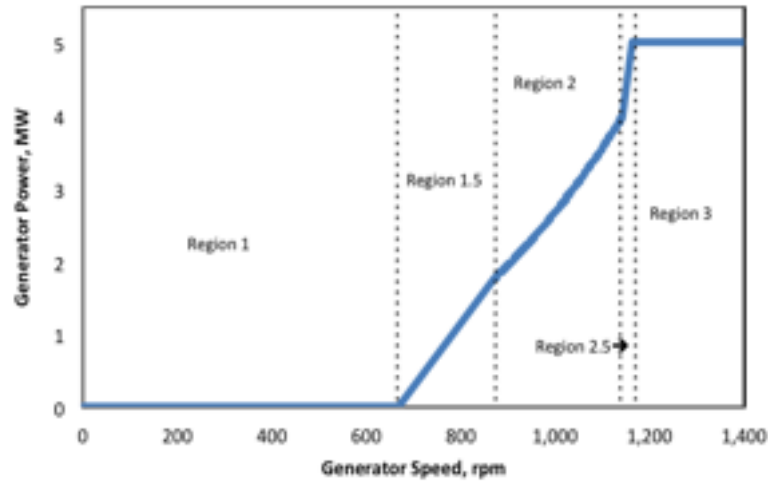
FIGURE 1.3: Power-speed curve for NREL 5-MW turbine.

At high wind speeds the collective blade pitch is manipulated to keep turbine speed and power generation constant. As wind speed increases, the turbine blades are pitched such that the turbine extracts a smaller fraction of the wind's power. As a result, the turbine is able to maintain the same power production even as the total available power in the wind increases. The purpose of pitch control is to manage loading on the turbine's mechanical components, and to prevent the turbine's power electronics from

being damaged by excessive power production. For the NREL 5-MW turbine pitch control is achieved with a nonlinear PI controller in which the controller gains vary depending on the current blade pitch angle.

1.3   Advanced Turbine Control Research

The advanced wind turbine control concepts being researched today are numerous and diverse. A comprehensive review of this field is outside the scope of this proposal, but in the following paragraphs I will briefly describe several areas of advanced wind turbine control that are related to the work in this thesis: Individual pitch control, active load control, and LIDAR assisted control.

In individual pitch control, the pitch of each turbine blade is controlled independently and the blades can be set at different pitch angles. This has several advantages over the collective pitch control described in the previous section. Individual pitch control can be used to reduce loading caused by rotor tilt and yaw alignment errors, airflow effects caused by wind turbine tower, or any other loads that vary cyclically with the rotation of the blade. Research has shown that cyclic pitch control could lead to a 30-40% reduction in fatigue loads on the turbine hub and a 20-30% reduction in fatigue loads at the blade roots.[10, 11] However, there is concern that the additional pitching will lead to premature failure of the blade pitching mechanism, or that it will require larger, more costly blade pitching mechanisms.[12]

Active flow control is the control of local airflow surrounding the blade. In the past, a great deal of research has focused on active flow control for aircraft. Recent research has sought to apply active flow technologies to commercial wind turbines as well. Active flow control typically operates on a small scale. It uses devices, such as the red trailing edge flaps shown in Figure 1.4, to exercise local control over the aerodynamic properties of the blade. These devices can independently control the aerodynamic properties of small portions of a wind turbine blade. The devices also typically have very quick response times. Because they respond quickly and because they can exercise local control over smaller portions of the turbine blade, active flow control devices have the potential to mitigate some loads that other control methods cannot.

In LIDAR assisted control a LIDAR (Light Detection and Ranging) system is mounted on the nacelle of a turbine and used to scan the wind field as it approaches the wind turbine. As illustrated in Figure 1.5, the LIDAR system is capable of measuring wind speed at several discrete distances upwind of the turbine. These measurements are used to estimate the wind speed that the turbine will experience in the future. The turbine

FIGURE 1.4: Wind turbine blades with trailing edge flaps for active load control.[3]

controller can use these future wind speed estimates to respond preemptively to changes in wind speed and to counteract changes in aerodynamic loading as they occur. The primary disadvantage to LIDAR control is the prohibitive cost of the LIDAR equipment.
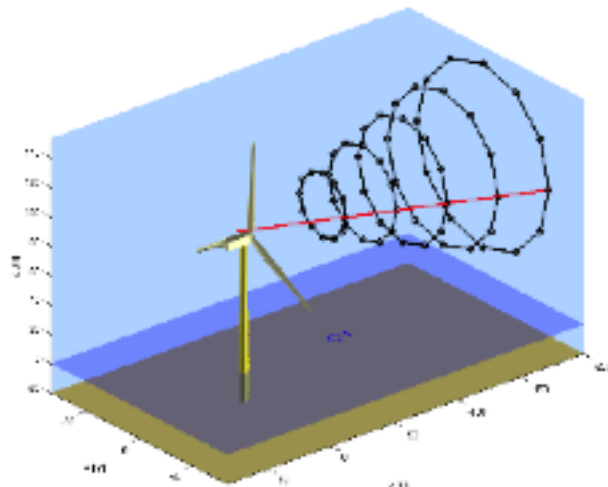
FIGURE 1.5: Illustration of upwind LIDAR measurement distances.[4]

1.4 Goals of This Research

This thesis seeks to improve wind turbine control by using information obtained from upwind turbines. In particular, pre-existing sensors on upwind turbines will measure wind speed fluctuations and dynamic turbine behavior. That information will then be used by the control system of a downwind turbine to anticipate wind speed fluctuations before they reach the downwind turbine. This technique holds the potential to improve power production and/or decrease turbine loads by allowing the downwind turbine to

react preemptively to changes in wind speed and track the optimum turbine conditions more closely.

Figure 1.6 shows the steady state power curve for the NREL 5-MW turbine. It represents the optimum power production at each wind speed. If the wind blows at a constant speed for long enough, the control system will bring the turbine's power production to a point on the blue line. However, since rapid wind speed fluctuations are common, the turbine often deviates from this power curve during normal operation. If the magnitude and/or time of these deviations can be reduced then the power curve can be tracked more closely and several potential benefits can be achieved.
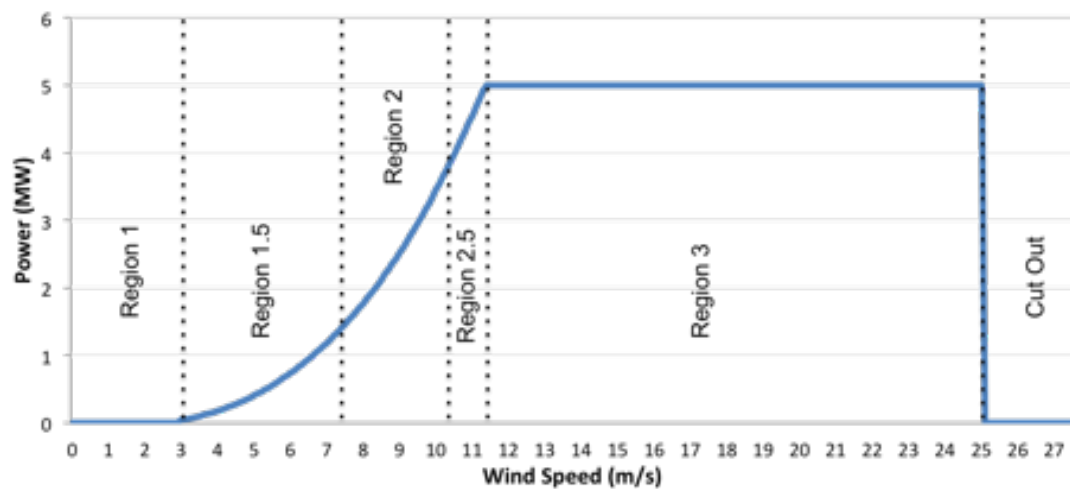
FIGURE 1.6: Steady state behavior of the NREL 5-MW.[2]

In region 2, deviations from the steady state power curve result in decreased aerodynamic efficiency and decreased power production. By tracking the power curve more closely in this region the power production of the turbine can be increased. In region 3, deviations from the steady state power curve cause higher loads on the mechanical components of the turbine and fluctuations in the power output of the turbine. By tracking the power curve more closely the peak mechanical loads and fluctuation in power production can be reduced.

Reducing peak mechanical loads has several advantages. It reduces wear and tear on the turbine's mechanical components, thereby reducing the long-term repair and maintenance costs. It can also lead to lower turbine-manufacturing costs or increased power production. Reductions in manufacturing costs are achieved by designing and sizing the turbine components based on the reduced loads. Alternately, increased power is achieved by "growing the rotor". Which means to increase the size of the turbine blades until the loading on the turbine components matches the original design loads.

Reducing the power fluctuations in region 3 can also be used to increase power production without any physical changes to the turbine. In part, the rated power of a turbine is set by the limitations of the turbine's power electronics. If improvements in wind turbine control can reduce deviations from rated power then the turbine can safely operate at a higher rated power without fear of overloading the power electronics. This technique is currently being used by General Electric with its WindBOOST control system. The WindBOOST control system update allows the GE 1.5 MW wind turbine to operate at a rated power of 1.6 MW without any changes to the turbine hardware. [13]

1.5   Dissertation Outline

In the following sections ...

Chapter 2

Using a Wind Turbine as a Sensor

2.1   Introduction

When using a wind turbine as a sensor, the fundamental questions are: What should we measure, and how should we measure it? In this chapter several possible answers to those questions are investigated. To minimize the cost of the control system we will restrict ourselves to using sensors that are already present on a typical wind turbine. This chapter will first evaluate several methods for estimating wind speed, but will also investigate other potentially useful measurements.

There are two advantages to measuring wind speed. First, both the steady state torque and steady state collective blade pitch are ultimately functions of the incoming wind speed (as shown in Figure 2.1). Second, the wind speed provides an estimate of the speed at which turbulent eddies in the wind travel. As a result, the wind speed can be used to estimate how long it will take for the wind gusts observed by the upwind turbine to reach the downwind turbine.

The following section will describe the generation of a simulation data set that is used to evaluate sensor techniques. The following three sections will discuss three methods for estimating the incoming wind speed of a turbine, nacelle top anemometer measurements, Turbine dynamics based estimation, and pressure measurement based estimation. The final section of the chapter will discuss the viability of using blade pitch and generator speed as feed forward signals.
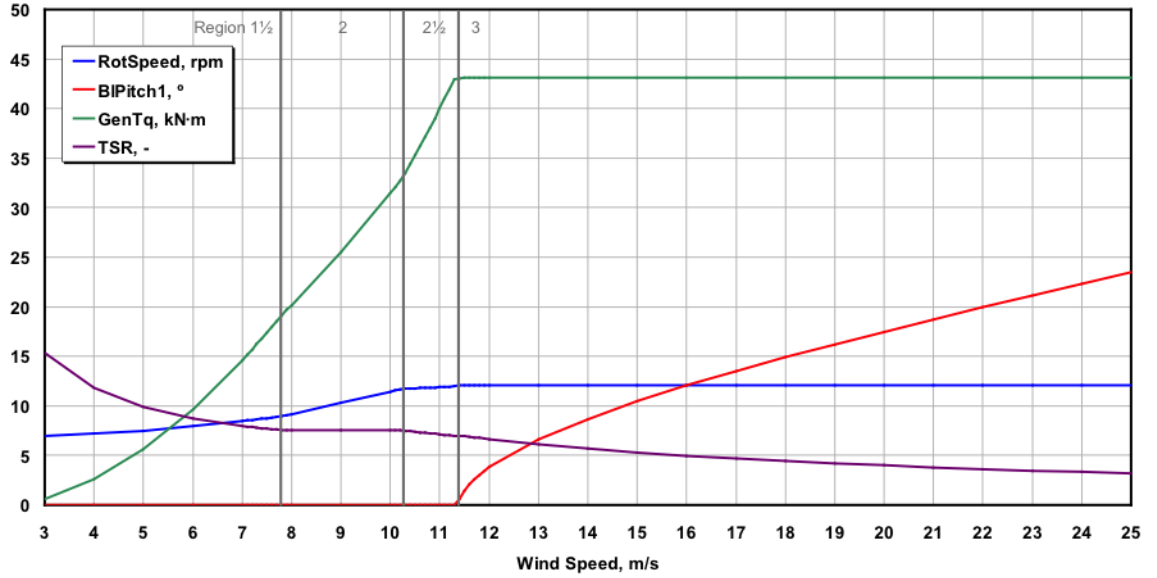
FIGURE 2.1: Steady state behavior of the NREL 5-MW.[2]

2.2 Data for evaluating sensor techniques

The rest of this chapter discusses several wind turbine sensor scheme's that could potentially be used for feed forward of downwind turbines. To gain insight into the performance of these scheme's a series of simulations were conducted. The simulations were carried out in FAST (Fatigue, Aerodynamics, Structures, and Turbulence), using wind conditions simulated by TurbSim. FAST is a medium fidelity wind turbine simulation tool developed by NREL and Oregon State University. FAST models both the aerodynamics and structural dynamics of horizontal axis wind turbines, and has been independently validated and verified[14]. TurbSim is a stochastic, full-field, turbulent-wind simulator. It uses a statistical model (as opposed to a physics based model) to numerically simulate a time series of three-component wind-speed vectors at points on a two-dimensional vertical rectangular grid (see Figure 2.2) [5]. All simulations described in this section assumed an NREL 5-MW turbine in great plains low level jet (GPLLJ) wind conditions.

A variety of mean wind speeds were simulated to capture performance over the turbine's whole operating range. 11 Mean wind speeds were simulated ranging from 4 m/s to 24 m/s in 2 m/s increments. At each wind speed 6 unique turbulent wind fields were generated using TurbSim. Each of these wind fields were used to drive a FAST simulation of the NREL 5-MW turbine. Each simulation was 10 minutes long. In total 66 10-minute simulations of a NREL 5-MW turbine in GPLLJ winds were performed. Sample input files for the simulations can be found in appendix A.
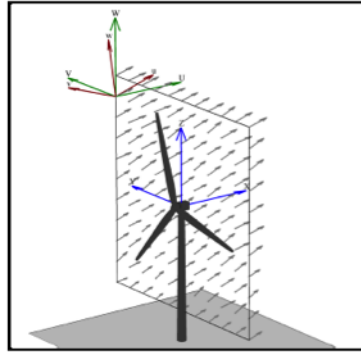
FIGURE 2.2: Illustration of TurbSim flow field.[5]

2.3 Wind speed estimate based on nacelle top anemometer

All utility scale wind turbines have nacelle-mounted anemometers. The wind speed measurements from the anemometer are used for purposes such as assessing wind turbine performance and forecasting future power production. The measurements from the anemometer are not used by conventional wind turbine control systems, but could potentially be used for wind turbine control.

In some ways, using a nacelle top anemometer is the simplest method to estimate incoming wind speed. The anemometer is designed to measure wind speed. It is located on top of the nacelle, which is near the center of the rotor's swept area. The anemometer and data acquisition system are already in place on all commercial wind turbines.

However, this method has several complications as well. The anemometer only measures wind speed at a single point. On modern utility scale wind turbines, where rotors are often more than 100 meters in diameter, a single point measurement may not be sufficient to accurately represent wind speed across the whole rotor. In addition, suitable anemometer data may not be readily available. For example, the data acquisition system on a Vestas V90 turbine provides the raw anemometer data. Instead it provides 10 minute average wind speeds that a proprietary filtering of the nacelle top anemometer data. For the sake of this investigation we will assume that the raw anemometer data can be obtained, perhaps with the help of the turbine manufacturer.

If suitable anemometer data is available, there may be difficulty obtaining an accurate wind speed measurement. Anemometer data has high frequency noise and occasional false values. The anemometer could have errors due to poor calibration. In addition, the nacelle top location of the anemometer means it is measuring wind that has passed through the rotor plane. The simulation results shown in Figure 2.3 were generated using SOWFA (Simulator fOr Wind Farm Applications), a simulatin tool that will be

discussed in future chapters. As Figure 2.3 shows, wind in the nacelle area can be significantly affected by the rotor. For the sake of this investigation, we will assume the anemometer data can be processed to obtain an accurate measurement of the incoming wind speed at the center of the rotor.
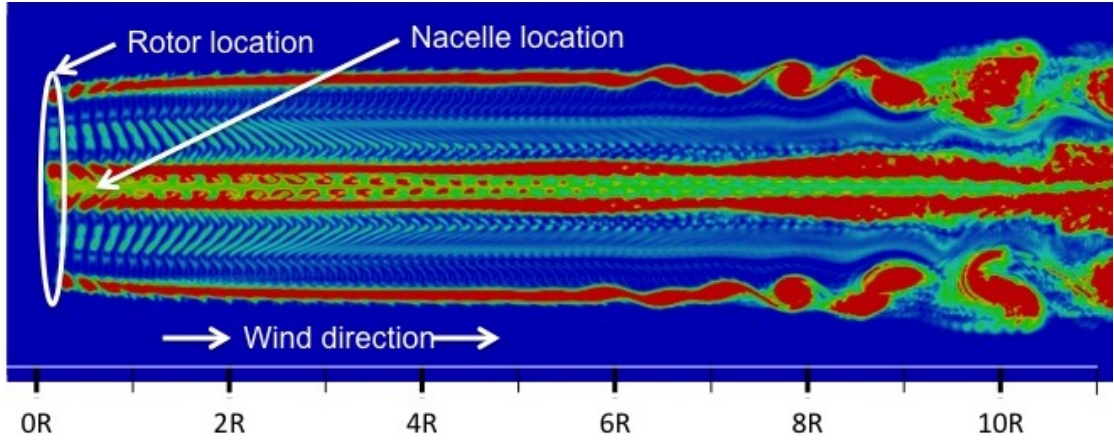
FIGURE 2.3: Vorticity downstream of an NREL 5-MW rotor in uniform 11 m/s wind.

2.3.1 Feasibility

The simulation dataset described in Section 2.2 was used to evaluate the feasibility of using a nacelle top anemometer to estimate incoming wind speed. FAST does not simulate the nacelle top anemometer. However, if we make the assumptions stated in the previous two paragraphs we can treat true the incoming wind speed at the center of the rotor as a filtered and processed signal from the nacelle top anemometer. The true incoming wind speed at the rotor center can be extracted from the TurbSim flow field, and will be treated as the nacelle top anemometer measurement for the remainder of this discussion(Figure 2.4-a). The average wind speed passing through the rotor of the turbine can also be calculated from the TurbSim flow field (Figure 2.4-b). By comparing these two values we get a feel for how well a nacelle top anemometer can represent the wind passing through the rotor of a utility scale turbine.

Figure 2.5 shows the wind speed at the anemometer as well as the average wind speed across the swept area of the rotor. The data shown in the figure is from the 13th simulation in the dataset described above, but this data is typical of the other 65 simulations as well. At first glance the anemometer wind speed looks noisy compared to the rotor average wind speed. Upon closer examination (Figure 2.6) we see that both the anemometer and the rotor average wind speed have high frequency fluctuations. However, the high frequency fluctuations in the anemometer wind speed have a much larger magnitude.
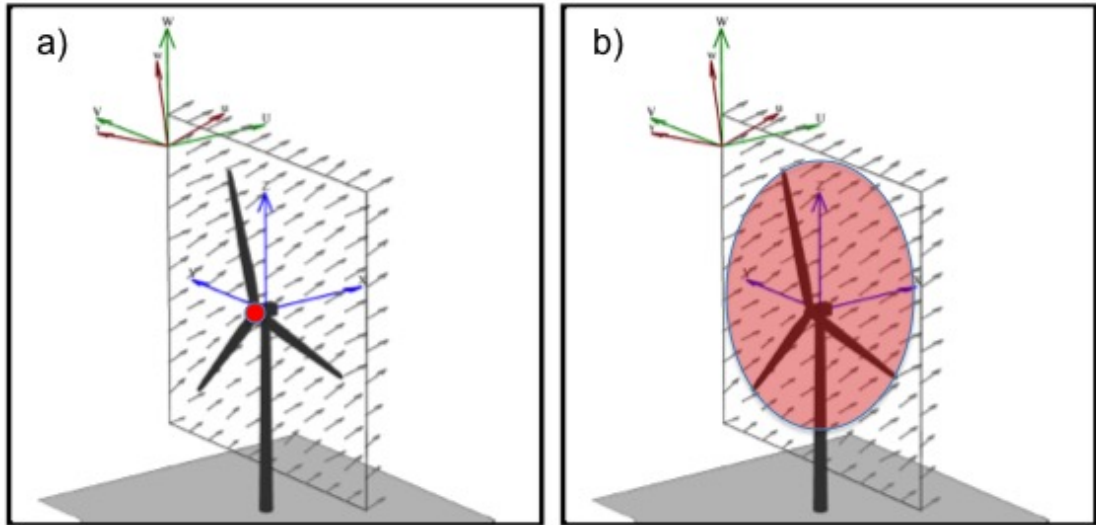
FIGURE 2.4: Measurement locations for the rotor center wind speed and rotor average wind speed.
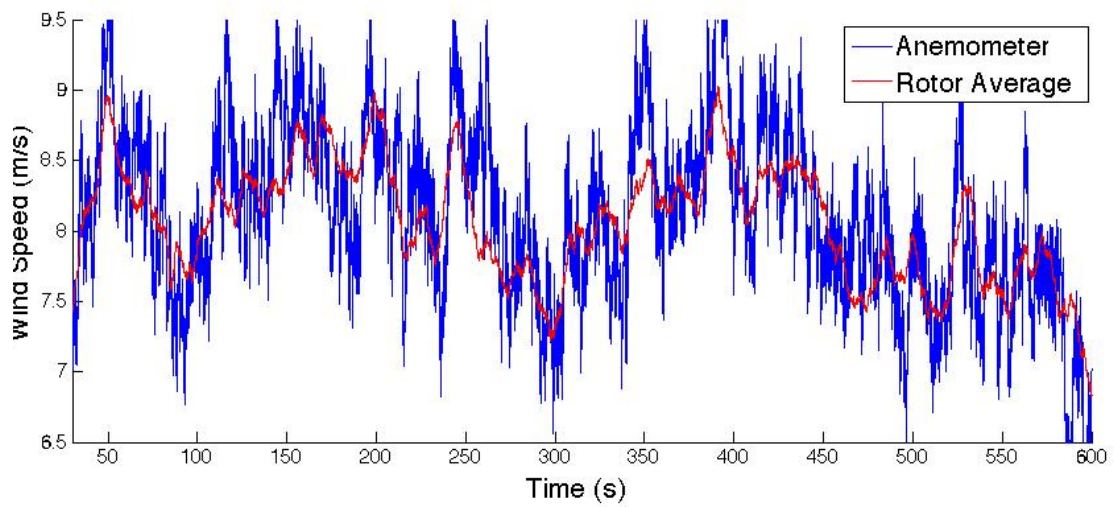
FIGURE 2.5: Anemometer measurement and rotor average wind speed for simulation #13 (8 m/s average wind speed).

The magnitude of these high frequency fluctuations is not very important from a wind turbine control point of view. Because utility scale wind turbines are such large machines, it isn't practical for the blade pitch and generator torque to track high frequency fluctuations in wind speed. In a typical utility scale turbine controller feedback signals are passed through a low pass filter before they are used for turbine control. To get a more meaningful comparison between anemometer wind speed and rotor average wind speed we should filter out the high frequency fluctuations.
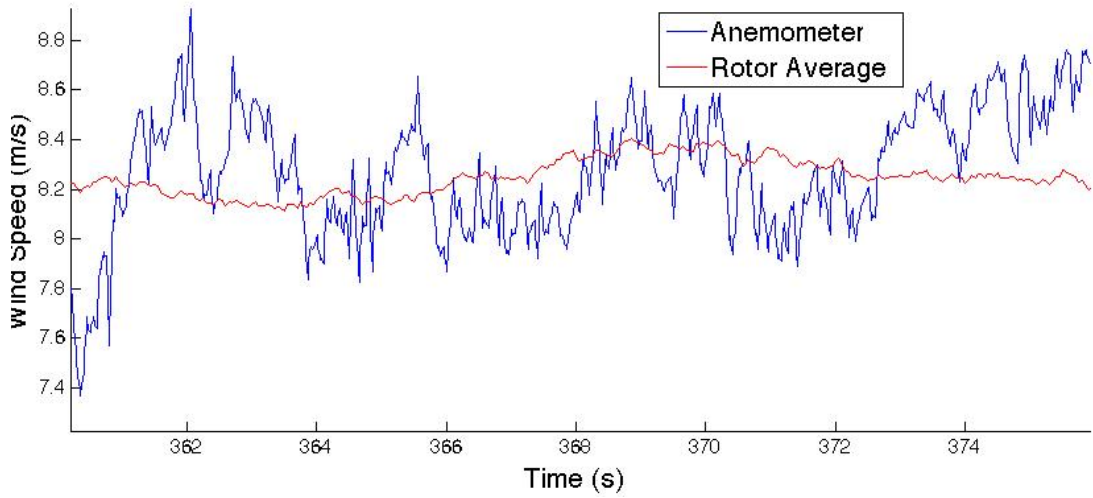
FIGURE 2.6: Anemometer measurement and rotor average wind speed for simulation #13 (8 m/s average wind speed).

Figure 2.7 shows the anemometer wind speed and rotor average wind speed from simulation #13 after they have been passed through a low pass filter. I chose to use a 4th order zero-phase filter with a 0.25 Hz cutoff frequency. A zero phase filter was chosen because it does not result in a delay of the filtered signal. A 0.25 Hz cutoff frequency was chosen because it is the corner frequency of the low pass filter used by the NREL 5-MW control system.
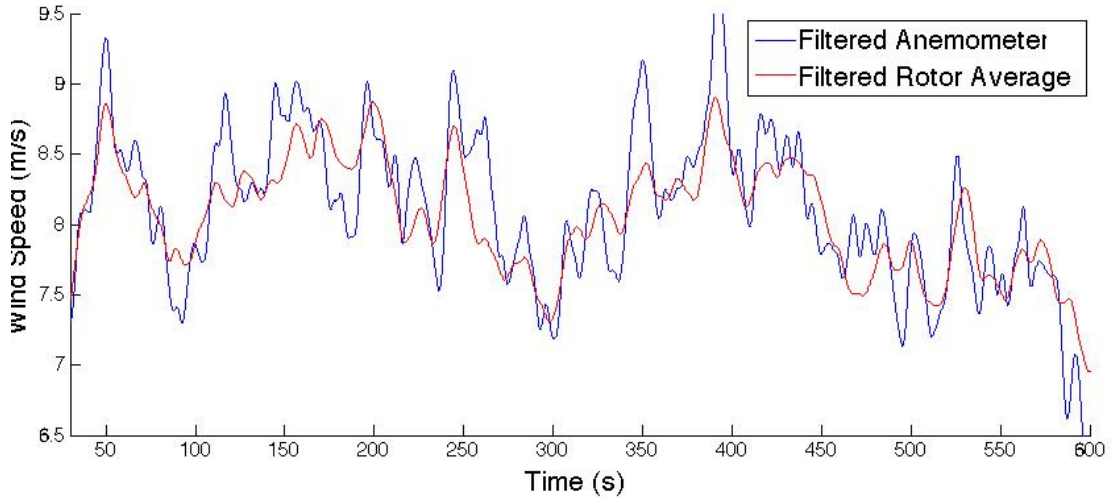
FIGURE 2.7: Filtered anemometer and rotor average wind speed for simulation #13.

Figure 2.8 shows the discrepancy between the filtered anemometer wind speed and the filtered rotor average wind speed for simulation #13. For this run the magnitude of the discrepancy ranges from almost 0 to as much as 0.954 m/s, and the average magnitude

of the discrepancy is 0.236 m/s. All 6 simulations run with an 8 m/s wind speed yield similar data, as can be seen in Figure 2.9. . Between these 6 simulations we have 57 minutes of data. If we average the magnitude of the discrepancy over all the data points in these 6 simulations we find the discrepancy between the filtered anemometer wind speed and the filtered rotor average wind speed averages 0.272 m/s when the NREL 5-MW turbine is in 8 m/s GPLLJ wind conditions.
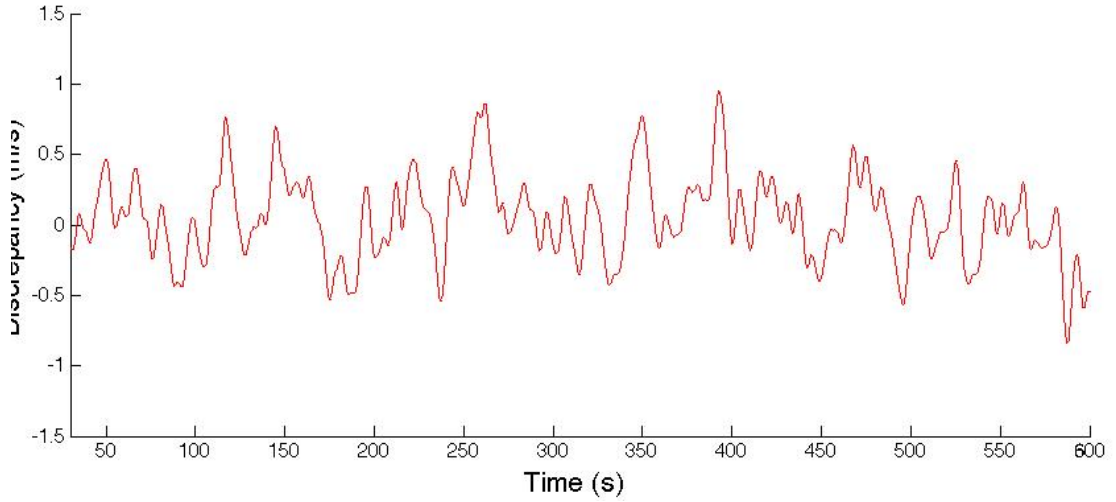
FIGURE 2.8: Discrepancy between anemometer and rotor average wind speed for simulation #13.
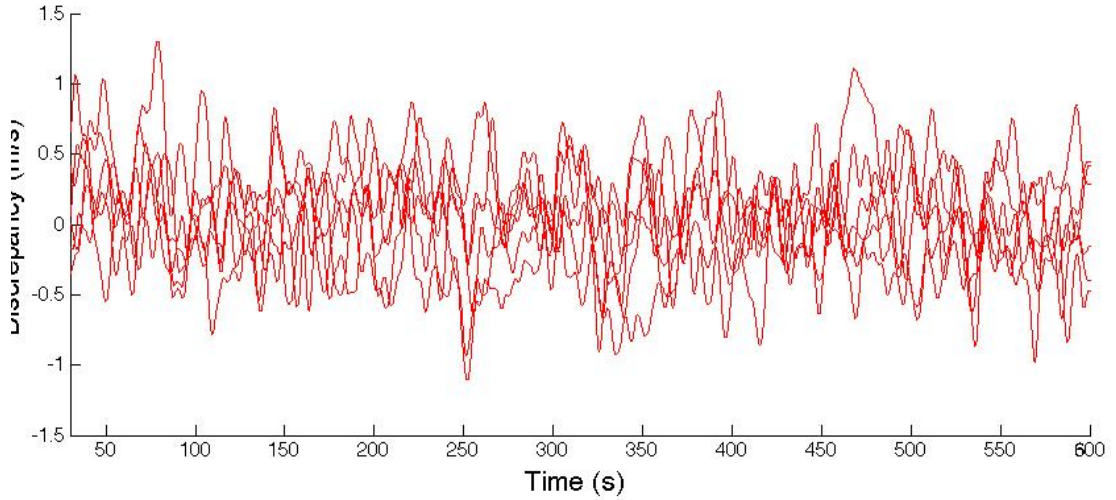
FIGURE 2.9: Discrepancy between anemometer and rotor average wind speed for all 8 m/s simulations.

Repeating that process for all the mean wind speeds simulated in the data set yields Figure 2.10 and Figure 2.11. Figure 2.10 shows average magnitude of the discrepancy between in m/s, while Figure 2.11 shows the same quantity expressed as a percentage

the mean wind speed. Each on the plot represents an average over all 57 minutes of simulation data at the corresponding wind speed. Figure 2.10 shows that the smallest average discrepancy is 0.269 m/s, which occurs at a mean wind speed of 6 m/s. When we examine the discrepancie as a percentage of the mean free stream wind speed (Figure 2.11) we see that the average discrepancie is approximately 3% of the mean wind speed over most of the operating range of the NREL 5-MW turbine., though the the average discrepancie is a larger percentage at low wind speeds.
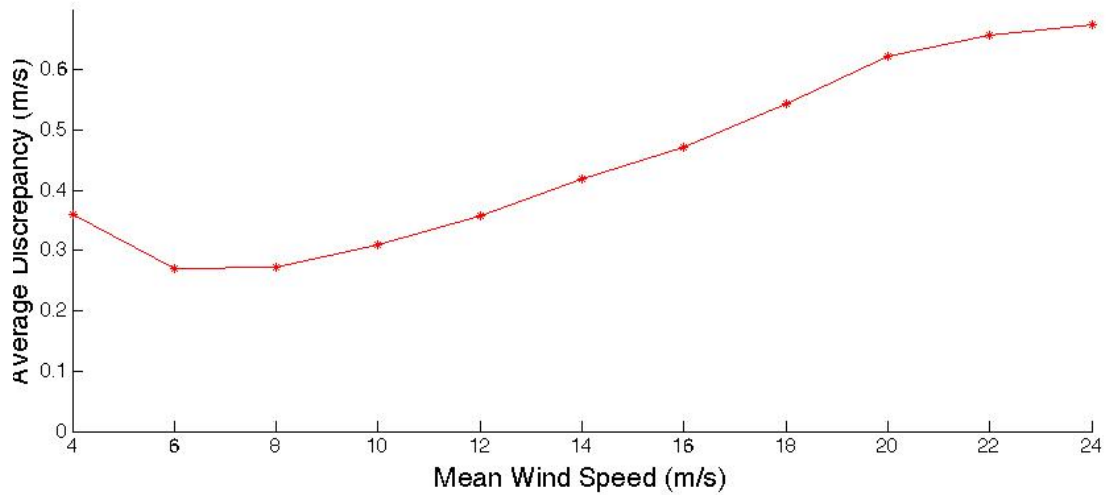
FIGURE 2.10: Average magnitude of discrepancy as a function of simulation mean wind speed.
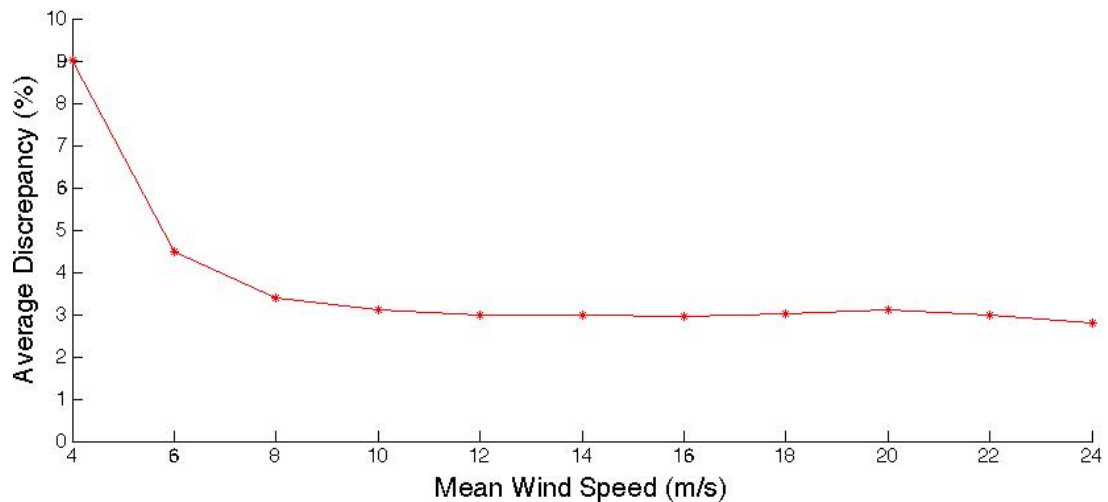
FIGURE 2.11: Average magnitude of discrepancy as a function of simulation mean wind speed.

2.4 Turbine Model Based Wind Speed Estimator

Incoming wind speed can also be estimated using an inverted model of the turbine. First the generator speed, generator torque, and pitch angle are measured. The inverted model is then used to determine the mean incoming wind speed that would cause the observed turbine operating conditions. In effect, the turbine itself is used as a wind speed sensor. [15–17]

We begin with a simplified model of the wind turbine in which the only degrees of freedom are the rotational speed of the rotor (Ω_{Rotor}), the collective blade pitch (θ), and the torque supplied by the generator (T_{Gen}). The dynamics of the turbine are given by equation 2.1 , where $I_{Drivetrain}$ is the low speed shaft equivalent inertia, T_{Aero} is the aerodynamic torque on the rotor, and N_{Gear} is the gear box ratio:

$$\dot{\Omega}_{Rotor} I_{Drivetrain} = T_{Aero} - T_{Gen} N_{Gear} \tag{2.1}$$

Essentially, equation 2.1 says the rotational acceleration of the rotor multiplied by the effective inertia of the rotor is equal to the sum of the torques applied to the rotor. The low speed shaft equivalent inertia ($I_{Drivetrain}$) is the rotational inertia of the rotor plus the apparent inertia due other components of the drivetrain. It can be calculated from the rotational inertias of the drivetrain components and the gearbox ratio (N_{Gear}). There are two torques applied to the rotor. The torque exerted by the generator is equal to the generator torque multiplied by the gearbox ratio. The aerodynamic torque exerted on the rotor by the incoming wind (U) is given by equation 2.2, where ρ is is air density, R is the rotor radius, C_p is the coefficient of power, and λ is the tip speed ratio:

$$T_{Aero} = \frac{1}{2}\rho R^3 \frac{C_p(\lambda, \theta)}{\lambda} U^2 \tag{2.2}$$

The tip speed ratio λ is the ratio between the speed of the turbine blade tips and the speed of the incoming wind. It can be calculated using equation 2.3. The coefficient of power C_p is a non-linear function of both tip speed ratio and collective blade pitch angle. A method for determining C_p will be discussed below

$$\lambda = \frac{\Omega_{Rotor} R}{U} \tag{2.3}$$

Equation 2.2 has four quantities that are not directly measureable: $T_{Aero}, C_p, \lambda, and U$. If equation 2.1 is used to substitute for T_{Aero} equation 2.2 becomes:

$$\dot{\Omega}_{Rotor}I_{Drivetrain} + T_{Gen}N_{Gear} = \frac{1}{2}\rho R^3 \frac{C_p(\lambda,\theta)}{\lambda}\left(\frac{\Omega_{Rotor}R}{\lambda}\right)^2 \qquad (2.4)$$

Which can be re-arranged to yield equation 2.5 . All the terms on the right side of equation 2.5 are known or easily measured from sensors on the wind turbine. Therefore, equation 2.5 can be used to calclate C_p/λ^3.

$$\frac{C_p(\lambda,\theta)}{\lambda^3} = \frac{2\dot{\Omega}_{Rotor}I_{Drivetrain} + 2T_{Gen}N_{Gear}}{\rho R^5 \Omega^2_{Rotor}} \qquad (2.5)$$

The coefficient of power C_p is a non-linear function of both tip speed ratio and collective blade pitch angle. It isn't possible to calculate C_p exactly, but for a given tip speed ratio and collective blade pitch it is possible to estimate the C_p of a turbine through simulation. Figure 2.12 illustrates how C_p of the NREL 5-MW turbine varies with λ and collective pitch angle. This plot was generated from a large number of simulations carried out with WTPerf [18]. Note that the maximum C_p corresponds to a $0°$ collective pitch angle and a tip speed ratio of 7.55. The turbine operates near this point when using variable speed control in region 2.
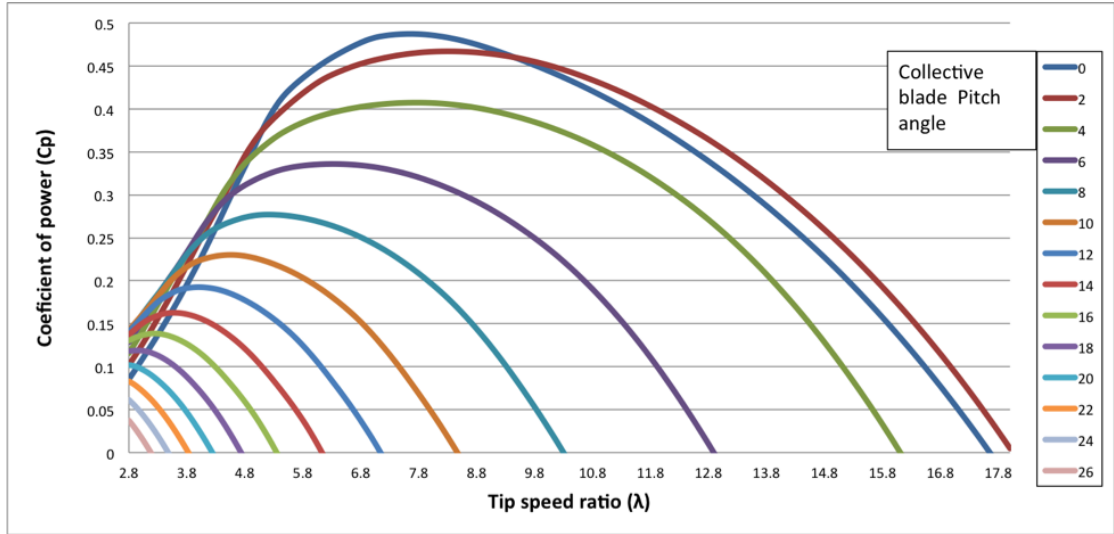
FIGURE 2.12: C_p dependence on λ and collective blade pitch.

The collective pitch angle is measured by turbine sensors, but both C_p and λ are unknown quantities that can not be directly measured or easily calulated. However, This problem can be fixed. If each C_p value estimated by WTPerf is divided by the corresponding λ cubed we get a relationship between $C_p\lambda^3$, λ, and collective pitch angle. Figure 2.13 illustrates how C_p/λ^3 of the NREL 5-MW turbine varies with λ and collective pitch angle.
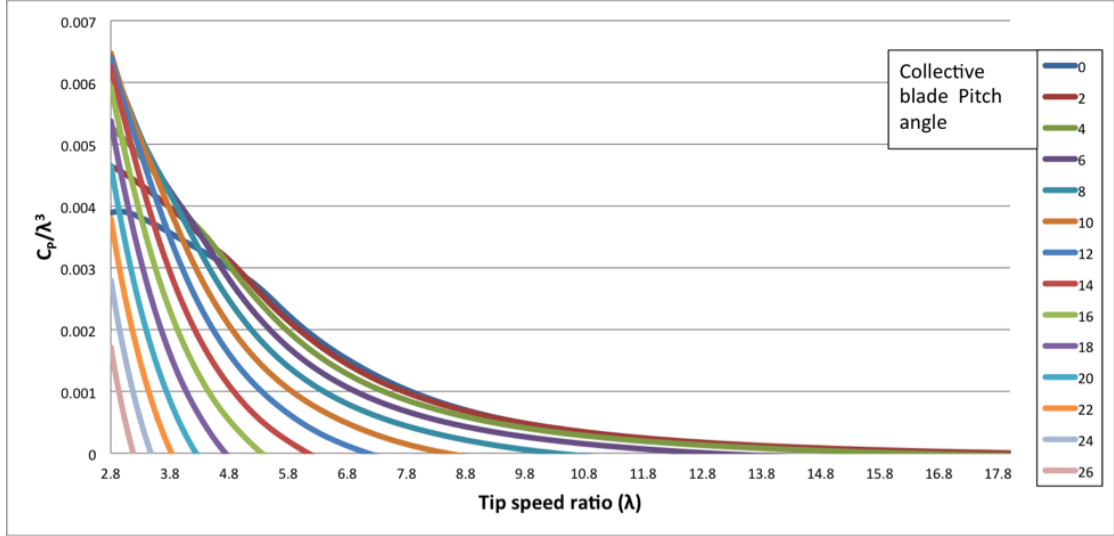
FIGURE 2.13: C_p/λ^3 dependence on λ and collective blade pitch.

The incoming wind speed can now be estimated. First the collective pitch angle is measured and C_p/λ^3 is calculated using equation 2.5. λ is then estimated by interpolating between the WTPerf simulation data points illustrated in Figure 2.13. Finally, λ is converted to incoming wind speed (U) using equation 2.3. Matlab codes carrying out these calculations can be found in appendix A.

2.4.1 Feasibility

The feasibility of using a wind turbine model based wind speed estimator was evaluated using similar methods to those used to evaluate the feasibility of using a nacelle top anemometer. We begin by comparing the average wind speed passing through the rotor of the turbine (calculated from the TurbSim flow field) to the wind speed estimated by the model based wind speed estimator. This gives us a feel for how well the estimator represents the wind passing through the rotor of a utility scale turbine.

The data in Figure 2.14 is from the 13th simulation in the dataset described above (the same simulation shown in Figure 2.5), but this data is typical of the other 65 simulations as well. The figure shows that the wind speed estimator is "noisier" than the rotor average wind speed. In this way it's similar to the nacelle anemometer measurements shown in Figure 2.5 and Figure 2.14 we see that high frequency fluctuations in the wind speed estimator are smaller than the high frequency fluctuations in the anemometer measurements.

Filtering the data to remove the high frequency fluctuations yields Figure 2.15. The wind speed estimator doesn't match the rotor average wind speed perfectly, but a comparison
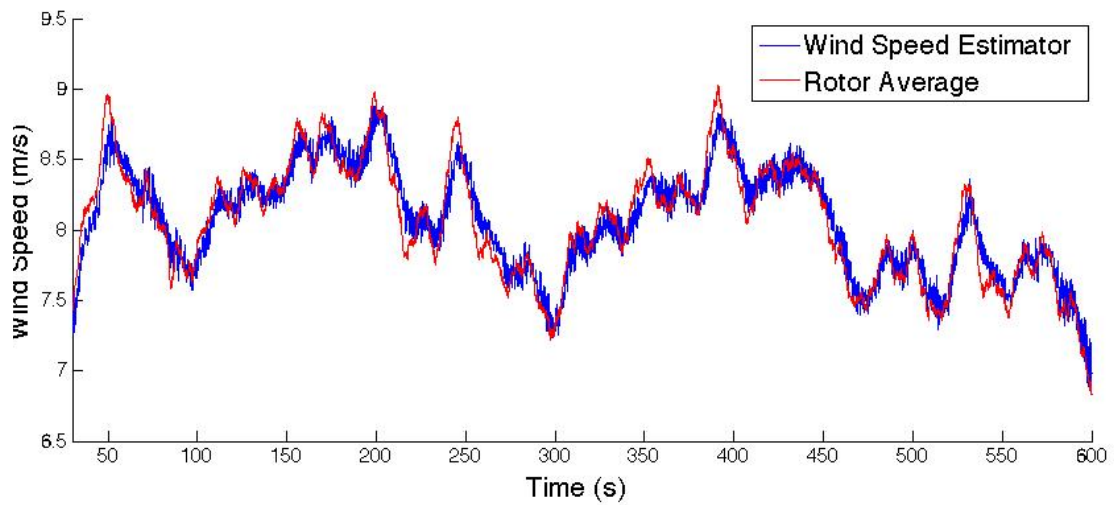
FIGURE 2.14: Wind speed estimate and rotor average wind speed for simulation #13.

between Figure 2.7 and Figure 2.15 shows that the wind speed estimator does a much better job than the nacelle top anemometer. This conclusion is reinforced by comparing Figure 2.8 to Figure 2.16.
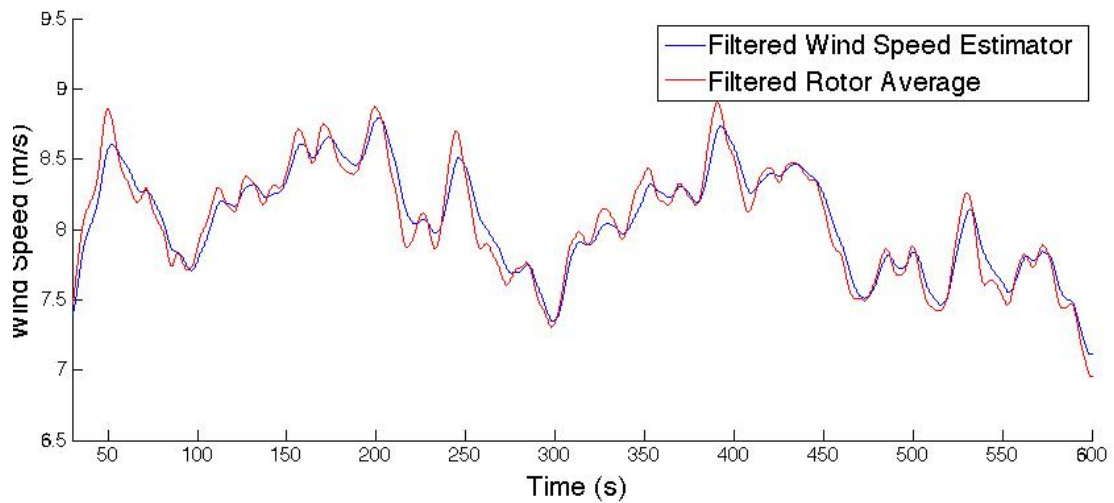
FIGURE 2.15: Filtered wind speed estimate and rotor average wind speed for simulation #13.

The data shown in Figures 2.14-2.16 are from a single simulation, but the data and the conclusions drawn from it are typical of all the simulation data examined. The wind sped estimator performed significantly better than the nacelle top anemometer. If we analyze the wind speed estimator data for all 66 simulations using the same process used to generate Figure 2.10 and Figure 2.11 we can get an idea of how much better the wind speed estimator performs. Figure 2.17 and Figure 2.18 compare the average discrepancy
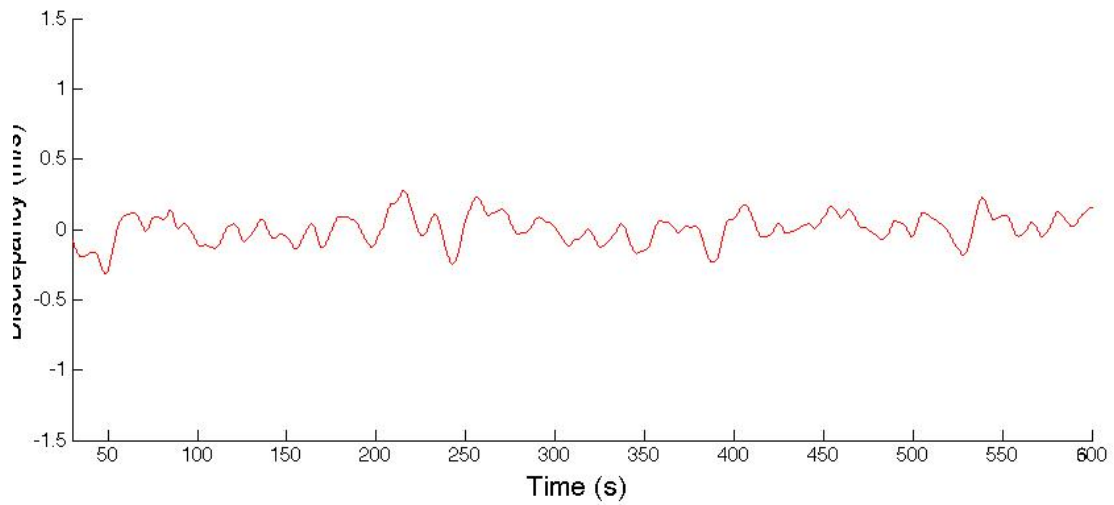
FIGURE 2.16: Discrepancy between wind speed estimate and rotor average wind speed for simulation #13.

between the wind speed estimator and the rotor average wind speed to the average discrepancy between the nacelle top anemometer and the average wind speed. It can be seen from these figures that the wind speed estimator outperforms the anemometer across the entire operating range of the turbine.
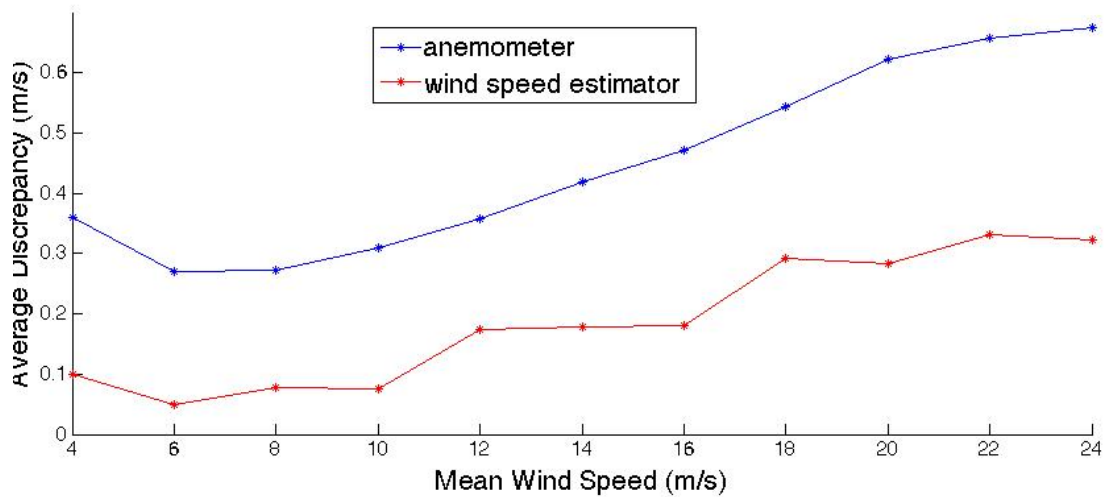
FIGURE 2.17: Average magnitude of discrepancy as a function of simulation mean wind speed.

2.4.2 Effect of rotor yaw misalignment

The simulations analyzed in the previous sections assume the turbine is pointed directly into the wind. However, in normal turbine operation there is often some misalignment
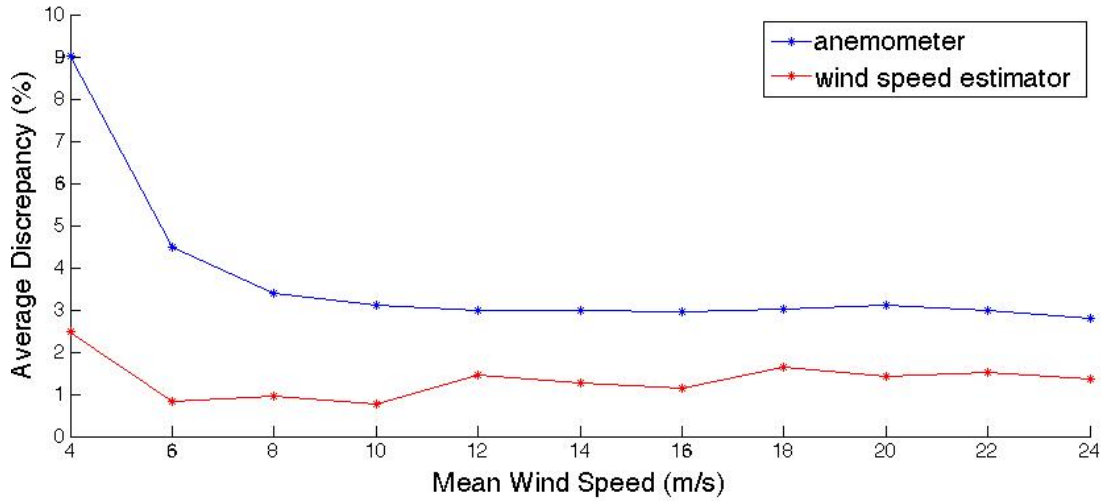
FIGURE 2.18: Average magnitude of discrepancy as a function of simulation mean wind speed.

between the wind direction and the pointing direction, or yaw, of the turbine. It is possible to design a turbine that is stable in yaw and will point itself into the wind without the help of a control system or actuators, but in practice this passive control technique is only used for very small turbines. Modern utility scale turbines use active yaw control[9].

The yaw control on a typical utility scale turbine uses a dead band controller with a nacelle mounted wind vane as a sensor and a nacelle yaw motor as an actuator. [ref wind energy handbook] In this control scheme the signal from the nacelle mounted wind vane is heavily averaged to reduce the effect of small brief changes in wind direction and to reduce the effect of the turbulence generated by the turbine rotor. That averaged wind direction is then treated as an estimate of the wind direction. The dead band controller compares the wind direction estimate to the current yaw of the turbine. If the misalignment is smaller than a pre-defined limit the controller does nothing, but if the misalignment exceeds the limit the controller engages the yaw motor and yaws the turbine into alignment with the wind. Since the NREL 5-MW turbine does not define a yaw control system, we will assume our turbine uses dead band control.

The amount of misalignment allowed by the dead band yaw controller will vary from one turbine to another. To evaluate the effect of yaw misalignment on wind speed estimation misalignments of 5°, 10°, 15°, and 20° were simulated. For each of these yaw misalignments the 66 test cases described above were simulated.

Figure 2.19 shows the effect of rotor misalignment on wind speed estimation for simulation case #13. As misalignment angle increases the wind speed estimator underestimates

wind speed. For 5° and 10° misalignments this effect appears small, but the effect is much larger for 15° and 20° misalignments. It's worth noting that the shapes of the wind speed estimate curves do not change much with increasing rotor misalignment. The misalignment primarily affects the magnitude of the wind speed estimates.
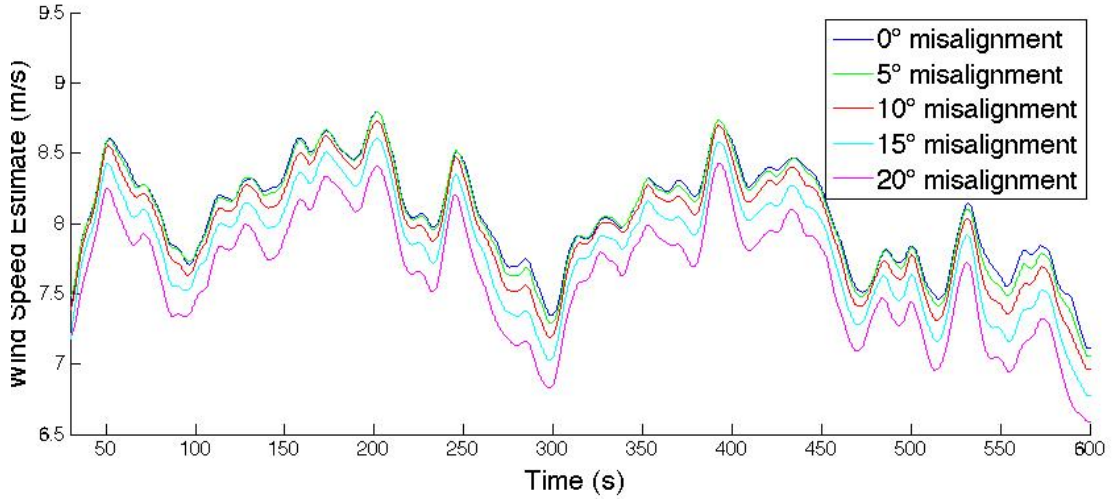
FIGURE 2.19: Effect of rotor misalignment on wind speed estimate for simulation #13.

Though the data shown in Figure 2.19 is from a single simulation case the conclusions drawn from it are typical of all simulation data that was examined. If we analyze the wind speed estimator data for all simulations cases using the same process used to generate Figure 2.11 we can get an idea of how rotor misalignment affects wind speed estimation error. As we saw in Figure 2.19 a misalignment of 5° or 10° causes only a small increase in the discrepancy between estimated wind speed and average rotor wind speed. Larger misalignments cause significantly larger discrepancies. It is worth noting only the 20° misalignment performs worse than the nacelle top anemometer (Figure 2.11).

It should not be surprising that a misaligned rotor underestimates wind speed. Our wind speed estimator is based on a simplified model of turbine rotor dynamics. Since wind parallel to the rotor plane does not exert an aerodynamic torque on the rotor our estimator does not measure that component of the wind. Essentially, our wind speed estimator is designed to measure the component of the wind that is perpendicular to the rotor plane. As Figure 2.21 shows, the apparent wind seen by the wind speed estimator is equal to the actual wind multiplied by the cosine of the misalignment angle.

If the misalignment angle is known it can be used to compensate for the difference between the apparent wind seen by the estimator and the actual wind. If the wind speed estimates shown in Figure 2.19 are divided by the cosine of the misalignment
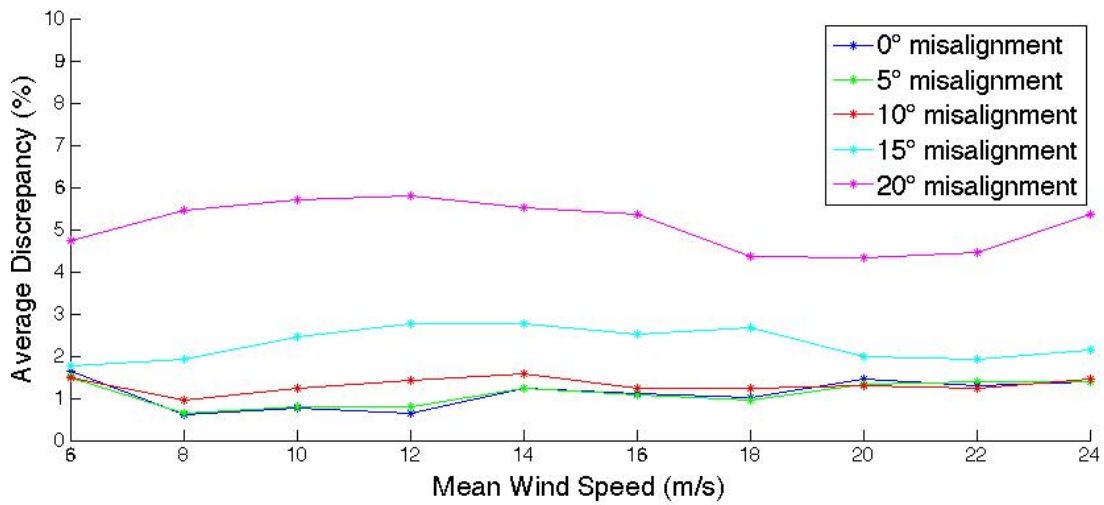
FIGURE 2.20: Effect of misalignment on average magnitude of wind speed estimate discrepancy.
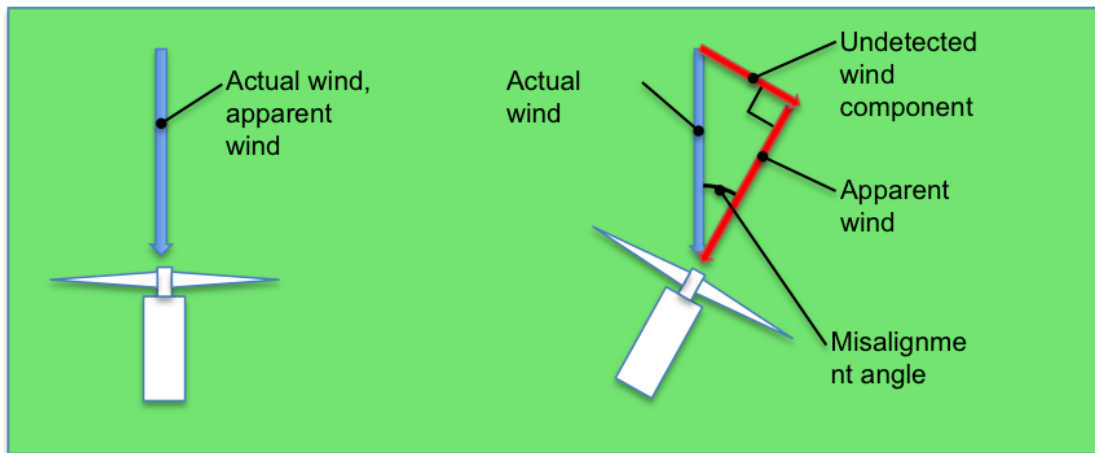
FIGURE 2.21: Effect of rotor misalignment on apparent wind.

angle it yields Figure 2.22. As the figure shows, the effect of misalignment on wind speed estimation has been greatly reduced.

Figure 2.23 shows the average discrepancy between misalignment-compensated wind speed estimates and rotor average wind speed. The misaligned simulations generally show more discrepancy than the perfectly aligned simulations. However, comparing Figure 2.20 to Figure 2.23 shows that misalignment compensation greatly reduces the discrepancy. In the 20° misalignment simulations the average discrepancy is reduced 60-75 % by angle compensation.

Though the misalignment angle will not be perfectly known, an estimate of the misalignment angle will be available and can be used for compensation. As stated earlier
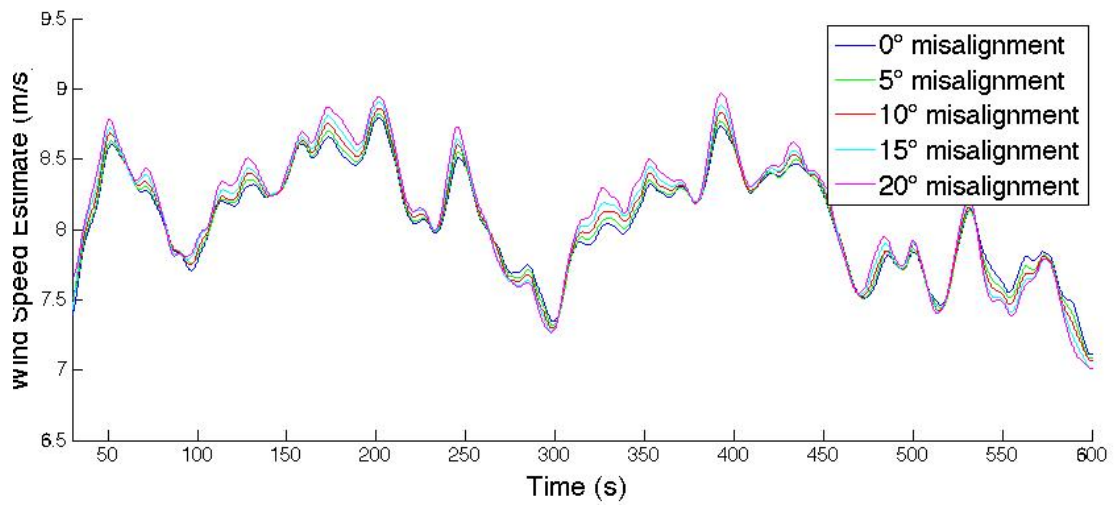
FIGURE 2.22: Angle corrected wind speed estimates for simulation #13.
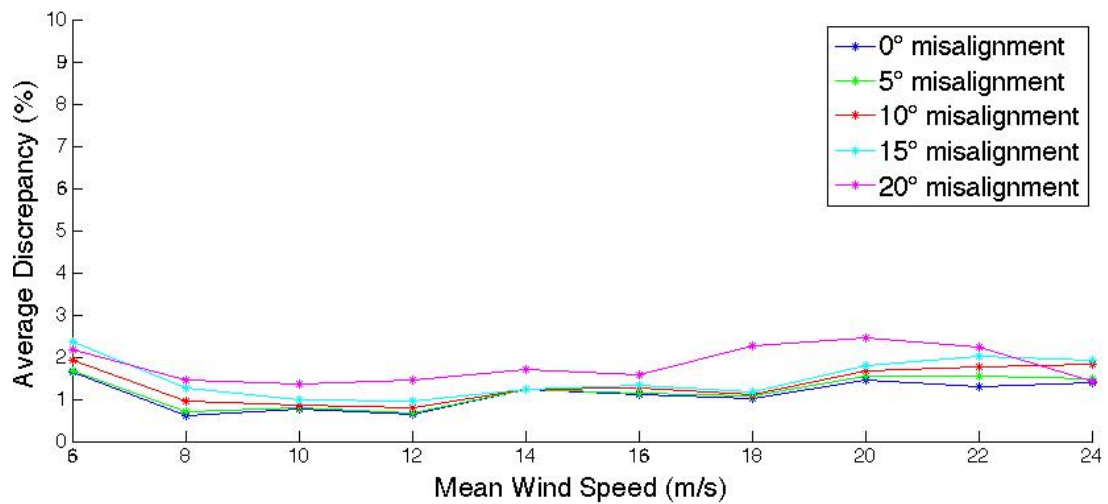
FIGURE 2.23: Average magnitude of discrepancy in angle corrected wind speed estimates.

in this section, the dead band yaw controller continuously estimates the misalignment angle but doesn't act unless the misalignment exceeds a pre-defined limit.

Yaw misalignment does have an effect on turbine model based wind speed estimation, but it does not appear that it will be a significant hindrance to using turbine model based wind speed estimation. Misalignments less than $10°$ only have a minor effect on performance. Larger misalignments do have a significant effect on performance, but it should be possible to reduce the effect by using misalignment angle compensation.

2.5   Convection speed estimation

The previous sections have discussed instantaneous wind speed estimation. These wind speed estimates can be used to observe how the wind speed is fluctuating as it passes through a wind turbine rotor. However, knowledge of how the wind speed is fluctuating is not sufficient information for feed forward control of downwind turbines. We must also know when these wind speed fluctuations will reach the downwind turbine. The time required for the wind speed fluctuations to pass from the upwind turbine to the downwind turbine can be calculated with the simple equation $t = D/U_{conv}$, where D is the downwind distance between the turbines and U_{conv} is the convection speed. The convection speed is the rate at which wind speed fluctuations propogate downwind. This section will discuss using a wind turbine to estimate the convection speed.

If we assume Taylor's frozen turbulence hypothesis we can estimate the convection speed based on wind speed measurements taken at a single location. In this secion the convection speed will be estimated using the turbine model based wind speed estimates discussed in Section 2.4. Taylor said "If the speed of the air stream which carries the eddies is very much greater than the turbulence speed, one may assume that the sequence of changes in u at a fixed point are simply due to the passage of an unchanging pattern of turbulent motion over the point." [19] In other words, the wind experienced by a point down wind of our sensor will be the same as the wind experienced by the sensor but it will be delayed by a time $t_D = (distance)/(U_{conv})$. It follows from Taylor's hypothesis that the convection speed of the turbulent fluctuations is equal to the local mean speed (U_{mean}).

There is much research into the validity and limitations of Taylr's frozen turbulence hypothesis for estimating the convection speed. [20–23] Though research shows that the convection speed is not allways equal to the mean speed they are frequently assumed to be equal in turbulent flow research. $U_{conv} = U_{mean}$ will be assumed for the remainder of this section. A more accurate estimate of the convection speed could be generated using more than one wind speed measurement location. For example, we could measure the time it took a gust of wind to travel between two turbines. However, this technique can not be used with the data set described in Section 2.2 because FAST only simulates a single turbine.

For the data set described in Section 2.2 the mean speed (U_{mean}) is known. U_{mean} is one of the turbsim input parameters used to generate the data set. As shown in equation 2.6 we can consider the wind passing through the turbine rotor to be a combination of the underlying mean wind sped (U_{mean}) and the wind speed fluctuations due to turbulence

(U_{turb}). If we average the hub height wind speed over a long enough timethe wind speed fluctuations due to turbulence will cancel out and we'll be left with the mean wind speed.

$$U = U_{mean} + U_{turb} \tag{2.6}$$

Figure 2.24 shows the wind speed estimate, the 60 second average wind speed, and the true mean wind speed for simulation #13. The wind speed estimate is generated using the method described in section 2.4. 60 second average values are generated by averaging 60 seconds of wind speed estimate data (from 30 seconds before to 30 seconds after the time of interest). The true mean wind speed is known and was specified as an input when simulating the incoming wind. There are two things worth noting in Figure 2.24. First, there are significant discrepancies between the 60 second average wind speed and the known mean wind speed of 8 m/s. At 182 seconds there is a 0.587 m/s, or 7.3%, discrepancy between the 60 second average wind speed and the true mean wind speed. Second, the 60 second average wind speed out performs the wind speed estimator when it comes to estimating the true mean wind speed. Both the maximum and average discrepency are lower for the 60 second average wind speed.
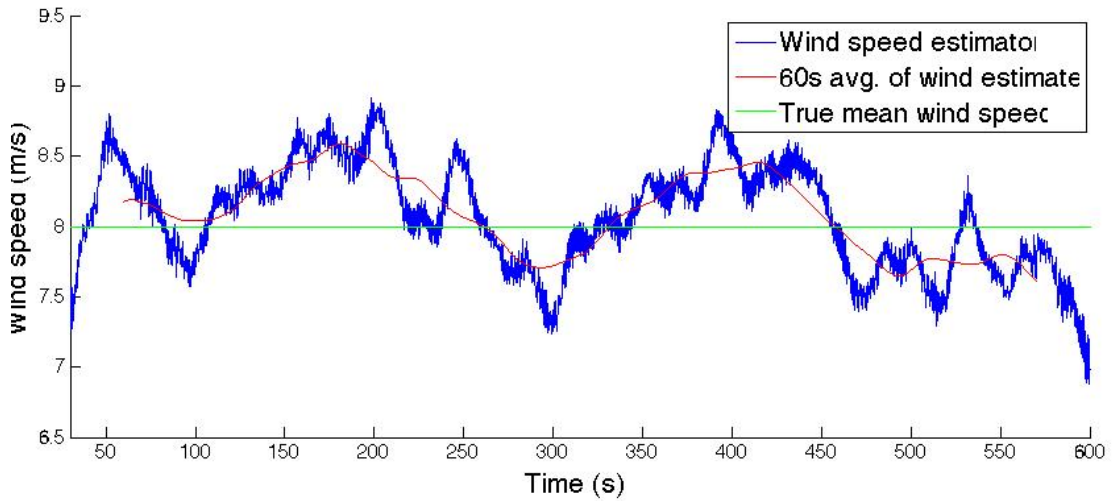
FIGURE 2.24: Estimating U_{mean} using a 60 s average of wind speed estimates for simulation #13.

By analyzing all of the test cases in our data set with a variety of averaging times we can generate Figures 2.24 and 2.25. These figures show the maximum and average discrepancies between the various averaged wind speed estimates and the known true mean wind speeds. In Figure 2.24 we see that longer average times result in smaller mean discrepencies between the average wind speed estimate and the true mean wind speed. This is expected. Longer averaging times would likely perform even better, but

570 seconds was the longest averaging time we could use with the current data set. The highest mean discrepancies (as a % of the true mean wind speed) are at low wind speeds. For some wind speeds (16 m/s - 22 m/s) Figure 2.24 seems to show diminishing improvement for averaging times over 240s. However, for the rest of the wind speeds Figure 2.24 does not seem to show a clear point of diminishing returns.

Figure 2.25 largely shows the same trends that we see in Figure 2.24, but the trends are a little less clear. Figure 2.25 shows a few unexpected results. For example, in 18 m/s wind Figure 2.25 an averaging time of 240s gives a larger maximum discrepency than any of the shorter or longer averaging times. I suspect that if we analyzed a lot more data some of these unexpected results would no longer be present.
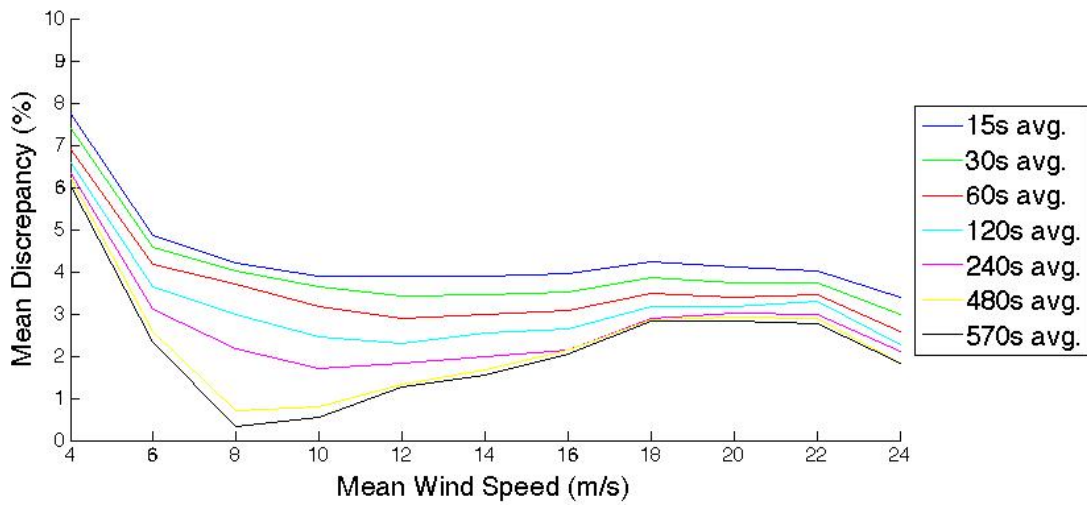
FIGURE 2.25: Mean discrepency between true U_{mean} and estimated U_{mean} for a variety of averaging times.

Though Figures 2.24 and 2.25 imply that the averaging time should be as long as possible, there is a practical reasons why a very long averaging time would be undesireable. When we simulate wind fields using TurbSim the mean wind speed remains constant, but research has shown that in real world conditions the mean wind speed does not remian constant indefinitely. In real world conditions the mean wind speed may be slowly changing [24]. If the mean wind speed is changing, we can minimize the impact on our wind speed averaging by keeping the averaging time short and by centering the averaging window on the time of interest. If we choose to center our averaging window on the time of interest, our averaging time is further constrained by the ammout of time it will take wind speed fluctuaions to propogate from the upwind turbine to the downwind turbine. For example, if the mean wind speed is 20 m/s and the downwind turbine is 1000 m behind the upwind turbine it will take about 50 seconds for the wind speed
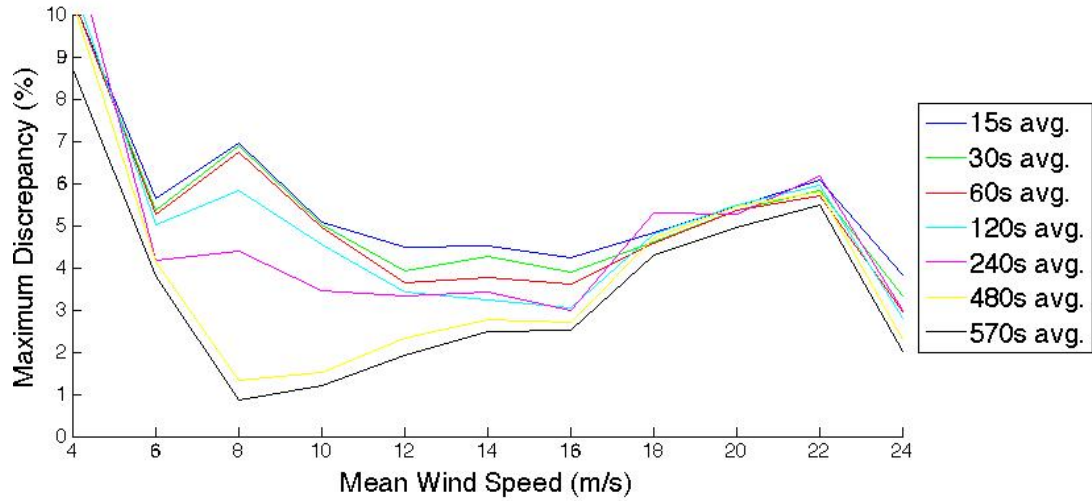
FIGURE 2.26: Max discrepency between true U_{mean} and estimated U_{mean} for a variety of averaging times.

fluctuations to travel from the upwind turbine to the downwind turbine. Therefore, our averaging time can not be more than 100 seconds.

2.5.1 A few thoughts on the limitations of

Though Taylor's hypothesis is often invoked in investigations of atmospheric turbulence, experimental results have shown that it is not universally accurate.[25, 26] In particular, Taylor's hypothesis is more accurate over short distances than over long distances and it is more accurate for low frequency wind speed fluctuations than high frequency fluctuations.

Chapter 3

Feed forward optimum pitch control.

3.1   Introduction

As discussed in Section 1.2, the closed loop control system of a typical utility scale wind turbine manipulates generator torque and collective blade pitch in order to control the power generation and rotor speed of the turbine. At low and medium wind speeds the blade pitch remains fixed at $0°$ while generator torque is manipulated to achieve the rotor speed that maximizes electricity generation. At high wind speeds the collective blade pitch is manipulated to manage loading on the wind turbine as well as to maintain constant rotor speed and power generation. For a given wind speed there is a desired rotor speed (Ω_{Rotor}), collective blade pitch (θ), and generator torque (T_{Gen}). Figure 3.1 shows these desired values for the NREL 5-MW turbine. If the wind remined constant the control system of the NREL 5-MW turbine would bring $\Omega_{Rotor}, \theta, and T_{Gen}$ to the values shown in figure 3.1 and maintain those desired conditions. However, since wind speeds often fluctuate (as shown in figure 3.2) and utility scale turbines are large mechanical devices that are unable to instantaneously adjust to changes in wind speed, turbines are frequently chasing the desired conditions instead of operating at the desired conditions.

Figures 3.3 and 3.4 illustrate the transient response of the NREL 5-MW turbine when subjected to sudden changes in wind speed. In both cases FAST has been used to model a NREL 5-MW turbine with the baseline controller defined in [2]. Figure 3.3 illustrates turbine behavior in region 2, wind speeds between 7.8 m/s and 10.3 m/s, while Figure 3.4 illustrates turbine behavior in region 3, wind speeds between 11.4 m/s and 25 m/s. Each figure shows wind speed, "Actual" and "Optimal" power, generator torque, and
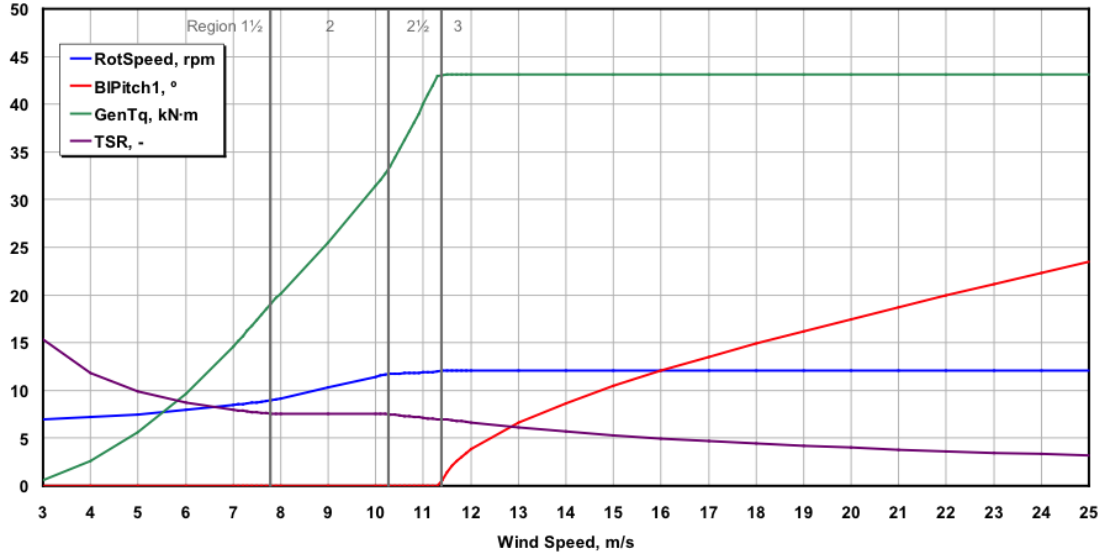
FIGURE 3.1: Steady state behavior of the NREL 5-MW.[2]
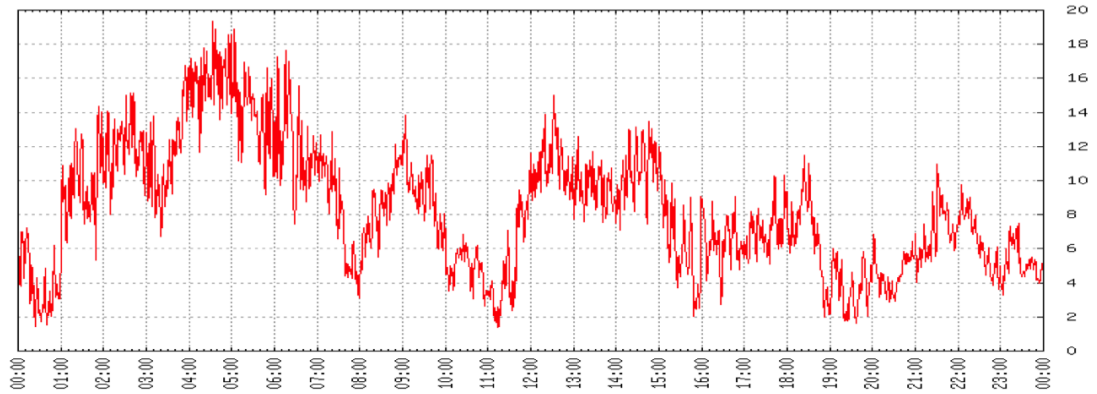
FIGURE 3.2: An example of wind speed fluctuations over 24 hours.[6]

blade pitch. "Actual" power is the power generated by the turbine. "Optimal" power is the desired steady state power generation for the current wind speed (based on the NREL 5-MW power curve shown in Figure 1.6). Generator torque and blade pitch are the two actuators used to control turbine performance.

In Figure 3.3 the turbine is subjected to a uniform incoming wind that changes between 8 m/s and 10 m/s every 20 seconds. These wind speeds are in region two, where optimal power production corresponds to the maximum aerodynamic efficiency of the turbine. Note that the turbine takes approximately 20 seconds to reach optimal generation after each change in wind speed. This corresponds to a reduction in efficiency. The optimal power curve generates 0.6% more power (15.6 kW on average) than the actual power curve. In this case turbine performance is regulated entirely by torque control. The turbine blades remain at 0° pitch.
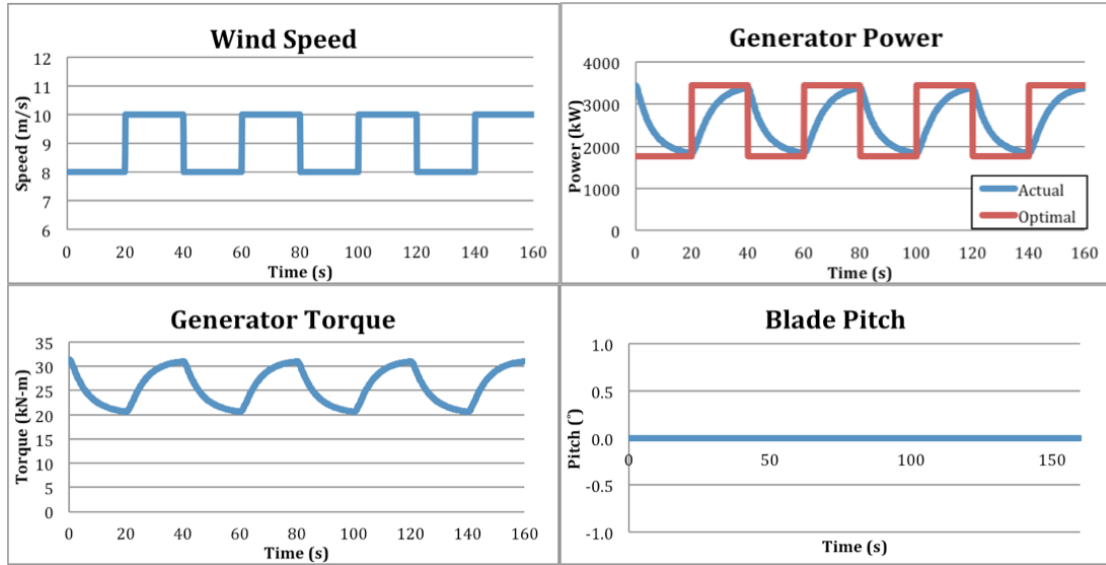
FIGURE 3.3: NREL 5-MW response to wind speed fluctuations in control region 2.

In Figure 3.4 the turbine is subjected to a uniform incoming wind that changes between 16 m/s and 18 m/s every 40 seconds. These wind speeds are in region three, where optimal power production is the rated power of the turbine, 5 MW. After each change in wind speed the turbine experiences both spikes and dips in power production. The largest fluctuations in power occur in the first 10 seconds after a change in wind speed. After 25 seconds the generated power is nearly constant at 5 MW. In this case turbine performance is regulated by both torque control and pitch control.
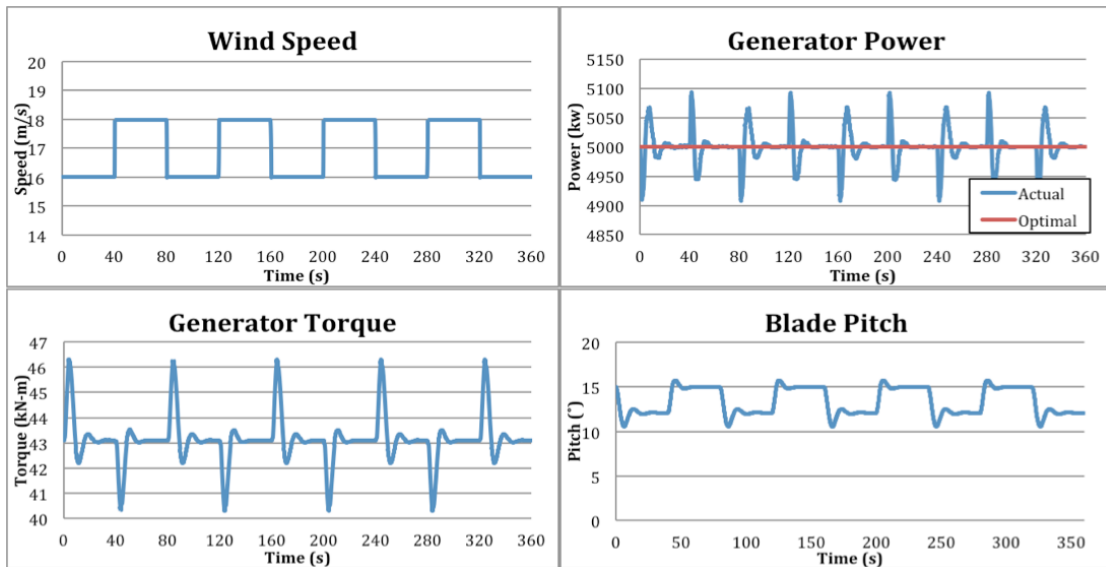
FIGURE 3.4: NREL 5-MW response to wind speed fluctuations in control region 3.

You can see from the previous figures that wind turbines respond reactively to changes

in wind speed. However, several researchers have shown that turbine performance can be improved if a turbine is able to pre-emptively react to changes in wind speed before they occur. Ozdemir, Seiler, and Balas showed that perfect preview knowledge of incoming wind speed could be used to increase power production or decrease gearbox loads by improving generator torque control in region 2 operation. The authors used state space optimal control techniques to control generator torque based on incoming fluctuations in wind speed. In some of their simulations they were able to achieve increases in power generation of 6% or decreases in gerabox loading of 30%.[27] Dunne, Pao, Wright, Jonkman, Kelley, and Simley have shown that perfect preview knowledge of incoming wind speed fluctuations could also be used reduce turbine loads by improving pitch control in region 3 operation. The authors examined three methods of feed forward pitch control based on wind speed preview information: non-causal series expansion, preview control, and optimized FIR filter methods. The autors simulated the response of the feed forward controllers to both turbulent wind and sudden gusts. Each of the feed forward controllers were capeable of reducing damage equivalent loads on the turbine blades and/or turbine tower. [28]. Schlipf, along with various collaborators, has shown that imperfect preview knowledge of incoming wind speed, obtained through a nacelle mounted LIDAR, can be used to improve turbine control.[4, 26, 29–31] Schlipf, Schlipf, and Kühn used simulations of the LIDAR and turbine to demonstrate that LIDAR based feed forward collective pitch control could reduce extreme and fatigue loads on turbine blades and the turbine tower. [31] However, Schlipf, Kapp, Anger, Bischoff, Hofsäß, Rettenmeier, and Kühn concluded that only minimal increases in power production could be achieved using LIDAR assisted generator torque control in region 2 operation.[30] Scholbrock, Fleming, Fingersh, Wright, Schlipf, Haizman, and Belen field tested a LIDAR assisted feed forward controller on the NREL CART3 research turbine. The authors observed reductions in damage equivalent loads for the turbine blade bending moments and rotor torque. [32]

The remainder of chapter examines the feasibility of feed forward pitch control using wind speed preview information generated by using wind speed estimates from an upwind turbine. The following section describes how FAST, a single turbine simulation tool, can be used to simulate a two turbine system. Section 3 describes the feed forward controller. Sections 4 and 5 examine how the feed forward controller performs when subjected to wind gusts and turbulent wind. Section 6 examines how sensitive teh feed forward controller is to errors in feed forward wind speed estimate data and the corresponding implications.

3.2 Using FAST to Model a 2 Turbine System

As discussed in Section 2.2, FAST is a medium fidelity wind turbine simulation tool. FAST models both the aerodynamics and structural dynamics of a single turbine. FAST can model a turbine's response to either uniform incoming wind or, with the help of TurbSim, statistically accurate turblent wind. Though FAST only models one turbine at a time it can be used to model a multi turbine system if a few assumptions are made. Figure 3.5 shows the two turbine system being simulated. The wind is blowing from left to right and the, the terain is flat, and the downwind turbine is slightly offset from the upwind turbine. When simulating this two turbine system in FAST the following assumptions are made:

- Taylor's hypothesis is valid. The wind speed fluctuations experienced by the upwind turbine will propogate downwind at some convection velocity without changing. Therefore, the downwind turbine will experience the same series of wind speed fluctuations as the upwind turbine but at a later time.

- The slight offset of the downwind turbine will be enough to keep the downwind turbine out of the upwind turbine's wake.

- The slight offset of the downwind turbine will be small enough that wind speed fluctuations will hit both the upwind and downwind turbines.

- Because the terrain is flat, complex terrain effects do not need to be considered.

FIGURE 3.5: Illustration of the two turbine system modeled in this chapter.

Figure 3.6 shows how FAST can be used to simulate the two turbine system illustrated in Figure 3.5. First a simulated wind field is generated. This can be a simple wind field, such as uniform incoming wind, or a turbulent wind field generated with TurbSim. Next, FAST is used to simulate how a turbine with a conventional control system will respond to the wind field. This first FAST simulation simulates the upwind turbine

in our two turbine system. Once the first FAST simulation is complete the simulation results are post-processed using the wind speed estimation techniques described in 2.4. In real world applicaions data from the upwind turbine would be continually processed and passed to the downwind turbine. However, since we are simulating the upwind and downwind turbine separately, it is easier to process all of the upwind turbine data at the same time. Finally, FAST is used to simulate the donwwind turbine. In this second simulation the turbine experiences the same wind field, but the turbine has feed forward pitch control and has access to wind speed preview data that was generated by post processing the results of the upwind turbine simulation. By comparing the simulation results from the first (upwind) and second (downwind) FAST simulations we can see how the feed forward pitch controller has affectetd turbine performance.
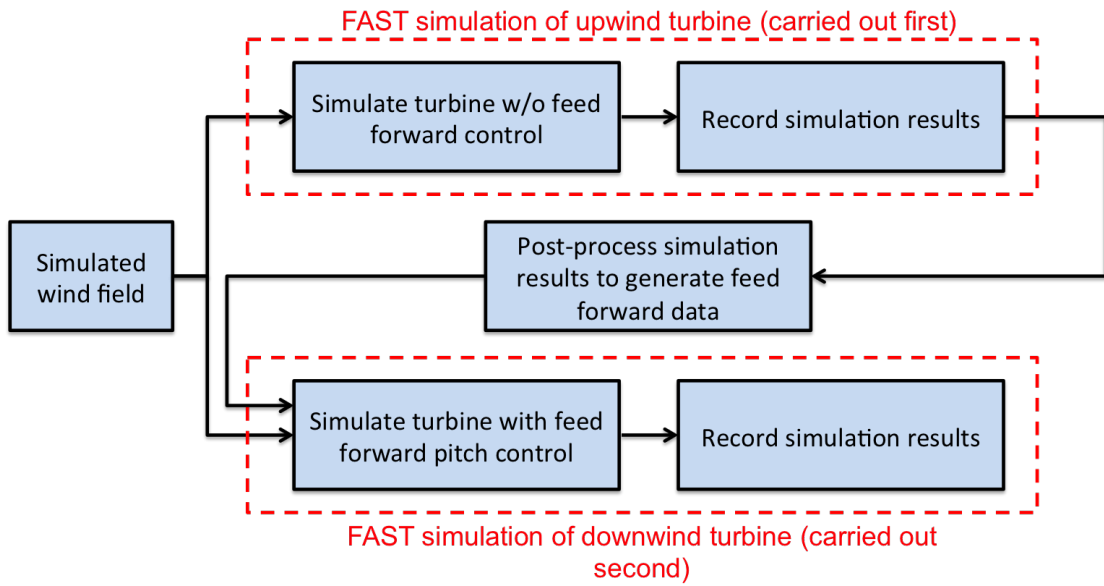
FIGURE 3.6: How FAST can be used to simulate a two turbine system.

3.3   Controller Design

3.3.1   Implementing Feed Forward Control

Figure 3.7 is a simple block diagram illustrating how the control system, turbine, and wind interact for a typical utility scale turbine. The behavior of the turbine is affected by the wind as well as the collective pitch (θ) and generator torque (T_{Gen}) commands sent by the closed loop controller. The closed loop controller monitors the turbine rotor speed (Ω_{Rotor}), the only feedback signal used in a typical utility scale turbine controller, to determine if the turbine is operating at a desired steady state operating point. If the turbine is not at a desired operating point the controller manipulates collective

blade pitch (θ) and generator torque (T_{Gen}) to bring the turbine to a desired operating point. In region 3 (high wind speeds) the controller tries to keep the turbine rotor speed (Ω_{Rotor}) and power generation constant. In region 2 (low and medium wind speeds) the controller tries to maintain the rotor speed that will maximize power generation. From a control standpoint the wind is a disturbance, it is an uncontrolled input that affects the behavior of the turbine. Generally, changes in the wind cause the turbine to move away from desired operating points while the closed loop controller acts to bring the turbine back to desired operating points.
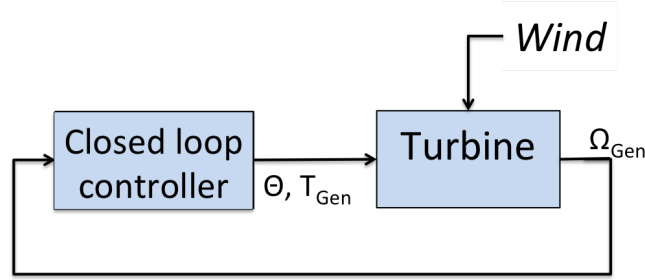
FIGURE 3.7: Simple block diagram of turbine w/o feed forward control.

Figure 3.8 is a simple block diagram illustrating the method we have chosen to incorporate feed forward control into the control system of a turbine. You can see that the feedback control loop shown in Figure 3.7 remains intact, but a feed forward controller, which issues supplimental collective pitch (θ_{ff}) and generator torque (T_{ff}) commands has been added. The closed loop controller shown in Figure 3.8 is identical to the one in Figure 3.7. This is not the only way to implement feed forward control, but this method does have some advantages. It is fairly simple in that it does not require us to re-design the entire control system. In addition, if the turbine were to lose the feed forward signal for any reason it would simple begin operating as if it were using a standard closed loop turbine control system. In fact this feed forward control implementation allows the turbine to smoothly transition between standard closed loop control and closed loop with feed forward controll. This trait is desireable for a variety of situations. For example, if the wind changes direction the turbine may find that it no longer has an upwind turbine to use as a sensor.

3.3.2 Closed Loop Controller

The closed loop controller is modeled in Simulink and coupled to FAST as described in the FAST user's guide [33], and the full Simulink model of the closed loop controller can be found in appendix **??**. The controller has all the properties of the NREL 5-MW controller defined by NREL in [2] plus a model of the collective blade pitch actuator.
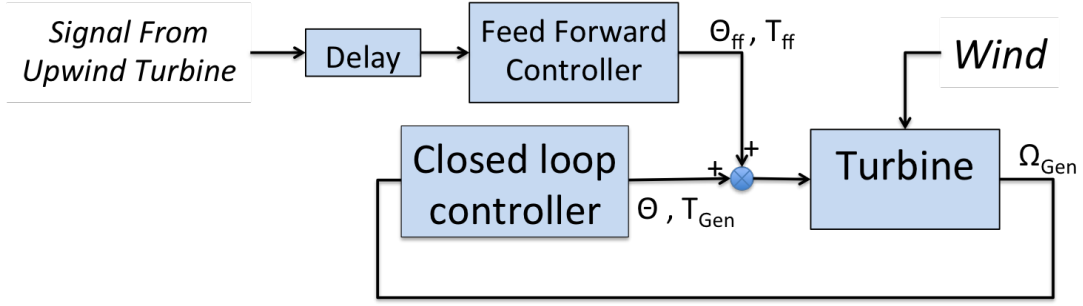
FIGURE 3.8: Simple block diagram of turbine with feed forward control.

Figure 3.9 illustrates the controller. The NREL 5-MW controller defined in [2] consists of a measurement filter, a torque controller, and a pitch controller. The measurement filter is a recursive, single pole low pass filter with a corner frequency of 0.25Hz. The purpose of this low pass filter is to mitigate high frequency excitations of the control system. The torque controller uses a torque schedule, basing generator torque on the rotational speed of the turbine. The pitch controller is a non-linear PI (proportional and integral) controller where the proportional and integral gains are a function of blade pitch.

Since this chapter is concerned with feed forward pitch control, the turbine will be operating in control region 3 for all simulations. The NREL 5-MW turbine operates in control region 3 when wind speeds are higher that the turbine's rated wind speed of 11.4 m/s. in control region 3 the pitch controller varies collective blade pitch in an attempt to maintain a constant rotational rotor speed (ω_{Rotor}) of 12.1 RPM. When the rotor is spinning at 12.1 RPM the generator supplies the rated generator torque (43,093.55 $N \cdot m$), but whe the 12.1 RPM the torque controller varies torque in an effort to maintain a constant power generation of 5 MW.

The controller shown in figure 3.9 also includes a model of the collective pitch actuator. Though the pitch actuator is not part of the control system it must be modeled in Simulink because current versions of FAST do not model pitch actuator dynamics. If pitch actuator dynamics are not modeled the closed loop controller is able to instantly change blade pitch. This is physically unrealistic and in some circumstances it leads to unrealistic control system behavior, such as high frequency fluctuations in pitch or unrealistic reactions to feed forward pitch control.

The pitch actuator is modeled as a second order system with dynamics describe by equation 3.1, where θ is the actual collective blade pitch, θ_c is the desired blade pitch requested by the controller, ξ is the damping ratio of the pitch actuator, and ω_o is the undamped natural frequency of the pitch actuator. Jonkman does define a NREL 5-MW blade pitch actuator in [2], but Jonkman has admitted that the pitch actuator defined in [2] is very fast and is unrealistic [34]. Instead we use $\xi = 0.7$ and $\omega_o = 1Hz$, which have
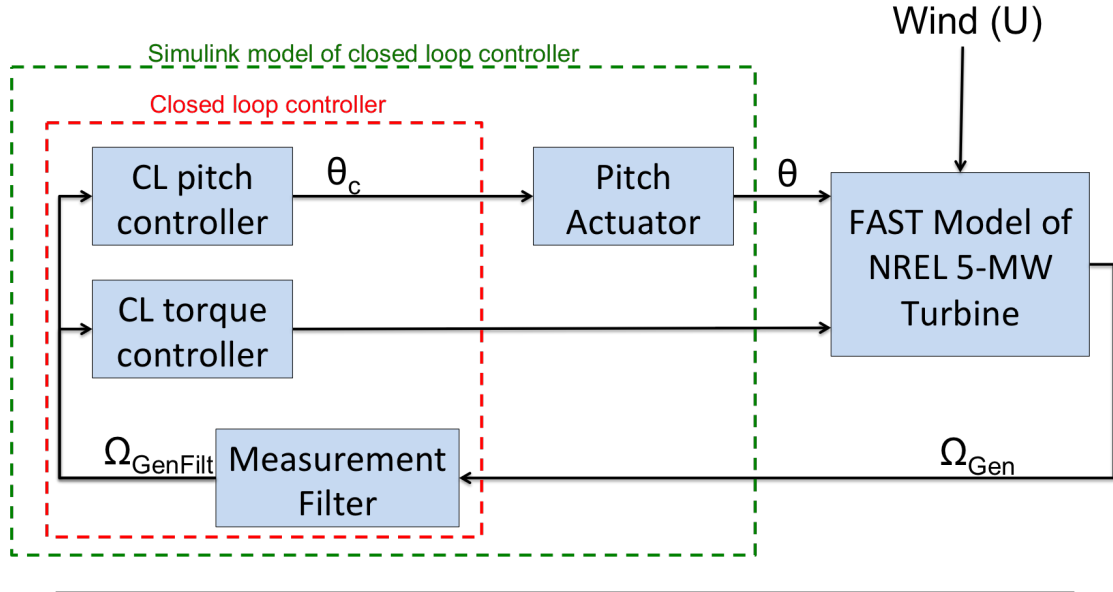
FIGURE 3.9: Closed loop control system.

been used to model NREL 5-MW pitcha actuators in previous research on feed forward turbine pitch control[28, 35].

$$\ddot{\theta} + 2\xi\omega_o\dot{\theta} + \omega_o^2\theta = \omega_o^2\theta_c \tag{3.1}$$

3.3.3 Feed Forward Controller

The feed forward controller is based on the dynamic feed forward pitch controller proposed by Shlipf in [26]. Figure 3.10 illustrates how the feed forward controller interfaces with the closed loop controller described in the previous section. As described in Section 3.3.1, the wind is a disturbance, an uncontrolled input that affects sytem behavior. Typically, changes in the wind cause the turbine to deviate from the desired operating conditions while the closed loop controller acts to bring the turbine back to the desired operating conditions. Ideally we would like the feed forward controller to cancel out the effect of the disturbance so the turbine never deviates from the desired operating conditions to begin with and the closed loop controler would not need to act.

As discussed in the previous section, the goal of region 3 pitch control is to maintain a constant rotor speed of 12.1 RPM. This constant rotor speed is maintained when the aerodynamic torque applied to the rotor by the wind is equal to the torque applied to the rotor by the generator and there is no net torque to accellerate or decellerate the rotor. If the rotor is spinning at 12.1 RPM and the wind speed is anywhere between the rated wind speed (11.4 m/s) and the cutout wind speed (25 m/s) of the turbine there
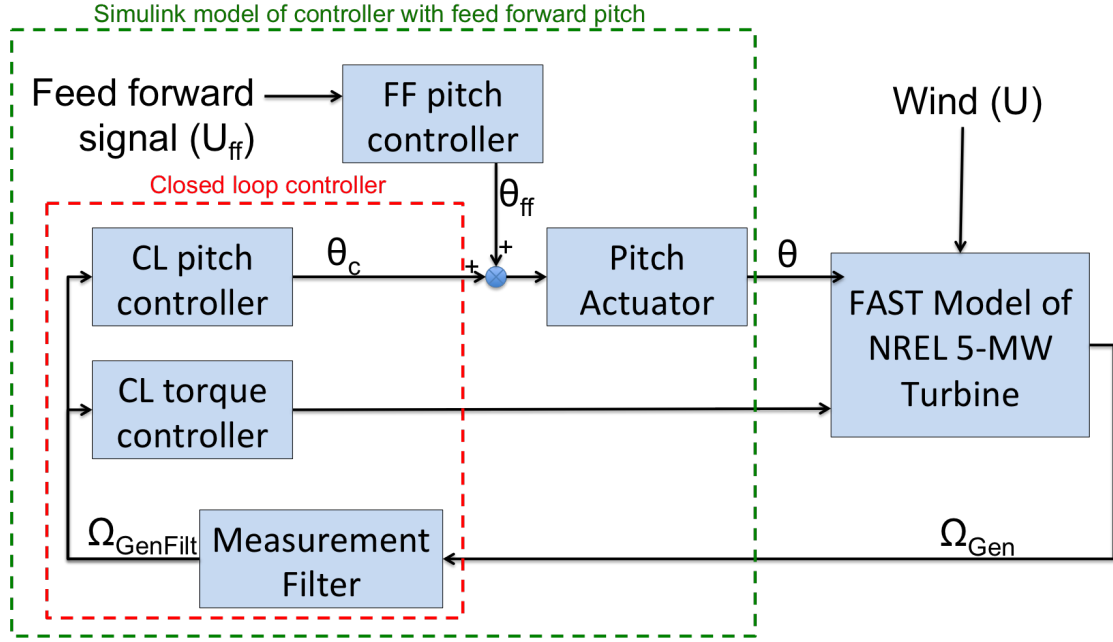
FIGURE 3.10: Controller with feed forward and closed loop control.

is a pitch angle (θ) that will cause an aerodynamic torque on the rotor that perfectly matches the torque applied to the rotor by the generator. We'll call this pitch angle the steady state pitch (θ_{ss}). Though the steady state pitch can't be calculated it can estimated through simulation. The relationship between steady state pitch and wind speed is shown in Figure 3.11.
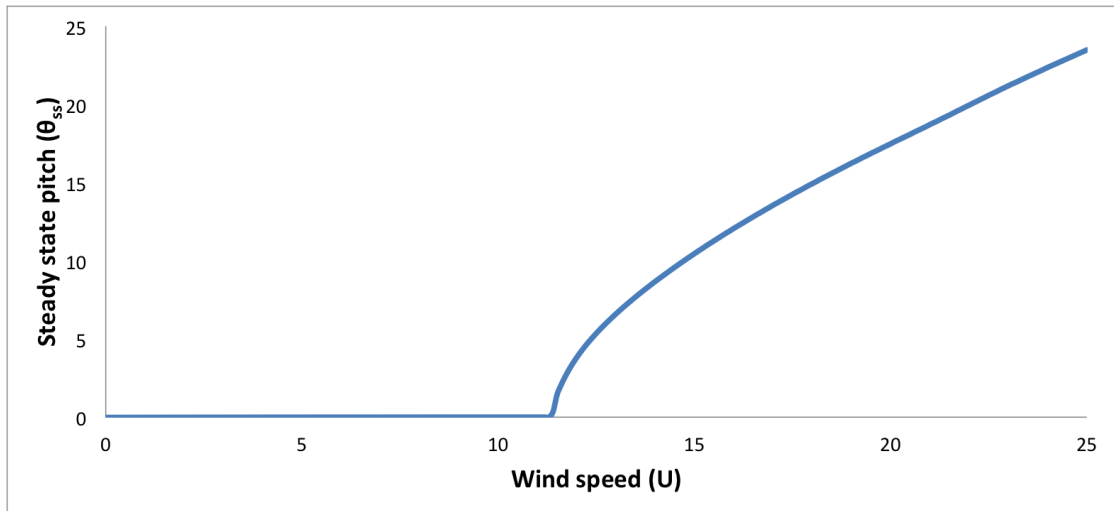
FIGURE 3.11: Steady state pitch (θ_s) as a function of incoming wind speed.

If the collective blade pitch of the turbine (θ) allways matches the steady state pitch (θ_{ss}) for the incoming wind speed (U) then the turbine will never deviate from the rated rotor speed of 12.1 RPM. If the feed forward signal U_{ff} is an accurate estimate of the

incoming wind speed (U) then it is possible to design a feed forward controller that causes the collective blade pitch to allways match the corresponding steady state pitch. Since all pitch commands pass through the pitch actuators we can only ensure the correct feed forward pitch signal if we first pass the feed forward signal U_{ff} through a function that inverts the dynamics of the blade pitch actuator. Therefore, the pitch commands supplied by the feed forward pitch controller (θ_{ff}) is given by the equations 3.2 and 3.3. θ_{ss} is the steady state pitch function that was experimentally determined and is illustrated in Figure 3.11. U_{ffd} is the dynamic feed forward velocity, which accounts for and cancels out the dynamics of the pitch actuator.

$$\theta_{ff} = \theta_{ss}(U_{ffd}) \tag{3.2}$$

$$U_{ffd} = (\ddot{U} + 2\xi\omega_o\dot{U} + \omega_o^2 U)/\omega_o^2 \tag{3.3}$$

If the feed forward wind speed estimate U_{ff} is perfectly accurate then the feed forward signal generated using equations 3.2 and 3.2 will completely compensate for fluctuations in wind speed and the closed loop controller will never issue a pitch command. However, we know that in practice U_{ff} will not be a perfect estimate of incoming wind speed and the closed loop controller will act whenever the feed forward pitch controller does not perfectly compensate for fluctuations in wind speed.

3.4   Performance With Perfect Wind Speed Knowledge

Now that the feed forward control system has been defined the performance of this feed forward control system can be examined. In the following sections we examine the performance of the feed forward controller when it has perfect knowledge of the incoming wind speed. Two wind cases are examined. The first case is a large gust. These occur infrequently, but can be very damaging to a turbine. The second case is a turbulent wind inflow, which is typical of what a turbine experiences in day to day operation. in In any real world implementation of this control system the feed forward controller will have imperfect knowledge of the incoming wind. As discussed in Chapter 2, a wind speed estimator provides imperfect estimates of both the wind speed (see Section 2.4.1) and convection velocity (see Section 2.5). In addition, we know that Taylor's frozen turbulence hypothesis is not entirely accurate in practice and the wind speed fluctuations experienced by the downwind turbine will not be identical to the wind speed fluctuations experienced by the upwind turbine. However, simulating

the feed forward control system with perfect knowledge of the incoming wind speed can provide valuable insight into the behavior of the feed forward control system, and can demonstrate the performance improvements that might be possible when the feed forward controller described in Section 3.3 is operated in ideal conditions.

3.4.1   Gust Response

Figure 3.12 shows an extreme operating gust for an NREL 5-MW turbine operating in 16 m/s wind according to IEC 61400-1 [36]. Though extreme operating gusts occur infrequently, they can be very damaging to a wind turbine when they do occur. To examine the system's response to this extreme operating gust, both the upwind turbine and downwind turbine are subjected to a uniform wind inflow (i.e. the wind has no turbulence and all points on the turbine rotor are subjected to the same wind speed) with the magnitude shown in Figure 3.12. Since we are assuming the feed forward controller has perfect knowledge of the incoming wind speed, the wind speed information in Figure 3.12 is also used as the feed forward wind speed estimate.
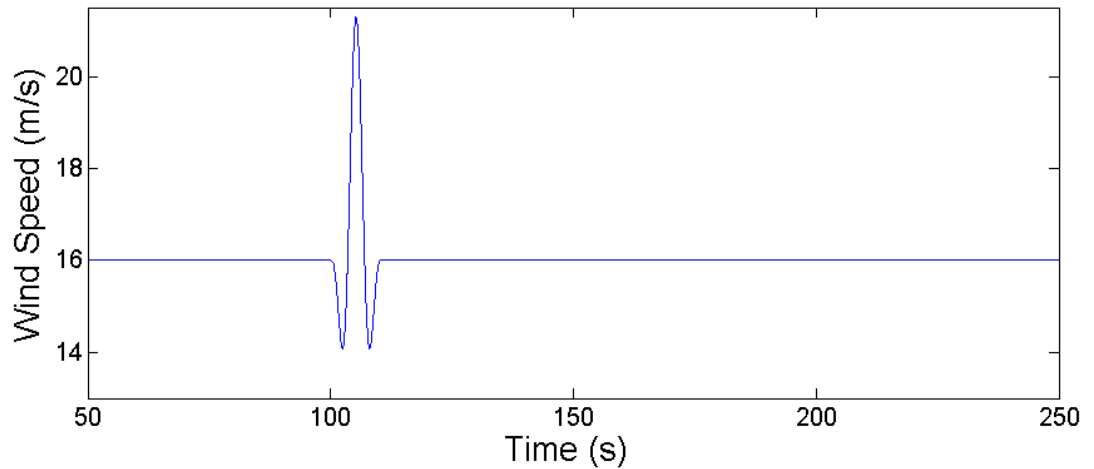
FIGURE 3.12: Extreme operating gust.

Figures 3.13 through 3.17 illustrate how the upwind and downwind turbines respond to the 16 m/s extreme operating gust, while Table 3.1 is a summary of some of the performance metrics that will be discussed in the following paragraph. By comparing the response of the upwind turbine, which does not have feed forward pitch control, to the response of the downwind turbine, which does have feed forward pith control, we can see how feed forward pitch control affects turbine performance.

In Figure 3.13 we see that the turbine with feed forward pitch control (the downwind turbine) responds to the gust sooner than the turbine without feed forward control (the

upwind turbine). This is unsurprising. As discussed in Section 3.1, a turbine using only closed loop control will respond reactively to changes in turbine behavior, which are caused by changes in wind speed. On the other hand, a turbine with feed forward control can respond to changes in wind speed before they affect turbine behavior. In fact, a perfect feed forward controller would prevent the wind speed changes from affecting turbine behavior at all. We can also see in Figure 3.13 that the turbine with feed forward control has higher maximum pitch angle when responding to the gust, and that the blade motion has less transient behavior after the gust passes.
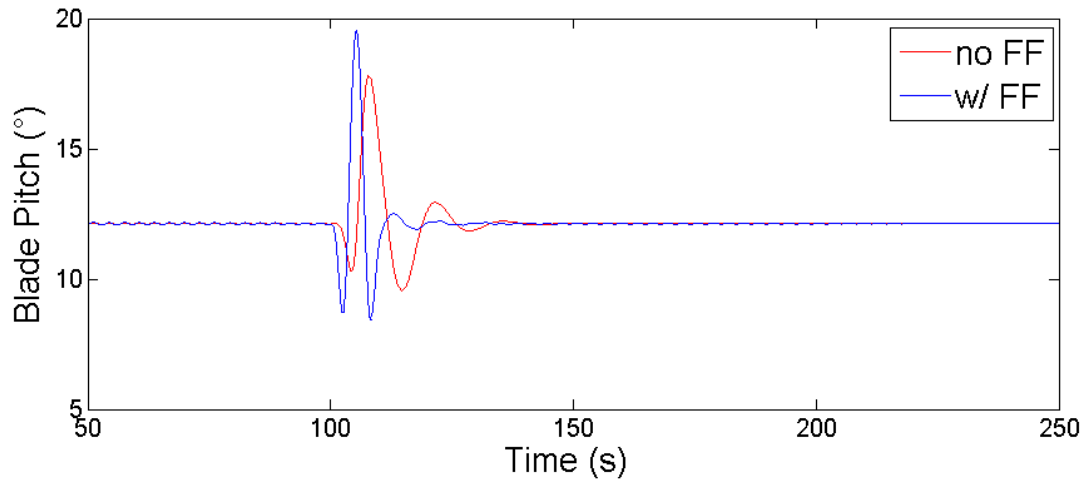
FIGURE 3.13: Blade pitch response to extreme operating gust.

Figure 3.14 shows that deviations from the rated rotor speed of 12 RPM are greatly reduced with feed forward control. The turbine with feed forward control has a maximum rotor speed of 12.07 RPM, which is only 0.6% over the rated speed. Without feed forward control, the rotor speed reaches a peak value of 14.15 RPM, which is 17.9% over the rated rotor speed. A 17.9% rotor over speed can be problematic as it may cause an emergency shut down of the turbine. According to Tobias Wehrhan of Oak Engineering LLC the threshold for an over speed shut down is usually 15-20% over the rated rotor speed, depending on the turbine (personal communication,March 19, 2015). Once an over speed shut down has been initiated, the turbine stops generating power until it can be safely restarted. This can lead to a significant loss of generated energy and therefore a loss of revenue for the turbine operator.

Figure 3.15 shows that deviations from the rated power are greatly reduced with feed forward control. It is desirable to limit spikes in power. Power spikes can cause an emergency shut down of the turbine if it drives the DC-bus voltage above safe levels, which is typically 15-18% above the nominal DC-bus voltage (Tobias Wehrhan, personal communication,March 19, 2015). FAST does not model the DC-bus voltage, so these
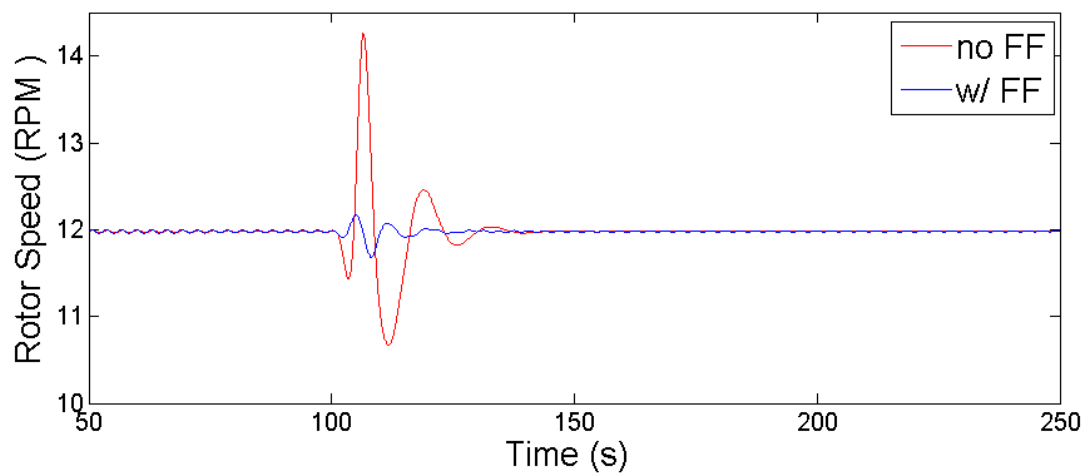
FIGURE 3.14: Rotor speed for turbine subjected to extreme operating gust.

results don't show how close the turbine without feed forward control comes to triggering an over voltage shut-down. Table 3.1 shows the total energy generated in each simulation. We see that the performance improvemments from feed forward control are achieved without a cost to energy generation. The turbine with feed forward control actually generates slightly more power than the turbine without feed forward control.
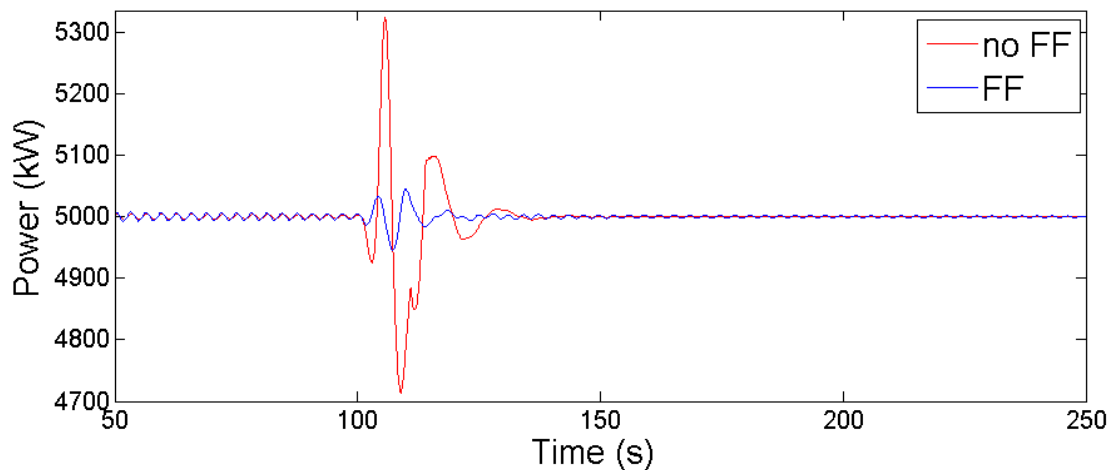
FIGURE 3.15: Power generation for turbine subjected to extreme operating gust.

Excessive structural loading can cause turbine components to immediately fail, or can cause excessive wear and tear that shortens the life of turbine components. When turbine components fail the turbine must be shut down and repaired. If we can reduce the frequency of shut downs and repairs we can increase the revenue (by increasing energy generation) and decrease the cost to the turbine operator. There are many turbine components that can experience damage from gust loading. In this section we

have chosen to examine two loads, the fore-aft bending moment at the base of the tower (Figure 3.16) and bending moment at the root of one of the turbine blades (Figure 3.17).We see similar behavior in both Figures. The turbine with feed forward control experiences lower loads during the extreme operating gust, while experiencing nearly identical loads at all other times. The feed forward controller reduces the maximum tower bending moment from 100,030 kNm to 50,900 kNm, a reduction of nearly 50%, and reduces the aximum blade root moment from 11,617 kNm to 7,351 kNm, a reduction of 37%.
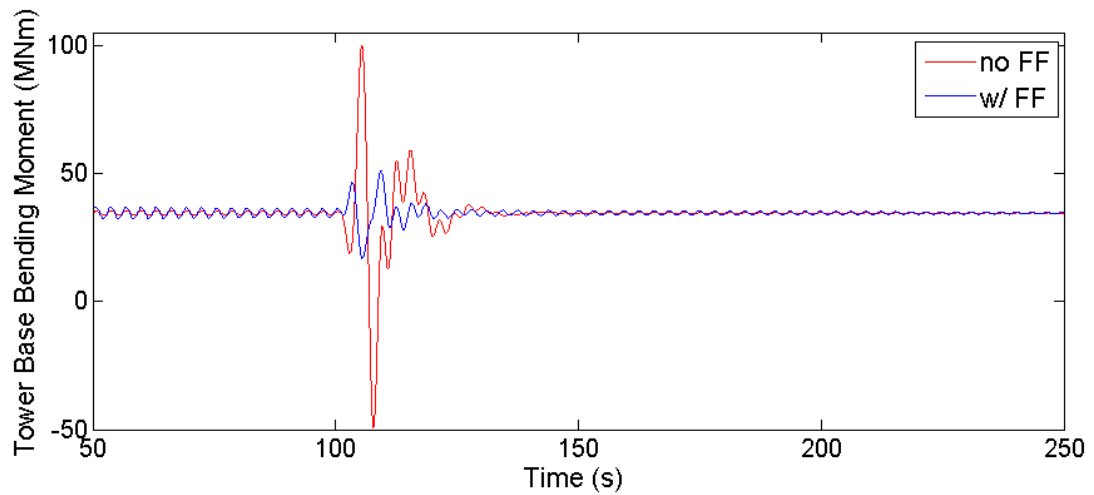
FIGURE 3.16: Tower base fore-aft moment for turbine subjected to extreme operating gust.
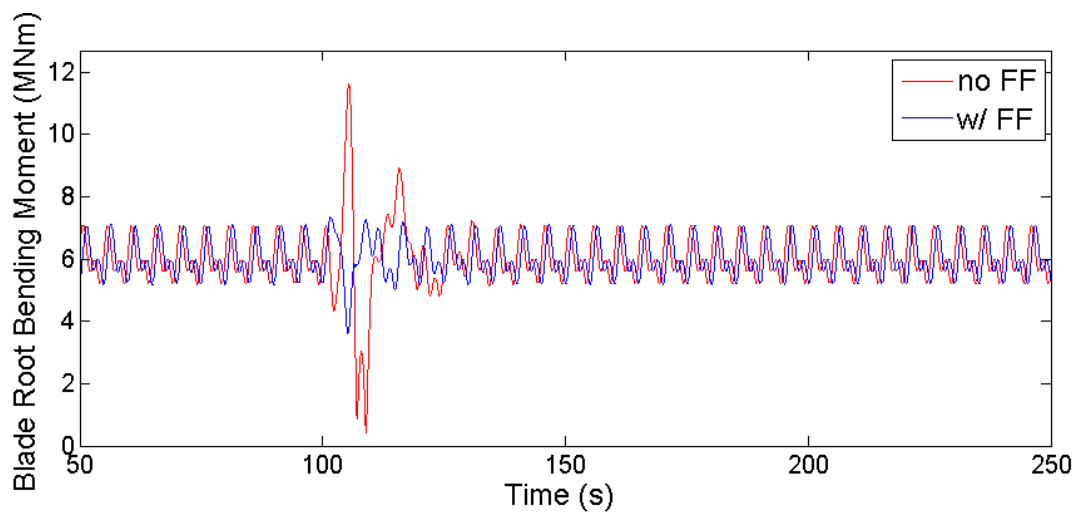
FIGURE 3.17: Blade root bending moment for turbine subjected to extreme operating gust.

Table 3.1 summarizes the performance metrics that have been discussed in this subsection. We see that feed forward control has significantly reduced structural loading of the

TABLE 3.1: Extreme operating gust response with perfect wind speed knowledge.

Turbine Control	Max tower base bending moment (MNm)	Max blade root bending moment (MNm)	Max rotor over speed (%)	Energy generated (kW hr)
Closed loop	100.00	11.62	17.9	831.74
Closed loop with feed forward	50.90	7.35	0.6	831.75

turbine without decreasing energy generation. This can potentially lead to a reduction in the repair and maintenance costs of the turbine without a reduction in revenue from the turbine. The turbine without feed forward control experienced a 17.9% rotor over speed, which may be enough to induce an emergency shutdown of the turbine. Over speed shut down faults are not modeled in theses simulations, but if the turbine without feed forward control experienced an over speed shut down then it would generate significantly less energy than the turbine with feed forward control. In that scenario the turbine with feed forward control would have lower repair and maintenance costs while having higher revenue from energy generation.

3.4.2 Turbulent Wind Response

In this subsection we examine how our two turbine system reacts to turbulent wind. Like the previous subsection both the upwind turbine and downwind turbine are subjected to the same wind speed fluctuations. The downwind turbine is equipped with the feed forward controller described in Subsection 3.3.3 and is assumed to have perfect knowledge of the incoming wind. The feed forward controller relies on knowledge of the incoming wind speed and the derivatives of the incoming wind speed. However, in a turbulent wind field the wind speed is not constant over the swept area of the rotor so there is no single measurement that can be considered the true incoming wind speed. In this subsection we will treat the average wind speed over the swept area of the rotor as the wind speed. Because this rotor average wind speed has some high frequency fluctuations it is passed through a single pole low-pass filter with a corner frequency of 0.5 Hz to generate the feed forward wind speed.

Figure 3.18 shows the rotor average wind speed and feed forward wind speed for 200 seconds of the turbulent wind field used in this subsection. The complete wind field is 600 seconds long and was generated by TurbSim using a 16 m/s mean wind speed and the GPLLJ turbulence model. This was one of the 66 test cases used in Chapter 2

and more details about this test case can be found in Section 2.2. Figures 3.19 through 3.20 illustrate how the upwind and downwind turbines respond to the turbulent wind field. All figures in this subsection have the same axes as the corresponding figures in Subsection 3.4.1. This helps illustrate the differences in magnitude between the wind turbine response to an extreme operating gust and the wind turbine response to a turbulent wind field with the same mean wind speed.
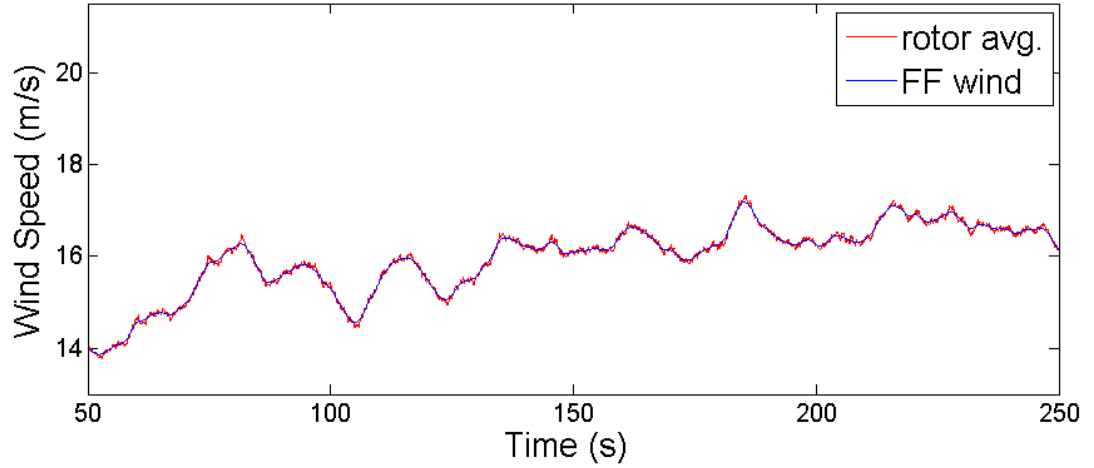
FIGURE 3.18: Rotor average wind speed and feed forward wind speed for 16m/s turbulent wind.

In Figure 3.19 we see the blade pitch response of each turbine. We see that the blade pitch response of each turbine follows a similar pattern of peaks and valleys. However, for the turbine with feed forward pitch control the peaks and valleys occurs a few seconds earlier. This is expected because both turbines are reacting to the same fluctuations in wind speed but the turbine with feed forward control can react to those wind speed fluctuations before they affect turbine behavior.

Figures 3.20 and 3.21 show that the feed forward controller reduces deviations in both rotor speed and power. With feed forward control the rotor speed stays within ???% of the rated rotor speed and the power stays within ???% of the rated power. Without feed forward control the rotor speed deviates as much as ???% from the rated speed and the power deviates as much as ???% from the rated power. Though the turbine with feed forward control performs better than the turbine without feed forward control it is important to note that neither turbine has a spike in rotor speed or power that could trigger an emergency shut down.

Figures 3.22 and 3.23 show the tower fore-aft bending moment and the blade root bending moment. In the previous subsection, when we examined the turbines' responses to an extreme operating gust, it was immediately obvious that feed forward control
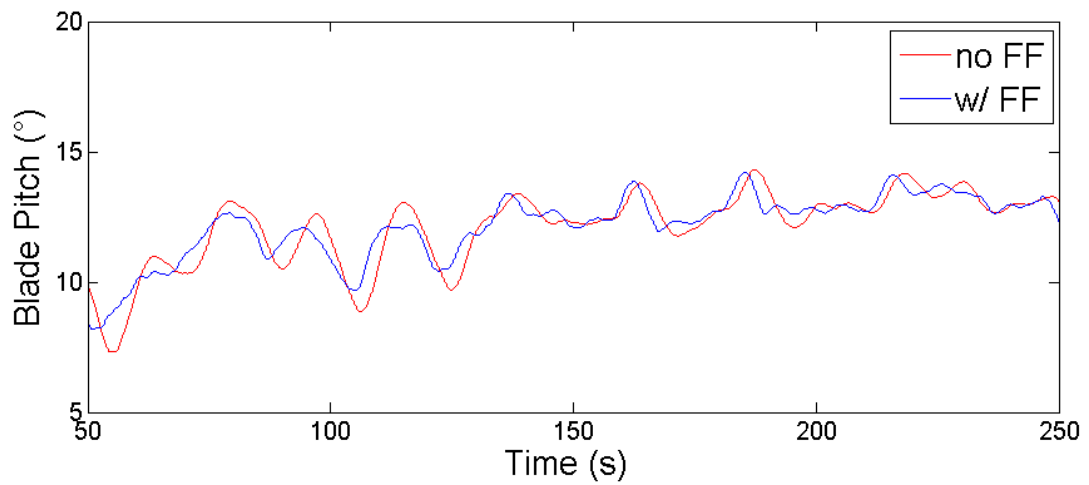
FIGURE 3.19: Blade pitch response to 16m/s turbulent wind.
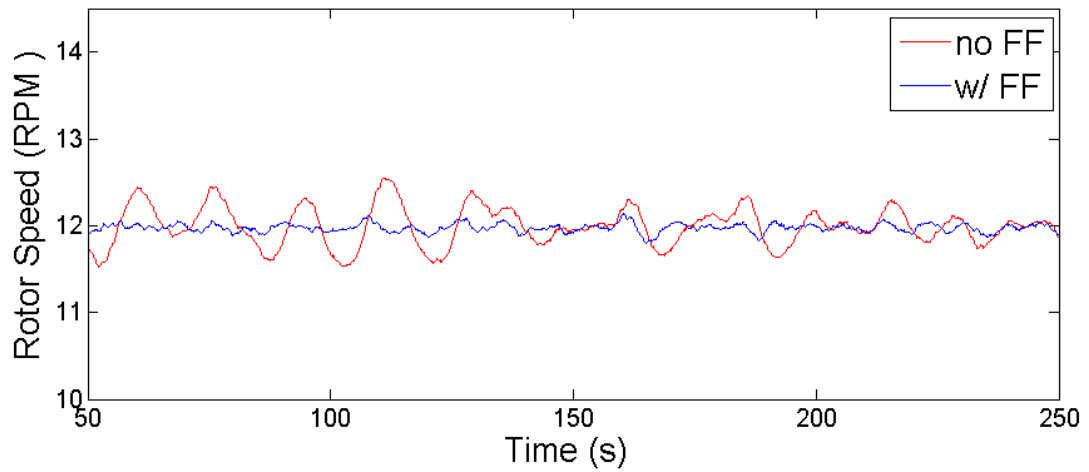
FIGURE 3.20: Rotor speed for turbine in 16m/s turbulent wind.

significantly reduced loads. In figures 3.22 and 3.23 it is not obvious that feed forward control is reducing loads. Though there are many moments in the simulation when feed forward control reduces loading, there are also many times when feed forward control causes higher loading. To determine which control system has better performance we must statistically analyze the loading.

In the previous subsection we analyzed loading by measuring and comparing the maximum loads experienced by the turbines. For these simulation results comparing the maximum loads doesn't make sense. In the previous subsection the turbine experienced a single large spike in loading when the extreme operating gust hit the turbines. In this subsection the turbine experiences many loading cycles that all have similar amplitudes.
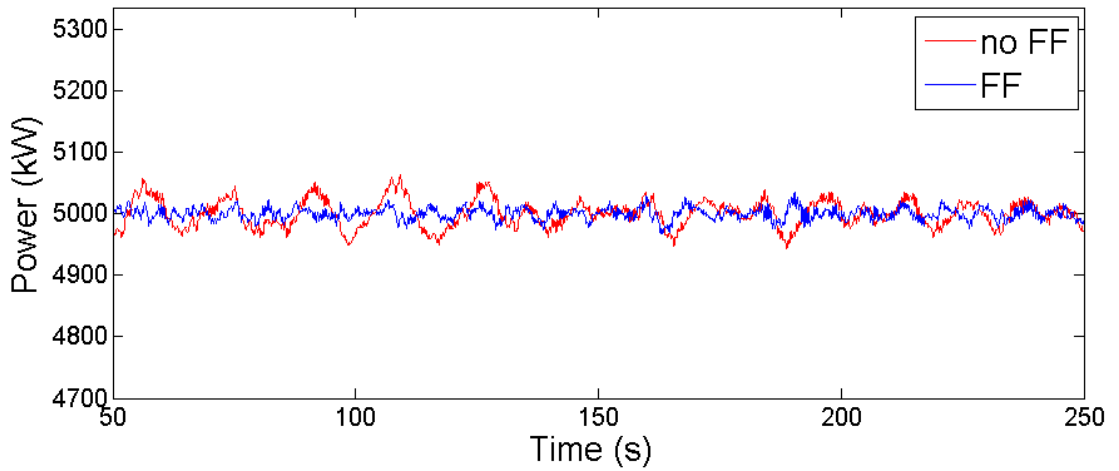
FIGURE 3.21: Power generation for turbine in 16m/s turbulent wind.
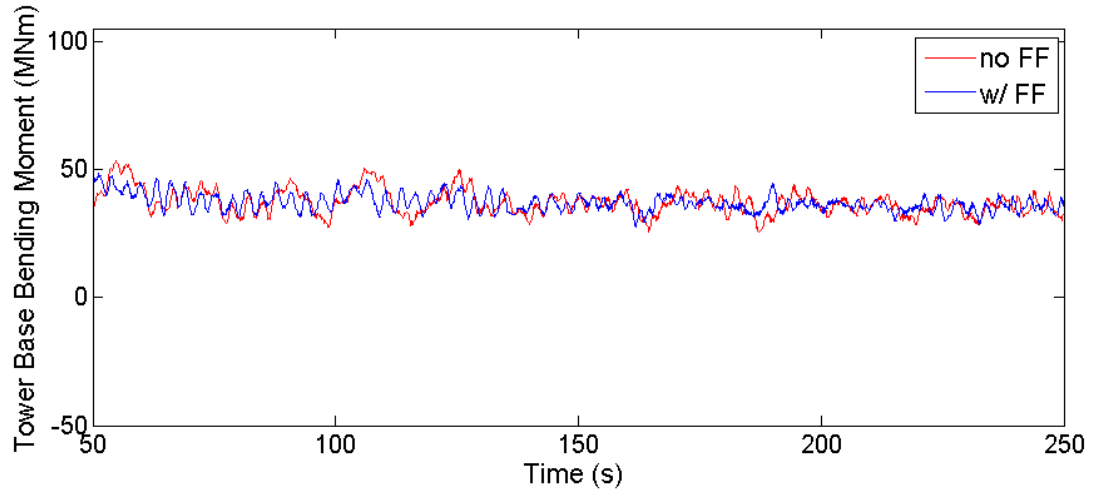
FIGURE 3.22: Tower base fore-aft moment for turbine in 16m/s turbulent wind.

Table 3.2 shows the mean and standard deviation of several turbine performance metrics. We see that feed forward control does not affect the mean values, but does decrease the variability of the performance metrics. Feed forward control reduces the standard deviation of the Power by more than 50%.

Reduced variability in power generation can be beneficial for grid integration of wind turbines. The standard deviation of the tower base bending moment and the blade root bending moment are reduces by 26% and 2% respectively.

Though a reduction in the standard deviation of the structural loads is noteworthy, it is more important to understand how the changes in structural loads will affect the wear and tear on turbine components. To estimate the wear and tear inflicted on the tower base and the blade root we can calculate the short term damage equivalent loads
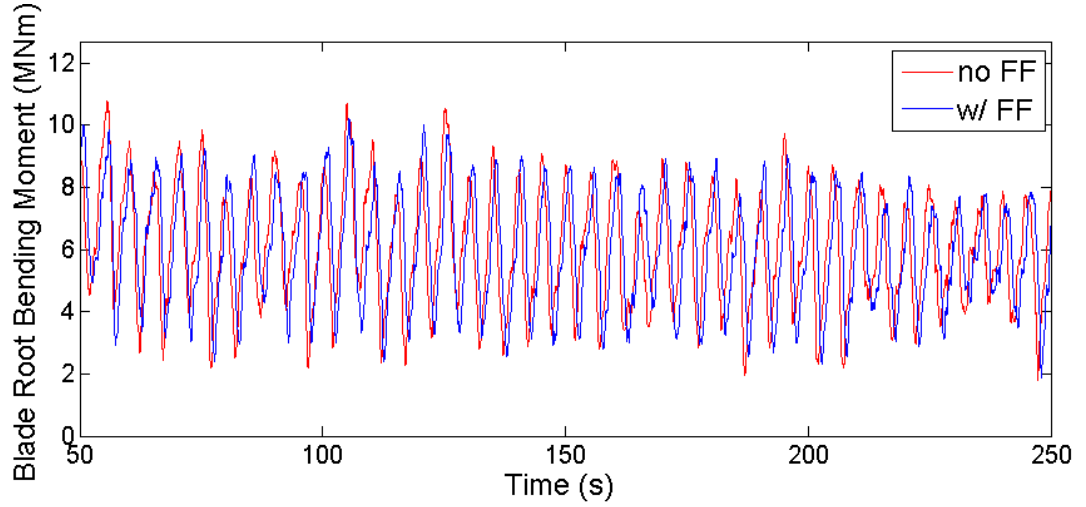
FIGURE 3.23: Blade root bending moment for turbine in 16m/s turbulent wind.

TABLE 3.2: Statistical summary of turbine performance in 16m/s wind.

Turbine Control	Tower base bending moment (MNm)		Blade root bending moment (MNm)		Rotor speed (RPM)		Power (kW)	
	mean	σ	mean	σ	mean	σ	mean	σ
Closed loop	36.60	4.64	5.96	1.84	12.0	0.212	5,000	21.8
Closed loop with feed forward	36.60	3.42	5.95	1.80	12.0	0.0547	5,000	10.7

(DEL). An explanation of damage equivalent loads and how they were calculated in this dissertation can be found in Appendix B.

Table shows that for this 10 minute simulation of 16m/s turbulent wind feed forward control reduces the damage equivalent loads for both tower base bending moment and blade root bending moment. This indicates that the turbine with feed forward control experiences less wear and tear on it's components, which may lead to less repair and maintenance costs over the life of the turbine.

3.5 Performance With Wind Speed Estimate From Upwind Turbine

The previous sections demonstrated how the feed forward pitch controller affects performance when it has perfect knowledge of the incoming wind. However, in practice

TABLE 3.3: Short term damage equivalent loads for 570s simulation of turbine in 16m/s turbulent wind.

Turbine Control	Tower base bending moment		Blade root bending moment	
	DEL (MNm)	Change in DEL	DEL (MNm)	Change in DEL
Closed loop	44.20	-	10.58	-
Closed loop with feed forward	35.60	-19.5%	10.02	-5.3%

the feed forward controller will not have perfect knowledge of the incoming wind. The feed forward controller will have an estimate of the incoming wind that is generated by using the upwind turbine as a sensor. In the following subsections we examine the performance of the feed forward controller when it has only an estimate of the incoming wind speed. The incoming wind speed estimate is based on the dynamic behavior of the upwind turbine and is generated using the process described in Section 2.4. The simulations described below assume Taylor's frozen turbulence, and assume that we will be able to perfectly determine the convection velocity. We know that neither of those assumptions will be entirely accurate in practice, but the simulations described in this section bring us a step closer to a realistic implementation of feed forward pitch control than the simulations described in the previous section.

3.5.1   Gust Response

Figure 3.24 shows an extreme operating gust for an NREL 5-MW turbine operating in 16 m/s wind according to IEC 61400-1 [36] and the feed forward wind speed estimate generated by the upwind turbine. This is the same extreme operating gust simulated in Section 3.4.1. The feed forward wind speed estimate does not perfectly capture the fluctuations in wind speed. In particular, the feed forward wind speed estimate has smaller peaks and valleys and contains some transient behavior after the extreme operating gust has passed.

Figure 3.25 shows the pitch response of the turbines. As we saw in previous simulations, the turbine with feed forward pitch control reacts to the extreme operating gust sooner than the turbine without feed forward pitch control. One noteworthy feature is the large dip in blade pitch for the turbine with feed forward pitch control. The blade pitch briefly drops to 5.4° at approximately 110 seconds. This is potentially dangerous behavior for the turbine with feed forward pitch control. For a given wind speed, decreasing the
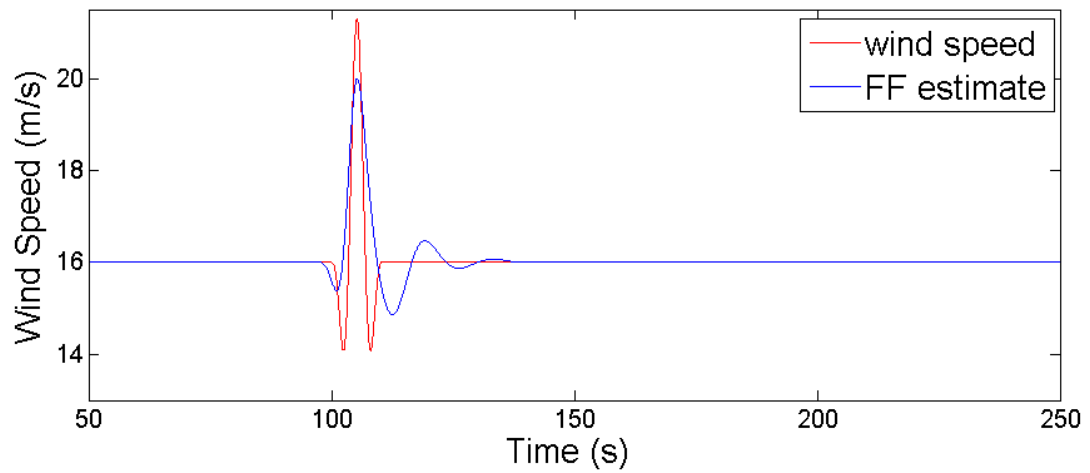
FIGURE 3.24: Extreme operating gust and feed forward wind speed estimate based on gust.

blade pitch results in an increase in the wind energy captured by the rotor. This leads to increased structural loads and increased rotor speed. If the blade pitch suddenly drops too low, as may be the case here, it can potentially lead to spikes in structural loads or rotor speed.
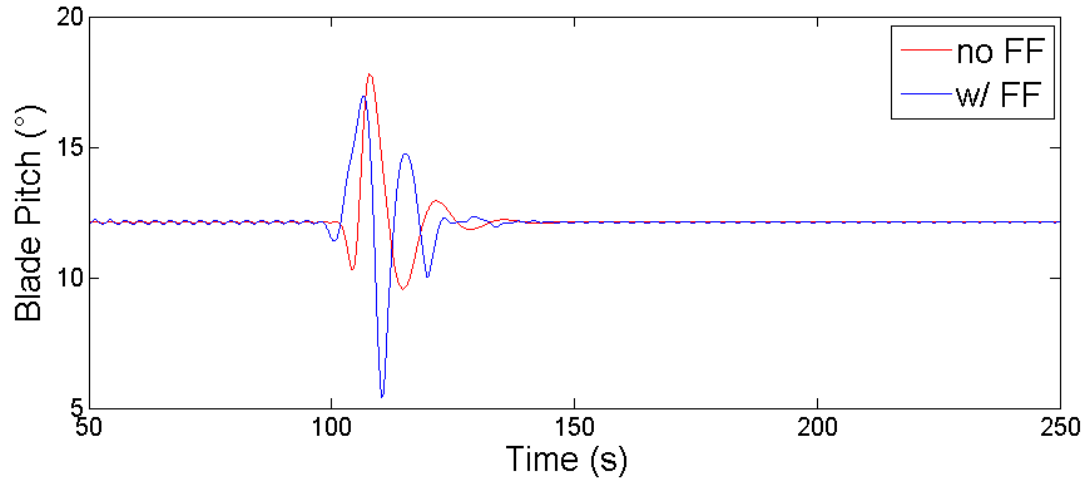
FIGURE 3.25: Blade pitch response to extreme operating gust.

Figure 3.26 shows that feed forward control significantly reduces deviations from the rated rotor speed of 12 RPM. The turbine without feed forward pitch control has a maximum rotor speed 17.9% above the rated speed. As discussed before, an overspeed of this magnitude could cause an emergency shutdown of the turbine. The turbine with feed forward pitch control has a maximum rotor speed 5.5% above the rated speed. For the turbine without feed forward control the maximum rotor speed occurs immediately

after the peak of the extreme operating gust. The turbine with feed forward pitch control also has a rotor overspeed immediately after the peak of the extreme operating gust, but the maximum rotor speed occurs approximately 10 seconds later, immediately after the sudden dip in blade pitch that was observed in Figure 3.25. This suggests that the larges rotor overspeed experienced turbine with feed forward pitch control was caused by the control action of the feed forward controller and not by the extreme operating gust.
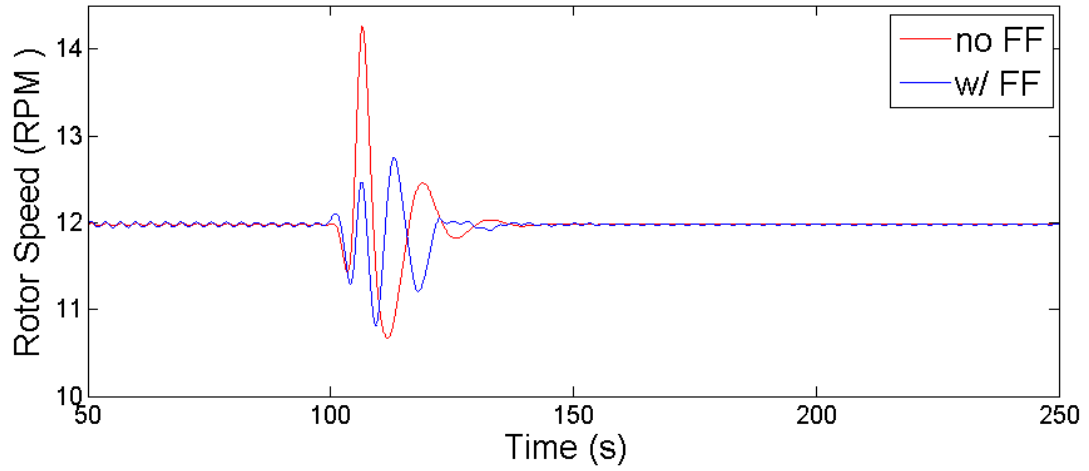
FIGURE 3.26: Rotor speed for turbine subjected to extreme operating gust.

In the remaining figures we see similar behavior to what we see in Figure 3.27. Feed forward pitch control improves performance by reducing deviations from rated power (Figure 3.27), maximum tower fore-aft bending moments (Figure 3.28), and maximum blade root bending moments (Figure 3.29). The turbine with feed forward pitch control experiences a peak in power production and structural loads immediately after the peak of the extreme operating gust. The turbine with feed forward pitch control then experiences an even larger peak in power production and structural loads immediately after the sudden dip in blade pitch that was observed in Figure 3.25.

Table 3.4 summarizes the performance metrics for this simulation. We see that feed forward pitch control reduces structural loading of the turbine and deviations from the rated rotor speed. The use of feed forward pitch control does decrease power generation by 0.54 kW-hours, but this is a very small decrease. If the wind plant sells energy for 8 cents per kW-hour the use of feed forward pitch control would result in a 4 cent decrease in revenue. Though feed forward pitch control does improve the turbine performance in this simulation, it is also worth noting that the feed forward pitch controller used in this simulation does not perform as well as a feed forward pitch controller with perfect knowledge of incoming wind speed (Table 3.1).
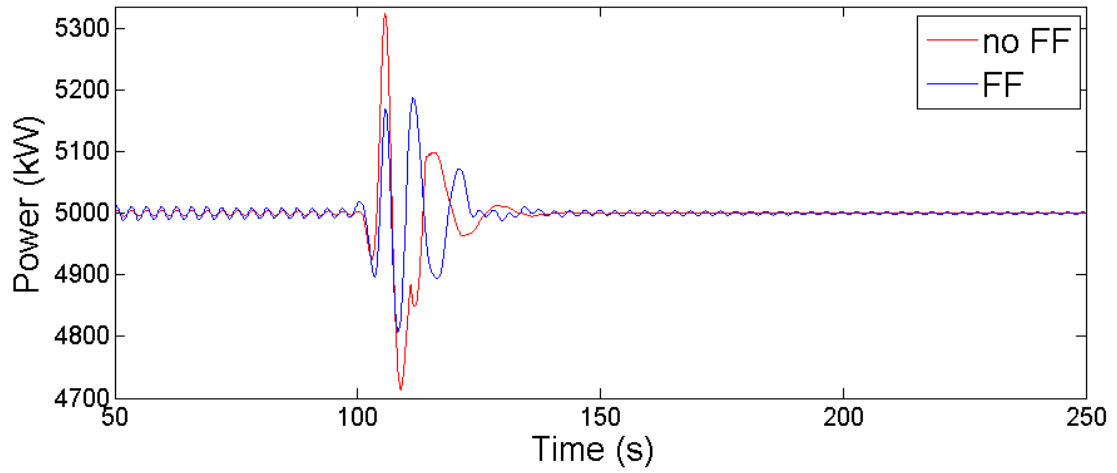
FIGURE 3.27: Power generation for turbine subjected to extreme operating gust.
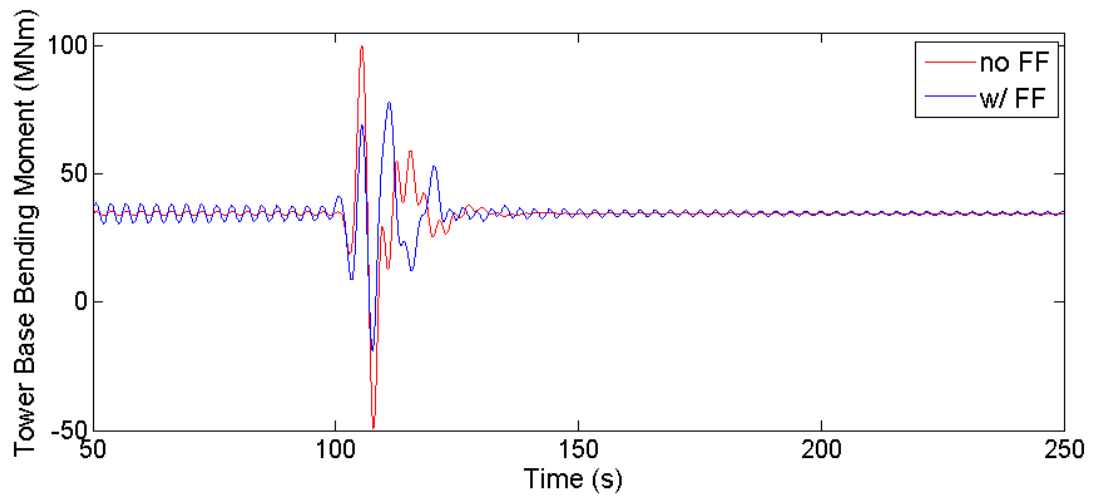
FIGURE 3.28: Tower base fore-aft moment for turbine subjected to extreme operating gust.

TABLE 3.4: EOG response with feed forward signal based on wind speed estimate.

Turbine Control	Max tower base bending moment (MNm)	Max blade root bending moment (MNm)	Max rotor over speed (%)	Energy generated (kW hr)
Closed loop	100.03	11.62	17.9	831.74
Closed loop with feed forward	77.70	10.51	5.5	831.20
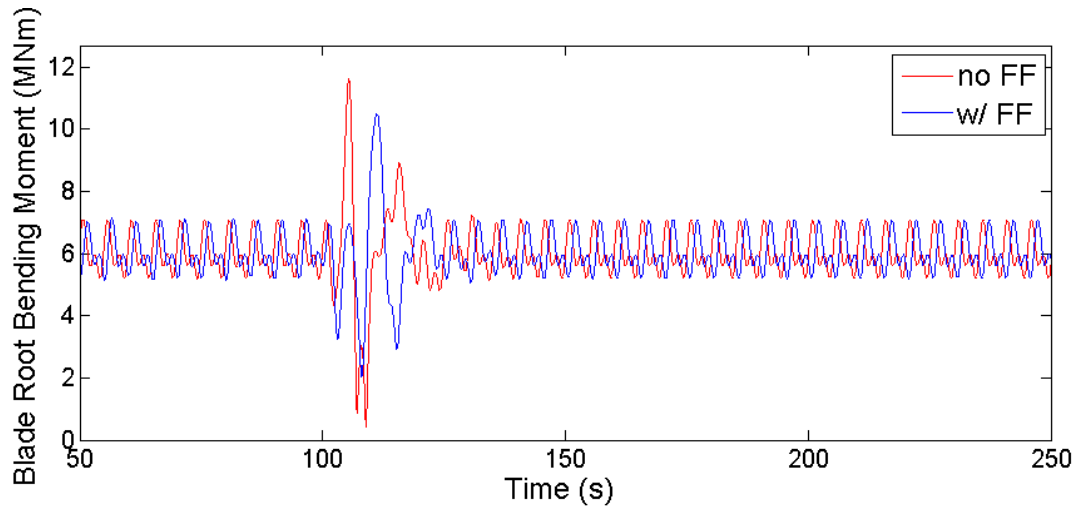
FIGURE 3.29: Blade root bending moment for turbine subjected to extreme operating gust.

3.5.2 Turbulent Wind Response

Figure 3.30 shows the rotor average wind speed and feed forward wind speed for 200 seconds of the turbulent wind field used in this subsection. This subsection uses the same turbulent wind field used in Subsection 3.4.2. Though the feed forward wind speed, estimated through the rotor dynamics of the upwind turbine, does not perfectly match the rotor average wind speed, it does capture most of the peaks and valleys of the wind speed fluctuations.
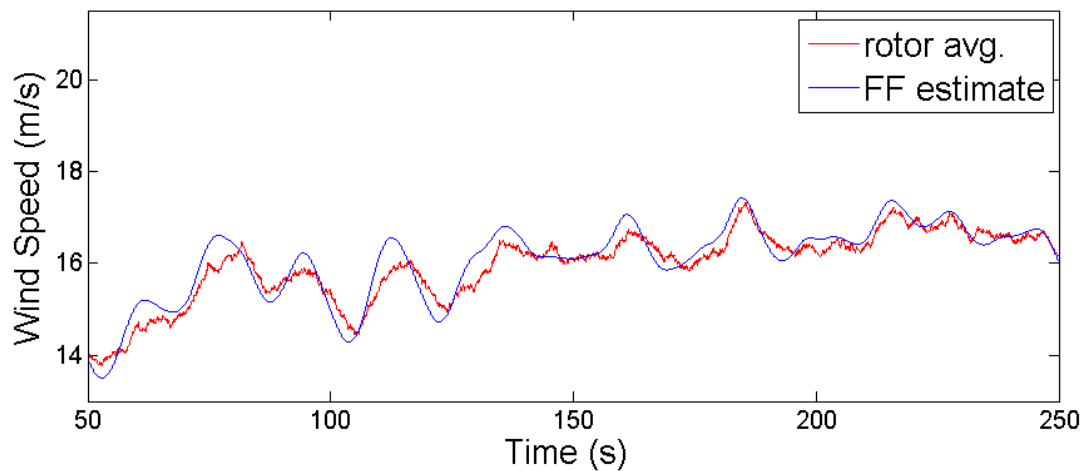
FIGURE 3.30: Rotor average wind speed and feed forward wind speed estimate of turbulent 16m/s wind.

Figures 3.31 through 3.35 show the dynamic behaviour of a turbine with and without feed forward pitch control. We see in these figures that feed forward control reduces

deviations in blade pitch (Figure 3.31), rotor speed (Figure 3.32), and power production (Figure 3.33). However, feed forward control does not reduce these deviations as much as we saw when the feed forward wind speed was the true rotor average wind speed (Subsection 3.4.2).
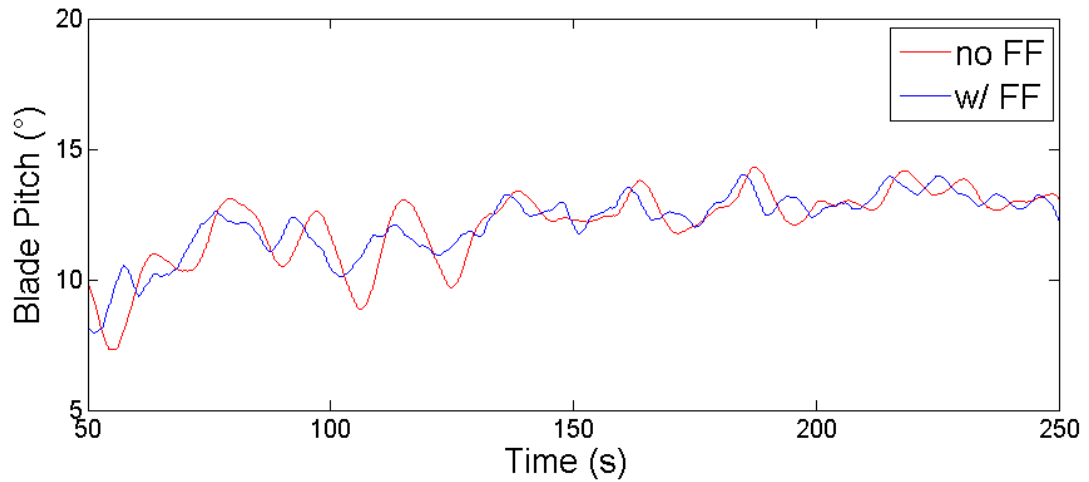
FIGURE 3.31: Blade pitch response to 16m/s turbulent wind.
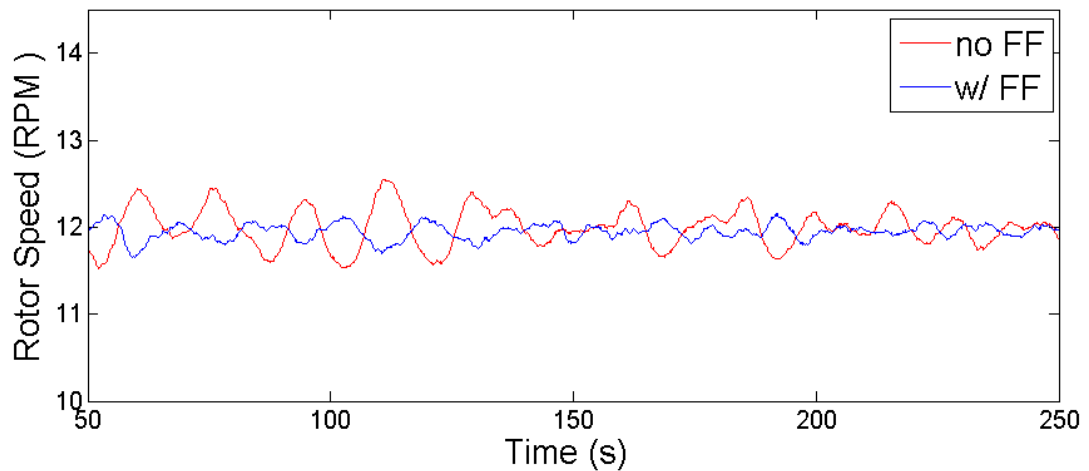
FIGURE 3.32: Rotor speed for turbine in 16m/s turbulent wind.

In Figures 3.34 and 3.35 it is difficult to determine how feed forward control affects the structural loading of the turbine components. However, Table 3.6 shows that feed forward control does in fact reduce the damage equivalent loads of the tower base bending moment (11.8% reduction) and the blade root bending moment (5.7% reduction).Note that these reductions in damage equivalent loads are not as large as the reductions observed when the feed forward wind speed was the true rotor average wind speed (Subsection 3.4.2).
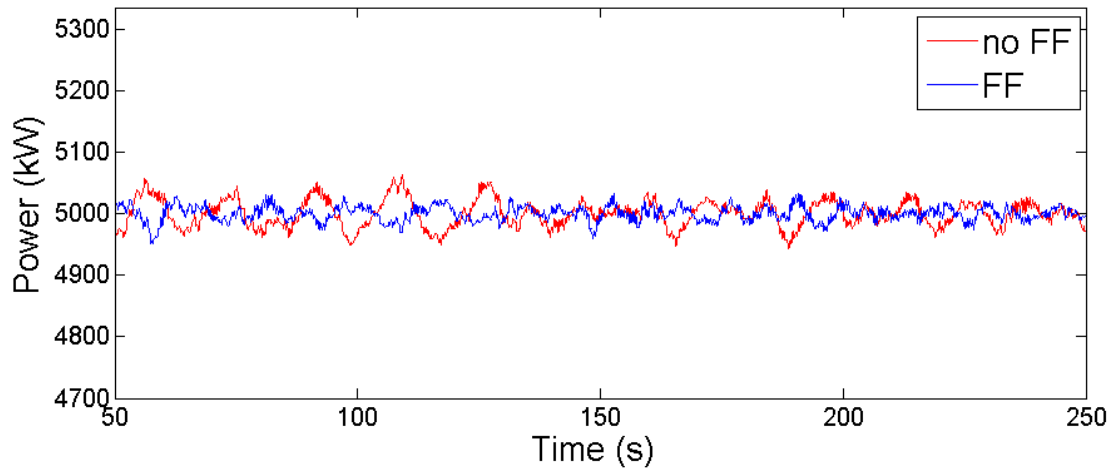
FIGURE 3.33: Power generation for turbine in 16m/s turbulent wind.
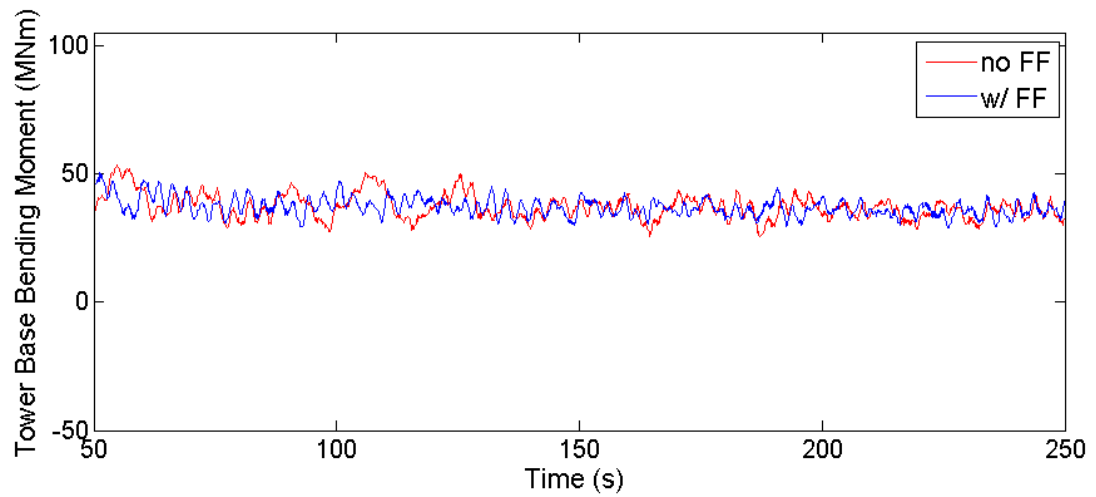
FIGURE 3.34: Tower base fore-aft moment for turbine in 16m/s turbulent wind.

TABLE 3.5: Statistical summary of turbine performance in 16m/s wind.

Turbine Control	Tower base bending moment (MNm)		Blade root bending moment (MNm)		Rotor speed (RPM)		Power (kW)	
	mean	σ	mean	σ	mean	σ	mean	σ
Closed loop	36.60	4.64	5.96	1.84	12.0	0.212	5,000	21.8
Closed loop with feed forward	36.50	3.60	5.95	1.79	12.0	0.081	5,000	12.0
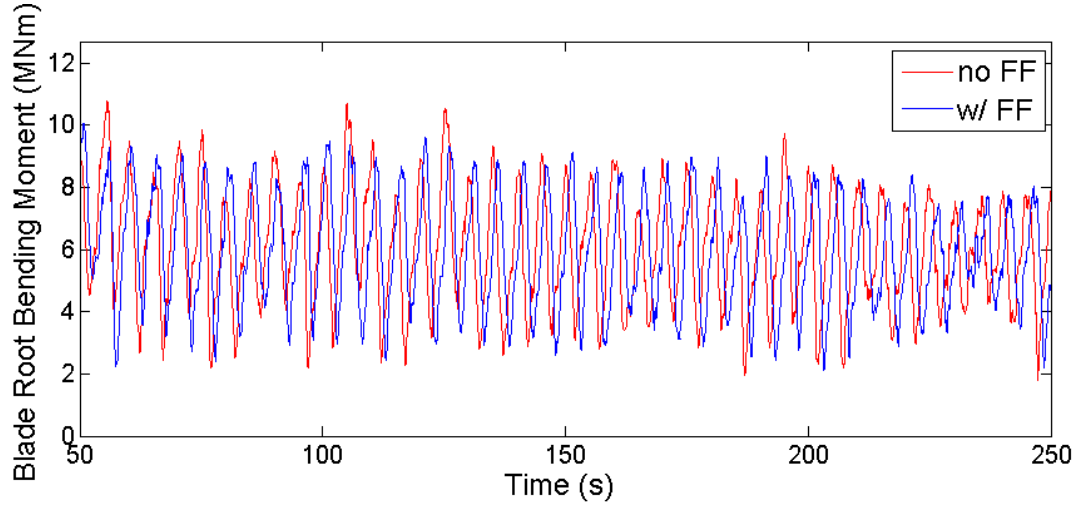
FIGURE 3.35: Blade root bending moment for turbine in 16m/s turbulent wind.

TABLE 3.6: Short term damage equivalent loads for 570s simulation of turbine in 16m/s turbulent wind.

Turbine Control	Tower base bending moment		Blade root bending moment	
	DEL (MNm)	Change in DEL	DEL (MNm)	Change in DEL
Closed loop	44.20	-	10.58	-
Closed loop with feed forward	39.00	-11.8%	9.98	-5.7%

3.6 Sensitivity to Errors in Feed Forward Data Timing

In the previous section we observed that feed forward pitch control based on wind speed estimates from an upwind turbine can improve performance and reduce structural loading provided Taylor's frozen turbulence holds and we are able to perfectly estimate the convection speed of the wind. However, experiments have shown that Taylor's frozen turbulence hypothesis is never completely accurate and it is impossible to perfectly estimate the convection velocity. In this section we bring our system one step closer to reality by considering the effect of errors in the convection velocity estimate.

In Section 2.5 we discussed a method fo estimating the convection velocity by calculating the mean wind speed estimate over some period of time. For the 66 test cases examined in Section 2.5 we found that the accuracy of the convection velocity estimate varied with both the true mean wind speed, and the time period over which the wind speed estimates were averaged. For wind speeds above the rated wind speed (the conditions

we are considering for feed forward pitch control) the mean discrepancy between the true and estimated convection velocity ranged from 2% to 4%.

By making a few reasonable assumptions about our system, we can get a rough estimate of the convection velocity error we might expect for the 16 m/s turbulent wind field our system was subjected to in sections 3.4.2 and 3.5.2. We can also determine how that convection velocity error would affect the timing of the feed forward wind speed estimates received by the downwind turbine. If we assume a 60 second averaging time, we might expect the error in our convection velocity estimate to average approximately 3.2% (Figure 3.26), or 0.5 m/s. If we assume the downwind turbine is 10 rotor diameters, or 1260 meters, behind the upwind turbine a 3.2% error in the convection velocity estimate will cause an error in the timing of the feed forward of approximately 2.5 seconds.

We can simulate the effect of an error in the convection velocity estimate by modifying the turbulent wind response simulation from Section 3.5.2. Instead of using perfectly timed feed forward wind speed estimates, the feed forward wind speed estimates is shifted in time. To determine how errors in the convection velocity estimate affect system performance we can calculate the resulting damage equivalent loads (DEL) on the tower bending moment and blade root moment.

Figure 3.36 illustrates how timing errors in the feed forward data affect the damage equivalent load of the tower fore-aft bending moment. A negative timing error indicates the feed forward data is ahead of the turbulent wind field. In other words, the system has overestimated the convection velocity and as a result the turbulent wind fluctuations are arriving at the downwind turbine later than the system expects them to.

The red line indicates the tower base DEL for the upwind turbine. Since the upwind turbine does not depend on feed forward data, the tower base DEL for the upwind turbine is constant across all simulations. The blue line indicates the tower base DEL for the downwind turbine. We see from the figure that a small negative error in the convection velocity estimate actually improves performance. The minimum damage equivalent load corresponds to a timing error of approximately -0.5 seconds. We also see that if the timing error is less than -2.2 seconds or greater than 0.8 seconds the turbine with feed forward control performs worse that the turbine without feed forward control. This is troubling because earlier in this section we estimated that our timing error for this wind speed would be in the neighborhood of ±2.5 seconds.

Figure 3.37 illustrates how timing errors in the feed forward data affect the damage equivalent load of the blade root bending moment. Again, a negative timing error indicates the feed forward data is ahead of the turbulent wind field, the red line indicates the DEL of the upwind turbine, and the blue line indicates the DEL of he downwind
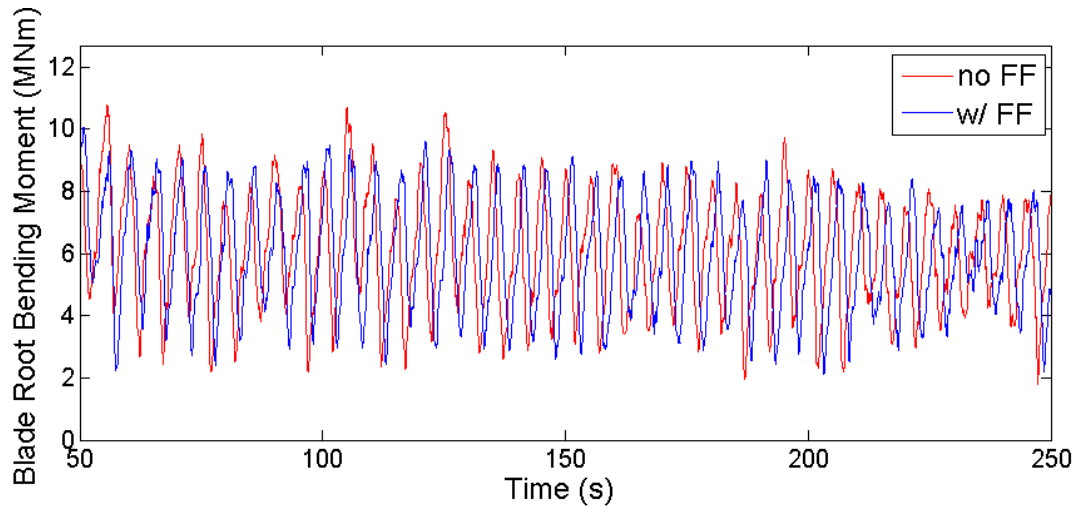
FIGURE 3.36: Tower base DEL for various timing errors in feed forward wind speed estimates.

turbine. We see that a small negative error improves performance. Like the tower base DEL, the blade root DEL is smallest when the timing error is -0.5 seconds. We also see that if the timing error is less than -4.8 seconds or greater than 2.3 seconds the turbine with feed forward control performs worse that the turbine without feed forward control. Blade root DEL is improved over a wider range of timing errors than we saw for tower base DEL, however our estimated timing error of ± 2.5 seconds would not guarantee that the downwind turbine with feed forward pitch control would perform better than a turbine with conventional closed loop control.
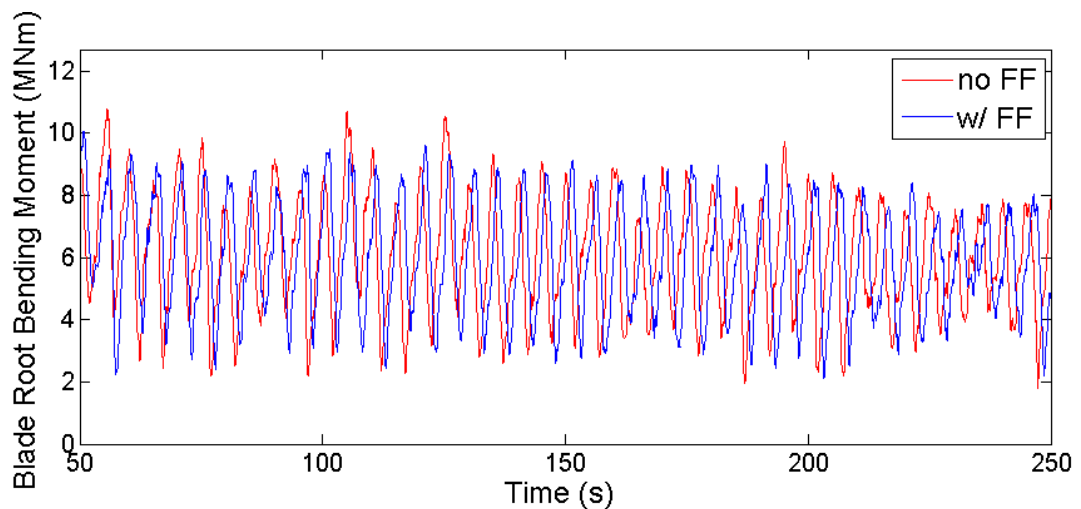
FIGURE 3.37: Blade root DEL for various timing errors in feed forward wind speed estimates.

Timing errors do not affect the average power production. Each simulations simulation had an average power production of 5,000 kW. However, timing errors do affect the

standard deviation of the power production. As shown in Figure 3.38, feed forward pitch control reduces the standard deviation of the power production when the timing error is small, but feed forward controll increases the standard deviation of the power production for timing errors greater than +2.2 seconds or less than -3.1 seconds. A small standard deviation is desirable as it indicates the power output of the turbine remains closer to the desired power output.
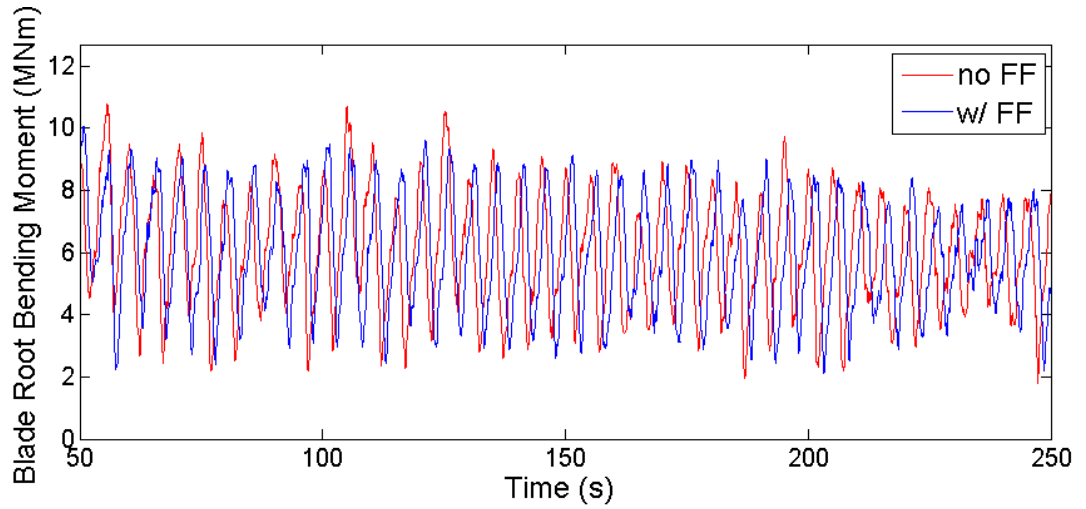
FIGURE 3.38: Standard deviation of power production for various timing errors in feed forward wind speed estimates.

All of the data presented in this section tells the same story. The feed forward pitch control system is sensitive to timing errors. Though the feed forward control system improves performance when timing errors are small it can degrade performance when significantly large timing errors are present. Based on the convection velocity estimate study carried out in Section 2.5, we can not guarantee timing errors will be small enough to ensure feed forward control will improve turbine performance. A control system that is just as likely to degrade performance as improve it is not particularly useful. As such, the results in this section show that in practice the proposed feed forward pitch control scheme proposed in this chapter is not very practical. At this point it is not worthwhile to carry out additional investigations into other real world complications the system would face, such as inaccuracies of the Taylors frozen turbulence hypothesis.

3.7 Summary and Conclusions

In this chapter a feed forward optimal pitch control scheme is introduced and investigated. In this control scheme an upwind is used as a wind speed sensor. Wind speed measurements are passed from the upwind turbine to a feed forward controller on a

downwind turbine. These wind speed measurements give the feed forward controller information about the wind speed fluctuations the downwind turbine will experience in the future. The feed forward controller determines the optimal pitch corresponding to the incoming wind speed fluctuations and issues supplementary pitch commands to the existing feedback control loop of the downwind turbine. These supplementary pitch commands enable the downwind turbine to preemptively respond to incoming wind speed fluctuations potentially improving energy capture and reducing damage to the turbine.

The control scheme is investigated through three rounds of simulation using the NREL FAST turbine simulation tool. The initial round of simulations uses a simplified idealistic model of the system, while the subsequent rounds systematically incorporate complicating factors that a real world system would encounter.

The first round of simulations (Section 3.4) assumes that the feed forward controller has perfect measurements of the incoming wind speed fluctuations, that the convection velocity has been estimated perfectly, and that the wind speed fluctuations experienced by the downwind turbine will be identical to the wind speed fluctuations experienced by the upwind turbine. Results show that in these conditions feed forward control significantly improves turbine performance with respect to both extreme operating gusts and turbulent wind.

The second round of simulations assumes that the convection velocity has been estimated perfectly, and that the wind speed fluctuations experienced by the downwind turbine will be identical to the wind speed fluctuations experienced by the upwind turbine. It does not assume that the feed forward controller has perfect measurements of the incoming wind speed fluctuations. Instead, the wind speed fluctuations are estimated using the dynamics of the upwind turbine. The results from the second round of simulations show smaller performance improvements from the use of feed forward optimal pitch control (compared to the first round of simulations). However, in these conditions feed forward control still significantly improves turbine performance.

The third round of simulations assume that the wind speed fluctuations experienced by the downwind turbine will be identical to the wind speed fluctuations experienced by the upwind turbine. Wind speed fluctuations are estimated using the dynamics of the upwind turbine and a variety of timing errors are introduced to simulate the effect of errors in estimating the convection velocity. Results from this round of simulations show that the feed forward optimal pitch control system is very sensitive to timing errors. If the timing of the data is off by more than a few seconds the feed forward control system can cause a turbine to perform more poorly than a turbine without feed forward control.

The feed forward optimal pitch control scheme presented in this chapter seemed promising trough the first two rounds of simulations. However, the system's high sensitivity to timing errors, and therefore the systems high sensitivity to errors in the estimation of the convection velocity, ultimately make this control scheme impractical in real world applications. In order to effectively use an upwind turbine as a sensor to improve the performance of a downwind turbine we must investigate alternate control schemes that will be less sensitive to timing errors.

Chapter 4

Turbine Derating Based on Feed Forward Signal From Upwind Turbine

4.1 Introduction

The overarching objective of this dissertation is to explore techniques for using an upwind turbine as a feed forward sensor to improve the control of downwind turbines. The previous chapter investigated a control scheme in which wind speed measurements from the upwind turbine were used to influence the blade pitch control of the downwind turbine. Initial simulations seemed promising, with the downwind turbine tracking the optimal pitch angle more closely, experiencing lower structural loading, and experiencing smaller rotor overspeeds. However, further simulations showed the control scheme was sensitive to timing errors in the feed forward data, and was likely impractical as a result.

This chapter investigates another method for improving the control of a downwind turbine using an upwind turbine as a sensor. The control scheme investigated in this chapter has been designed to overcome the shortcomings of the control system investigated in the previous chapter while maintaining many of the same performance goals. The following sections will show that this feed forward control scheme can be very insensitive to timing errors in the feed forward data, that the control system can potentially reduce wear and tear on turbine components by reducing loads caused by large gusts of wind, and that the control system can potentially increase energy capture by reducing overspeed shutdowns in response to large gusts of wind.

The feed forward control scheme investigated in this chapter relies on selective turbine derating to reduce structural loads and rotor overspeeds. Turbine derating, sometimes referred to as turbine curtailment, is when the power produced by a turbine is intentionally reduced below the nominal operating conditions of the turbine. When a turbine is derated, the reduction in power production is generally accompanied by a reduction in structural loads as the turbine extracts less energy from the wind. There are a variety of turbine derating strategies, several of which are investigated by Deshpande and Peters [37], but they all involve reducing either the generator speed and/or the generator torque. This is not surprising since the power generated by the turbine is approximately equal to the generator speed times the generator torque.

Turbine derating can be done for a variety of reasons, and can be done at the request of an electrical utility, or can be done by the wind plant operator in an attempt to improve plant performance. The derating requirements imposed by utilities vary, but to date, most utility requested turbine derating occurs due to lack of sufficient transmission capacity on the utility grid, or in response to high wind generation at times of low electrical load.[38]. A utility may also ask a wind plant to derate turbines to help utility grid frequency regulation [39, 40]. A wind plant operator may derate a turbine to reduce structural loads and increase the longevity of turbine components.[41]. In applications where wind turbine maintenance is difficult to schedule, such as offshore wind farms, a turbine that experiences a small amount of damage could be derated and operated at a diminished capacity until a convenient time can be found for inspection and repairs.[42, 43]. Derating can be used to implement a "soft cut out" scheme in which the turbine will be derated in very high wind speeds instead of being completely shut down once the cut out wind speed is reached. [44] If detailed knowledge of the incoming wind speed is known, then a turbine can be dynamically derated to optimize power capture without exceeding structural loading limits.[44–46] In some cases, derating some of the turbines in a wind plant can increase the total power production of the plant.[47]

The remainder of this chapter describes and investigates a control scheme that uses turbine derating in an attempt to mitigate the detrimental effects of a large wind gust propagating through a wind farm. The following section describes the derating scheme used by the feed forward controller. Section 4.3 investigates the relationship between derating, power generation, structural loads, and rotor overspeed when a turbine is subjected to a large wind gust. Section 4.4 investigates the transition between a rated and derated state. Section 4.5 describes the feed forward control system design. Section 4.6 examines the performance of the feed forward control system when subjected to a large gust of wind.

4.2 Turbine Derating

The power generated by a turbine is given by $P_{gen} = T_{gen}\Omega_{gen}\eta_{gen}$ where T_{gen} is the generator torque, Ω_{gen} is the generator speed, and η_{gen} is the efficiency of the generator. For a given wind speed, a turbine can be derated by reducing Ω_{gen} and/or η_{gen} below the normal operating values. Derating a turbine typically causes a reduction in both the power generation and structural loads of the turbine. However, reducing structural loads is not always a goal of turbine derating. Therefore, the load reduction capabilities of derating are not always thoroughly examined in literature. Several derating methods have been proposed in literature. In this section three of those derating methods are investigated to determine which method is best suited for our feed forward controller.

Method 1 is based on "derating strategy C" proposed by Deshpande and Peters in "Wind turbine controller design considerations for improved wind farm level curtailment tracking."[37] In this method the rated generator speed remains unchanged and the turbine is derated by reducing the rated generator torque. The torque-speed curve of the generator torque controller is scaled to accomodate this change. Method 2 is based on the derating strategy proposed by Frost, Goebel, and Obrecht in "Integrating Structural Health Management with Contingency Control for Wind Turbines."[48] In this method the torque-speed curve of the torque controller remains unchanged. The turbine is derated by changing the point on the torque speed curve at which the turbine switches to a region 3 control strategy. Essentially this method derates the turbine by reducing both the rated generator torque and the rated generator speed. Method 3 is based on the derating method proposed by Petrovic and Bottasso in "Wind Turbine Envelope Riding."[46] In this method the rated generator torque remains unchanged while the turbine is derated by reducing the rated generator speed. To accomodate the reduction in the rated generator speed ,the torque-speed curve of the generator torque controller is scaled and a minimum pitch angle is imposed on the blade pitch controller.

To evaluate the three derating methods, all three derating methods are simulated for a pair of test cases. In test case one the turbine has been derated by 30% and is operating in steady 16 m/s when it experiences an extreme operating gust. In test case two the turbine has been derated by 30% and is operating in steady 12 m/s wind when it experiences an extreme operating gust. In both test cases the extreme operating gust is defined according to IEC 61400-1 [36] for a class 1 turbine in category A turbulence. Figures 4.1 through 4.4 illustrate how the derating strategies affect the power generation, tower base fore-aft bending moment, blade root bending moment, and rotor speed. As expected, derating the turbine by 30% results in a 30% reduction in power production for all three derating strategies. The deviations in power production caused by the extreme operating gust are slightly larger for derating method 3, but otherwise all three derating

strategies have a very similar effect on power production. In Figure 4.2 we see that all three derating strategies have a similar effect on tower base fore-aft bending moment before and after the extreme operating gust, with a 30% derating corresponding to a ?????findThis???? % reduction. However, the derating methods have differing effects on the peak tower base fore-aft bending moments induced by the extreme operating gust. Derating method 1 has a peak moment of 88.4 MNm, a 13.5% reduction compared to a non derated turbine, while derating method 2 has a peak moment of 85.2 MNm, a 16.6% reduction. Derating method 3 performs significantly better with a peak moment of 65.8 MNm, a 35.6% reduction. Figure 4.3 tells a similar story. All three derating methods have a similar effect on blade root moments when the turbine is in constant wind, but they have differing effects when the turbine is experiencing an extreme operating gust. Once again, derating method 3 out performs the other two methods with respect to reducing peak structural loads. Derating method 1 reduces the peak blade root moment by 17.5%, method 2 reduces the peak blade root moment by 17.0%, and method 3 reduces the peak blade root moment by 29.5%. Figure 4.4 shows that the three derating strategies have very different effects on rotor speed. It is not surprising that the derating method based on reducing the rated torque (method 1) has the least effect on rotor speed, the derating method based on reducing the rated generator speed (method 3) has the greatest effect on rotor speed, and the derating method based on reducing both the rated speed and rated torque (method 2) falls somewhere in between. With derating method 1 the turbine sees a peak rotor speed of 14.18 RPM, only a 1.1% reduction from the non-derated turbine. That peak rotor speed is 17.2% over the turbine's rated rotor speed of 21.1 RPM. With derating method 2 the turbine sees a peak rotor speed of 13.57 RPM, a 5.4% reduction, which corresponds to a peak overspeed of 12.1%. With derating method 3 the turbine sees a peak rotor speed of 10.40 RPM, a 27.5% reduction, which is not an overspeed.

Test case 2, where a turbine is derated by 30% and is operating in steady 12 m/s wind when it experiences an extreme operating gust, shows similar trends to test case 1. Plots of the power generation, tower base fore-aft bending moment, blade root bending moment, and rotor speed for test case two are not shown here. However, the performance observed in both test cases has been quantified and summarized in Table 4.1 and Table 4.2. The table shows that derating method 3 is significantly better than methods 1 and 2 at reducing both the structural loads and the rotor overspeeds caused by an extreme operating gust. Since derating method 3 does the best job of mitigating the negative effects of a large gust of wind it is best suited for our feed forward controller. All further simulations described in this chapter use derating method 3. A more detailed description of derating method 3 and how it is incorporated into the NREL 5-MW controller can be found in Section 4.5.
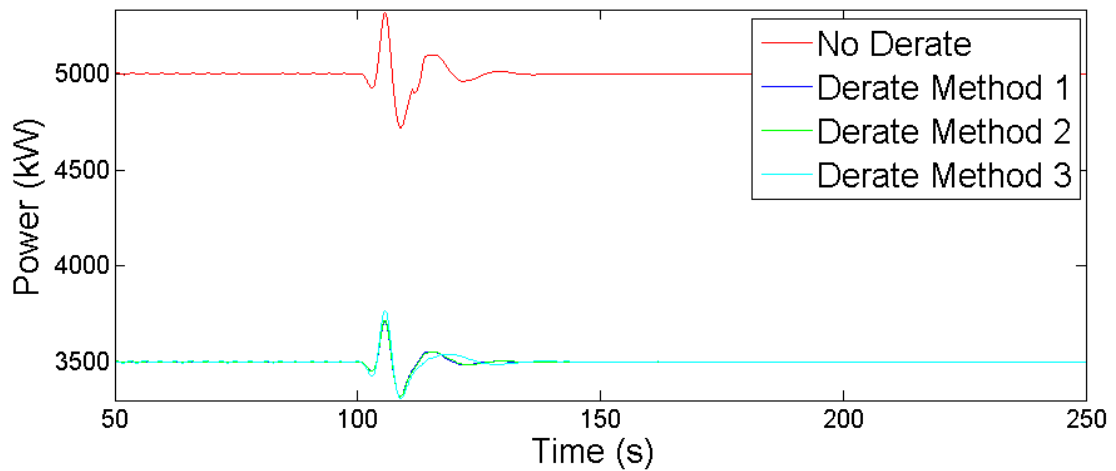
FIGURE 4.1: Power generated during 16m/s EOG for 30% derated turbine.
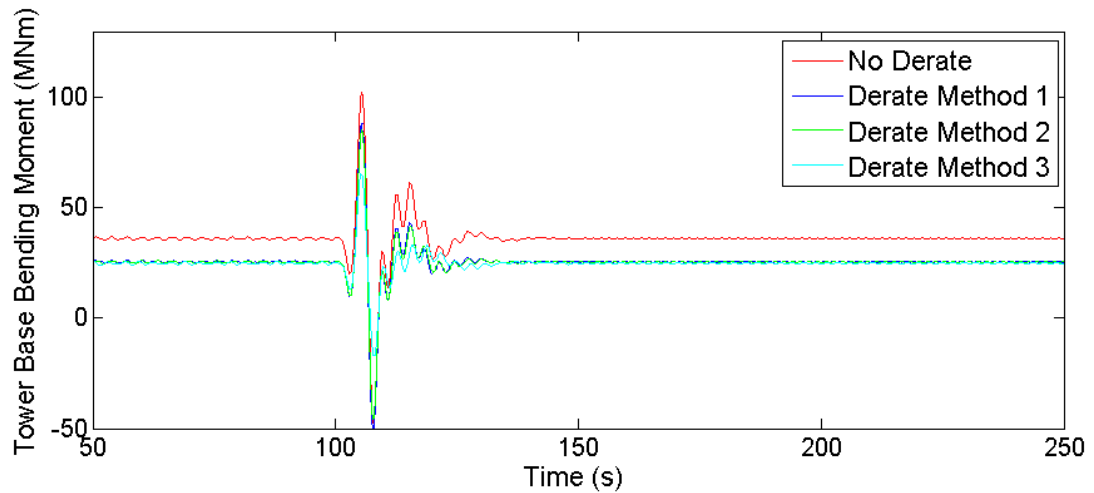
FIGURE 4.2: Tower fore-aft bending moment for 30% derated turbine during 16m/s EOG.

4.3 Effect of Derating on Dynamic Turbine Response

This section investigates the relationship between derating and the dynamic turbine response. In particular we are interested in determining how derating affects the structural loading and rotor overspeed a turbine experiences when subjected to a large gust. To study these relationships a series of simulations were run subjecting a derated NREL 5-MW turbine to an extreme operating gust at a variety of mean wind speeds and a variety of derating factors. The series of simulations included mean wind speeds of 6 m/s, 8 m/s, 10 m/s, 12 m/s, 14 m/s, 16 m/s, 18 m/s, and 20 m/s, as well as derating factors of 0%, 5%, 10%, 15%, 20%, 25%, and 30%. For all simulations the turbine is
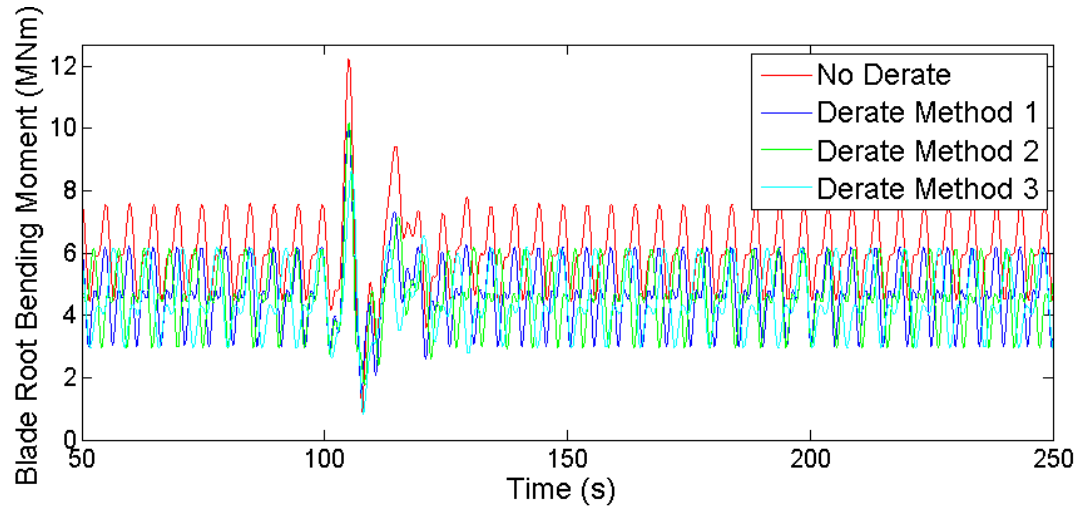
FIGURE 4.3: Blade root moment for 30% derated turbine during 16m/s EOG.
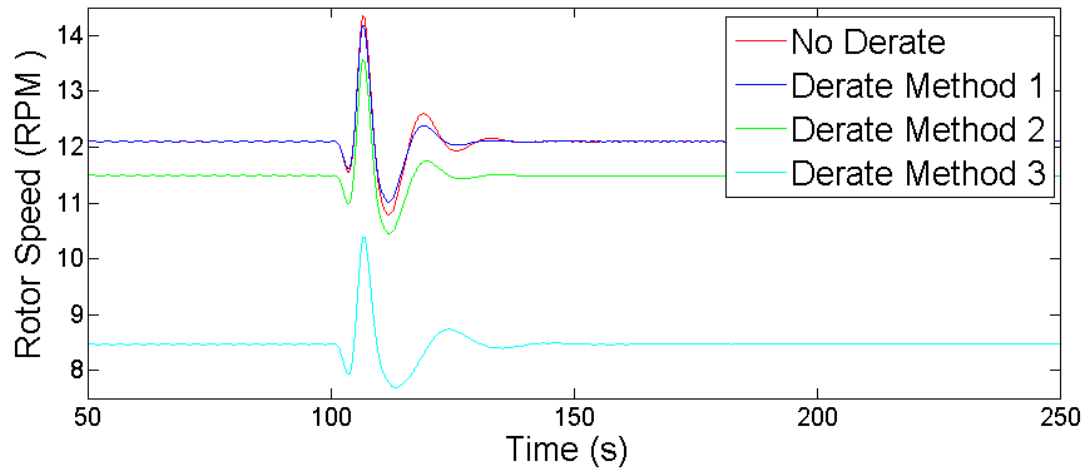
FIGURE 4.4: Rotor speed for 30% derated turbine during 16m/s EOG.

TABLE 4.1: Effect of derating methods for test case 1: 16 m/s EOG with 30% derating.

	Max tower base bending moment		Max blade root bending moment		Max rotor speed	
	(MNm)	reduction	(MNm)	reduction	(RPM)	reduction
No derating	102.2	-	12.25	-	14.35	-
Derating method 1	88.40	13.5%	10.11	17.5%	14.18	1.1%
Derating method 2	85.19	16.6%	10.17	17.0%	13.57	5.4%
Derating method 3	65.81	35.6%	8.64	29.5%	10.40	27.5%

TABLE 4.2: Effect of derating methods for test case 2: 12 m/s EOG with 30% derating.

	Max tower base bending moment		Max blade root bending moment		Max rotor speed	
	(MNm)	reduction	(MNm)	reduction	(RPM)	reduction
No derating	124.7	-	11.84	-	14.07	-
Derating method 1	91.36	26.7%	11.84	26.1%	13.77	2.1%
Derating method 2	89.71	28.1%	11.78	26.5%	13.17	6.4%
Derating method 3	70.20	43.7%	8.30	48.2%	10.38	26.2%

operating in uniform, constant wind when it experiences an extreme operating gust (as defined by IEC 61400-1 [36] for a class 1 turbine in category A turbulence).

Figure 4.5 shows the relationship between derating factor and average power production for several of the mean wind speeds simulated. As expected, there is a 1 to 1 relationship between the derating factor and the reduction in power generation. Each 1% of derating corresponds to a 1% decrease in power production. The other wind speeds simulated also showed this same relationship.
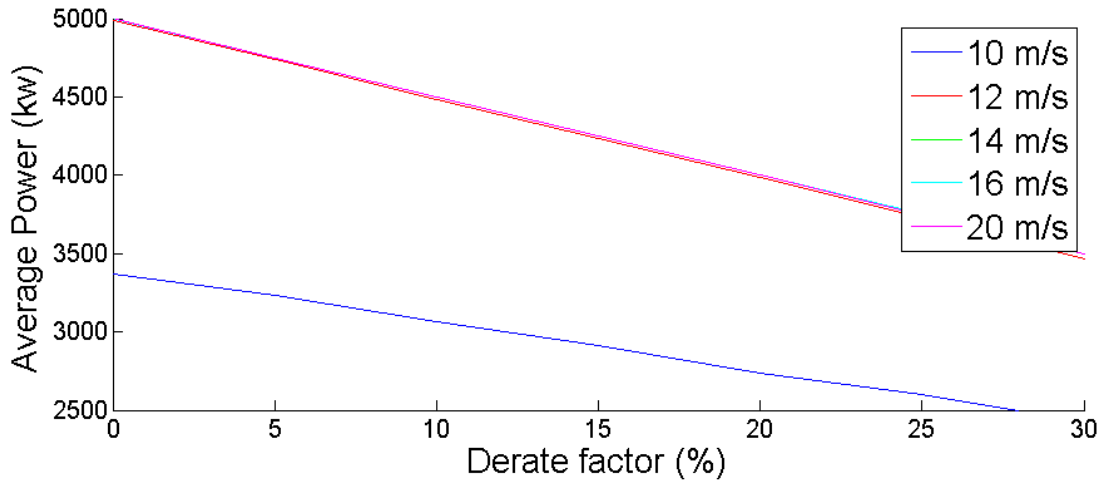
FIGURE 4.5: Effect of derating on avg. power for EOGs at various wind speeds.

Figure 4.6 shows the relationship between derating factor and the maximum tower base fore-aft bending moment for several of the mean wind speeds simulated. One thing we see in this figure is that the turbine experiences the largest tower bending moments in simulations where the mean wind speed is equal to the rated wind speed of 12 m/s.

The maximum tower bending moment decreases slowly and steadily as the mean wind speed is increased above 12 m/s. The maximum tower bending moment also decreases steadily, but more precipitously, as the mean wind speed decreases below 12 m/s. We also notice that the relationship between derating factor and maximum tower bending moment appears nearly linear. ????talk about slopes????
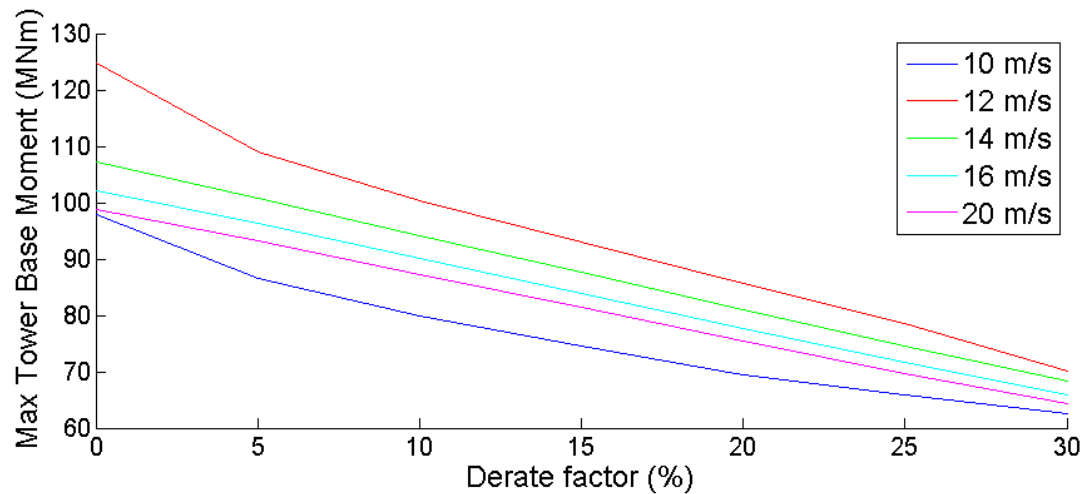
FIGURE 4.6: Effect of derating on max tower moment for EOGs at various wind speeds.

Figure 4.7 shows the relationship between derating factor and the maximum blade root bending moment. For low derating factors we see again that highest loads occur when the mean wind speed is equal to the rated wind speed of 12 m/s and the maximum loads gradually decrease as the mean wind speed either increases or decreases away from the rated wind speed. However, at higher derating factors all of the test cases at or above the rated wind speed (12 m/s - 20 m/s) seem to converge. When the turbine is derated 25% or 30% the 12 m/s and 14 m/s simulations actually cause slightly larger maximum blade root moments. Again the relationship between derating factor and maximum load reduction appears nearly linear. ????talk about slopes????

Figure 4.8 shows the relationship between derating factor and the maximum rotor speed, while Figure 4.9 shows the corresponding maximum rotor overspeed. We see in these figures that the simulations with higher mean wind speeds have higher maximum rotor speeds and therefore higher maximum rotor overspeeds. As with the previous plots in this section we see a nearly linear relationship between ????not totally sure what to say here?????
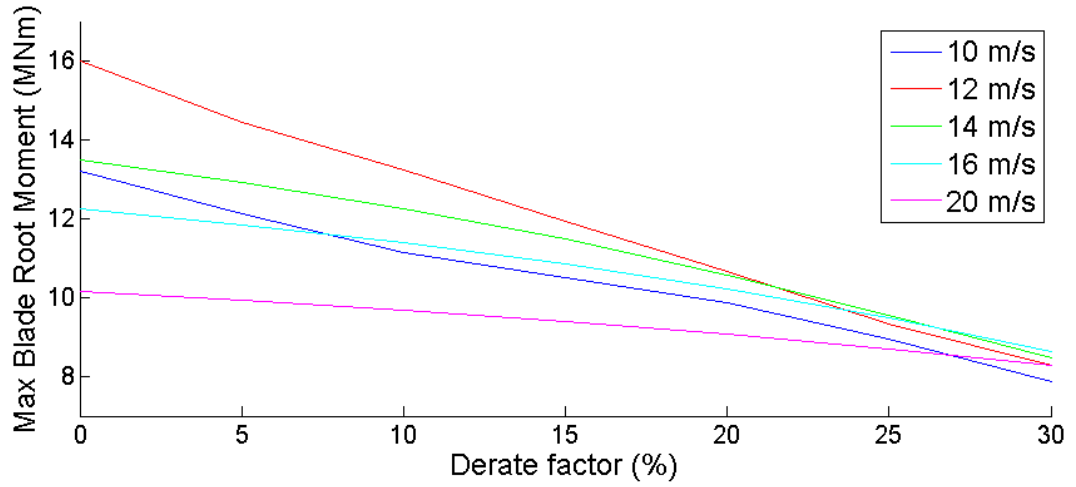
FIGURE 4.7: Effect of derating on max blade root moment for EOGs at various wind speeds.
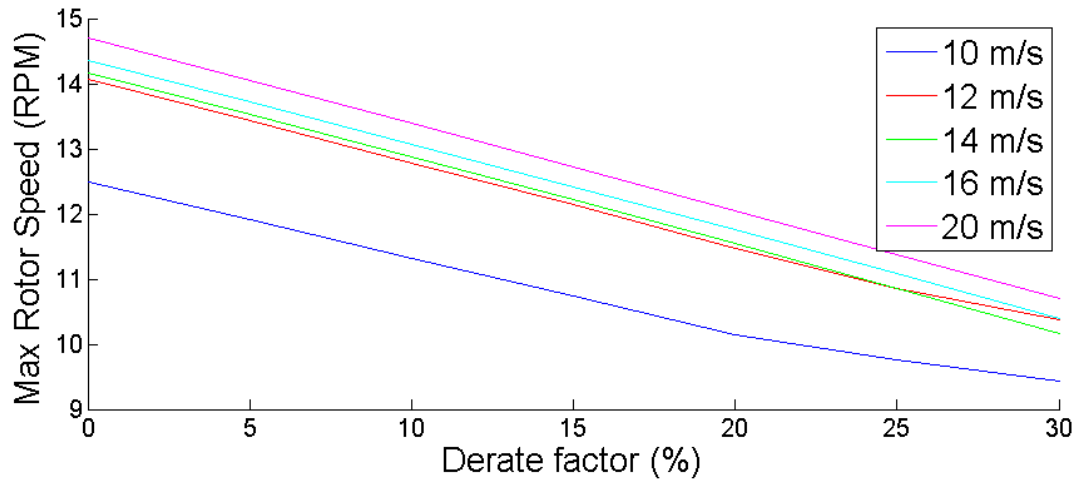
FIGURE 4.8: Effect of derating on max rotor speed for EOGs at various wind speeds.

4.4 Transitioning Between Rated and Derated Operation

The previous subsection demonstrated that operating in a derated state can significantly reduce the structural loading and rotor overspeeds experienced by a turbine. However, the control scheme proposed in this chapter uses selective derating. In this control scheme the turbine will be derated when reductions in loading and rotor speed are necessary, but the turbine will operate normally when those reductions are not needed. To implement this control scheme we must understand how the turbine behaves while it is transitioning into and out of derated operation. This subsection examines the transient behavior of the turbine during these transitions and how undesireable transient behavior can be mitigated.
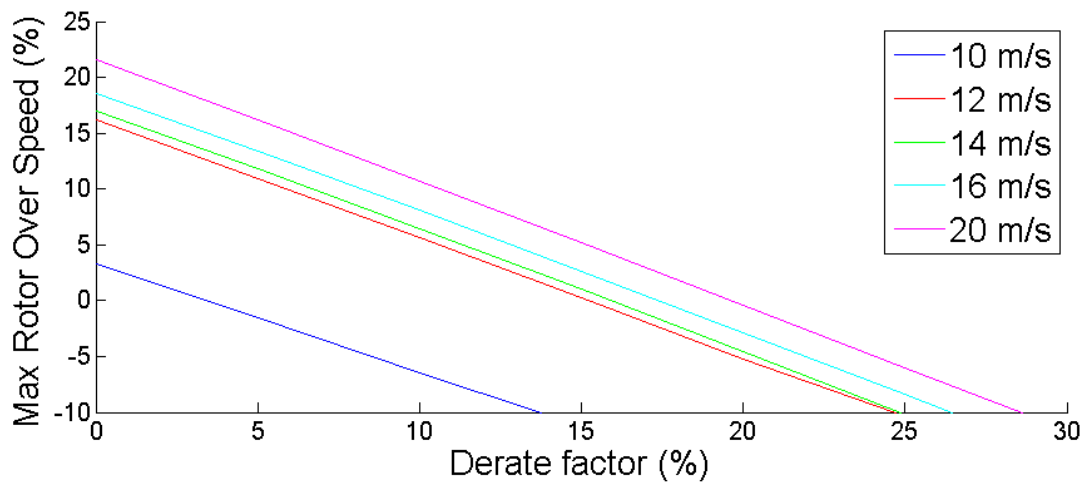
FIGURE 4.9: Effect of derating on max rotor overspeed for EOGs at various wind speeds.

When the rating of a turbine is abruptly changed the turbine exhibits undesireable transient behavior. This transient behavior is illustrated by Figures 4.10 through 4.12. The figures show a test case in shich the turbine operates in a steady, uniform 16 m/s wind. At 100 seconds the turbine is abruptly derated by 20%, then at 200 seconds the turbine is abruptly returned to it's full rating. A 20% derating corresponds to a rotor speed reduction from 12.1 RPM to 9.68 RPM. In Figure 4.10 we see that when the turbine is abruptly derated the rotor undershoots the desired rotor speed by 0.94 RPM then oscillates before settling to within 2% of the the desired rotor speed at approximately 130 seconds. When the turbine is abruptly returned to full rating it exhibits similar behavior, overshooting the desired rotor speed by 1.62 RPM (a 13.4% overshoot) before oscillating and settling to within 2% of the desired rotor speed at aproximately 230 seconds.

The tower fore-aft bending moment also exhibits undesireable oscillations with settling times of approximately 30 seconds (Figure 4.11). These oscillations apear to have both a higher frequency component and a lower frequency component. The higher frequency oscillation (2 rad/s) corresponds to the first natural frequency of the tower. The lower frequency oscillation is caused by oscillations in the collective blade pitch. When the turbine's collective pitch controller reduces the blade pitch, in order to increase aerodynamic rotor torque and increase the rotor speed, it also increases the aerodynamic thrust on the rotor, which increases the fore-aft tower moment. Similarly, when the collective pitch controller increases blade pitch it reduces the fore-aft tower moment.

As Figure 4.12 shows, the blade root bending moment also exhibits undesireable transient behavior when the turbine abruptly transitions into or out of derated operation.
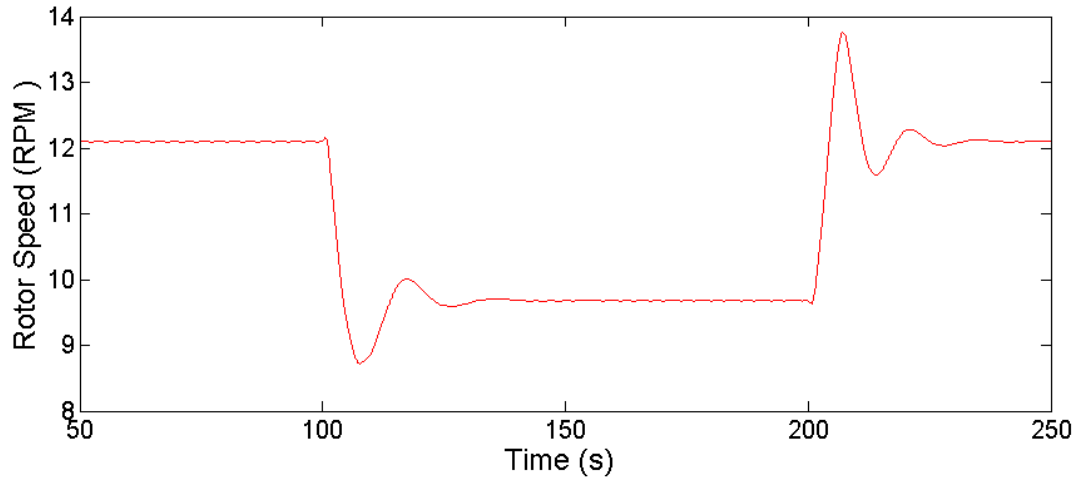
FIGURE 4.10: Effect of sudden rating changes on rotor speed.
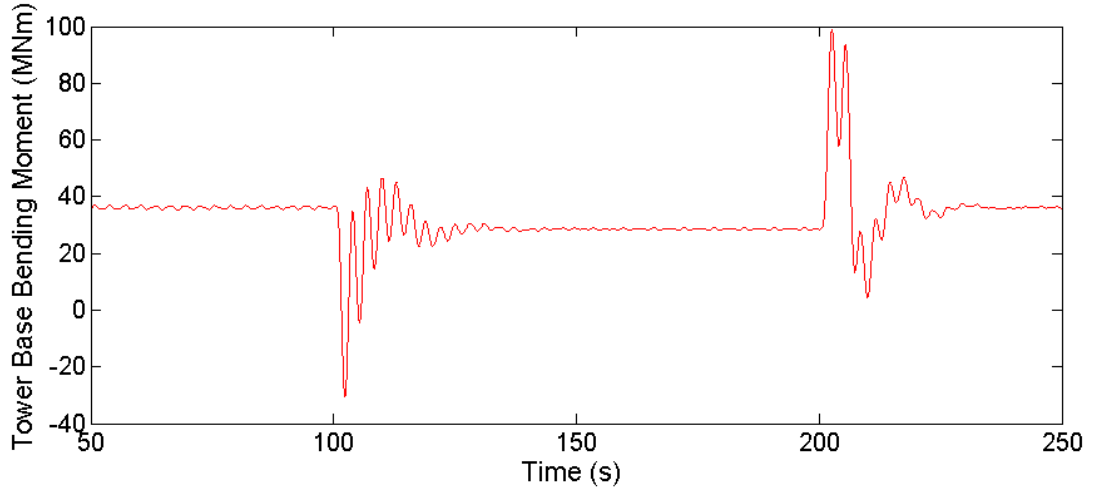
FIGURE 4.11: Effect of sudden rating changes on tower bending moment.

However, the cyclic nature of the blade root loading makes it difficult to discern the frequency or settling time of the transient behavior. Undesireable oscillations, like those shown in figures 4.10 through 4.12, were seen at all wind speeds.

We can reduce the excitation of undesireable oscillations by using a smoother transition into and out of derated operation. One way to smooth the transition is to pass derating commands through a low pass filter like the one described by the transfer function shown in Equation 4.1. This low pass filter is a critically damped second order system with two poles at $-P_{filter}$. Passing derate commands through this filter turns abrupt derating comands into smoother transitions, as seen in Figure **??**. The 98% settling time of the filtered command is determined by the value of P_{filter} and is given by $t_s = 5.8 \times P_{filter}$.
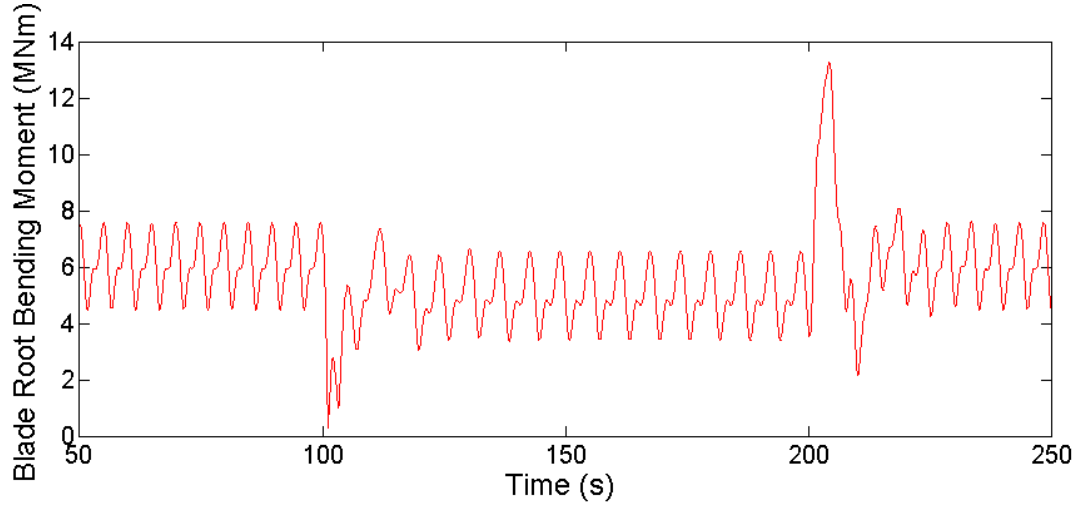
FIGURE 4.12: Effect of sudden rating changes on blade root bending moment.

$$\dot{\Omega}_{Rotor} I_{Drivetrain} = T_{Aero} - T_{Gen} N_{Gear} \qquad (4.1)$$

Choosing $P_{DRFilt} = 0.2$ gives filtered command settling time of 29.5 seconds, which is approximately equal to the settling time of the transient oscillations caused by abrupt changes in turbine rating. As Figures 4.13 through 4.15 show, using this filtered command to transition into and out of derated operation results in improved transient behavior while maintaining the same settling time. In figure 4.13 we see that the filter eliminates the oscillations, overshoots, and undershoots in rotor speed. In Figure 4.14 we see that the filter eliminates the higher frequency oscillation. The lower frequency oscillation, caused by variations in the collective pitch angle, are still present but have reduced in magnitude. In figure 4.15 we see that the filter also improves transient behavior in the blade root bending moment.

In general, lengthening the settling time of the filter reduces undesireable transient oscillations and reduces the magnitude of any overshoots or peak loads associated with transitioning into or out of derated operation. Figures 4.16 through 4.18 show the relationship between filter settling time and the maximum overshoots observed in the derating transition simulations. In practice the maximum acceptable settling time would be limited by the time it takes a gust of wind to travel from the upwind turbine to the downwind turbine. This time will depend on both the wind speed and the layout of the wind farm, however, some simple calculations can be made to help choose a reasonable filter settling time. The NREL 5-MW turbine has a rotor diameter of 126 meters. If the turbines are spaced 10 rotor diameters appart then in 12 m/s wind, the wind speed at which loads are highest and this control scheme would likely be most benneficial, a
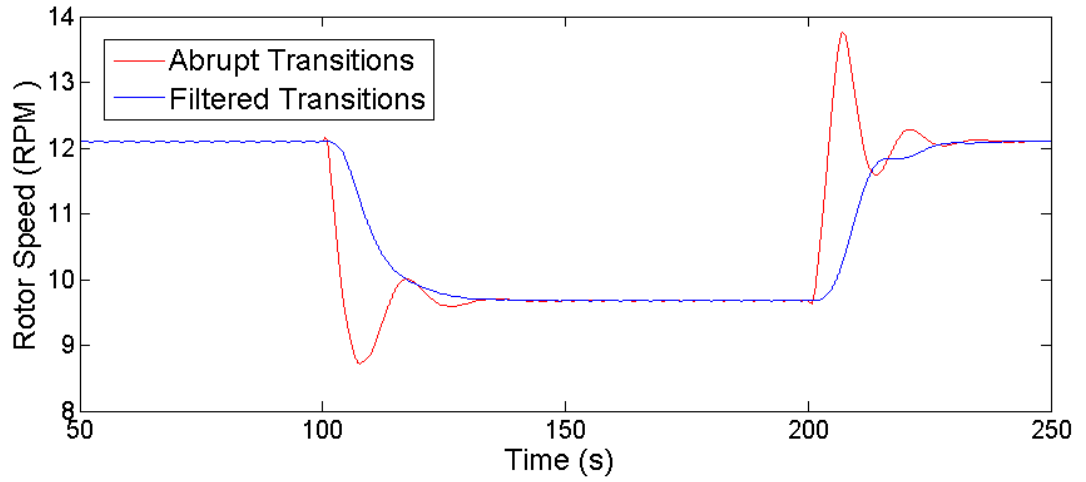
FIGURE 4.13: Improvements in rotor behavior from filtered derate commands.
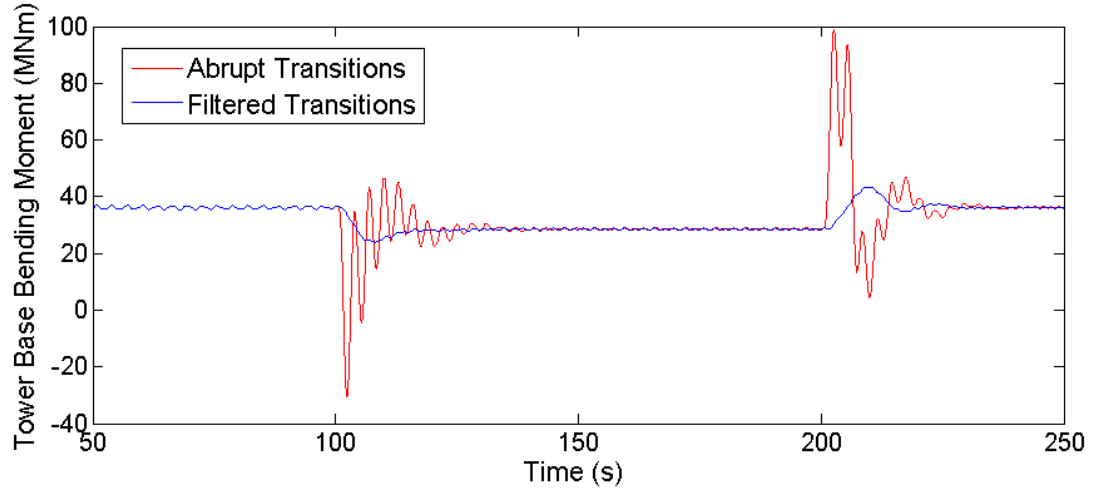
FIGURE 4.14: Improvements in tower bending moment from filtered derate commands.

gust would travel between turbines in approximately 105 seconds. In 25 m/s wind, the highest wind speed in which the NREL 5-MW turbine will operate at all, the gust would travel between turbines in approximately 50 seconds. If the turbines are spaced 5 rotor diameters appart then a gust would travel between turbines in approximately 53 seconds for 12 m/s wind and in approximately 25 seconds for 25 m/s wind.

A low pass filter, given by equation 4.1 with $P_{filter} = 0.2$, will be used to smooth the turbine transitions into and out of derated operation. $P_{filter} = 0.2$ corresponds to a filter settling time of 29.5 seconds. Though this filter could potentially cause problems for tightly packed turbines in very high wind speeds a filter settling time of 29.5 seconds would be practical for almost all operating conditions of the NREL 5-MW turbine. As
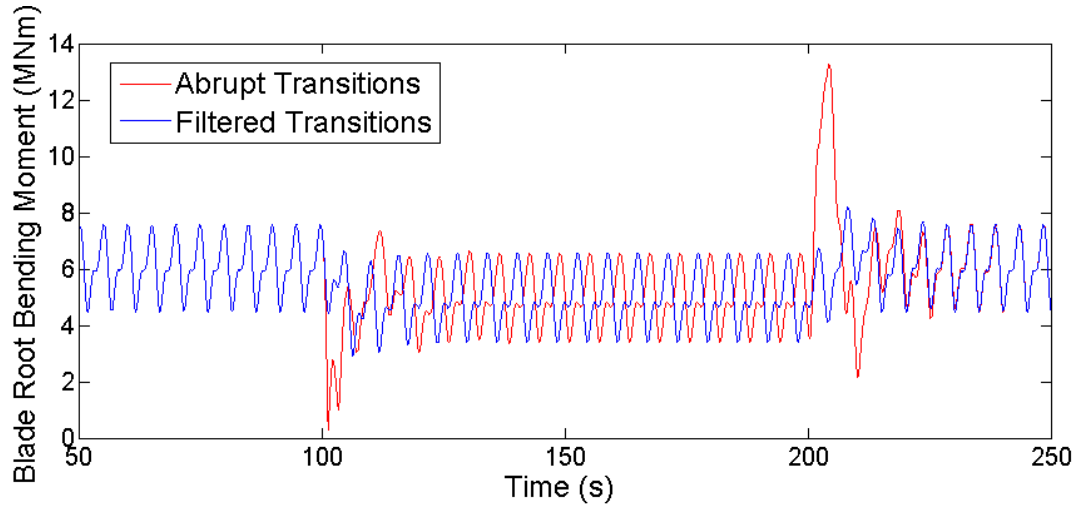
FIGURE 4.15: Improvements in blade root moment from filtered derate commands.
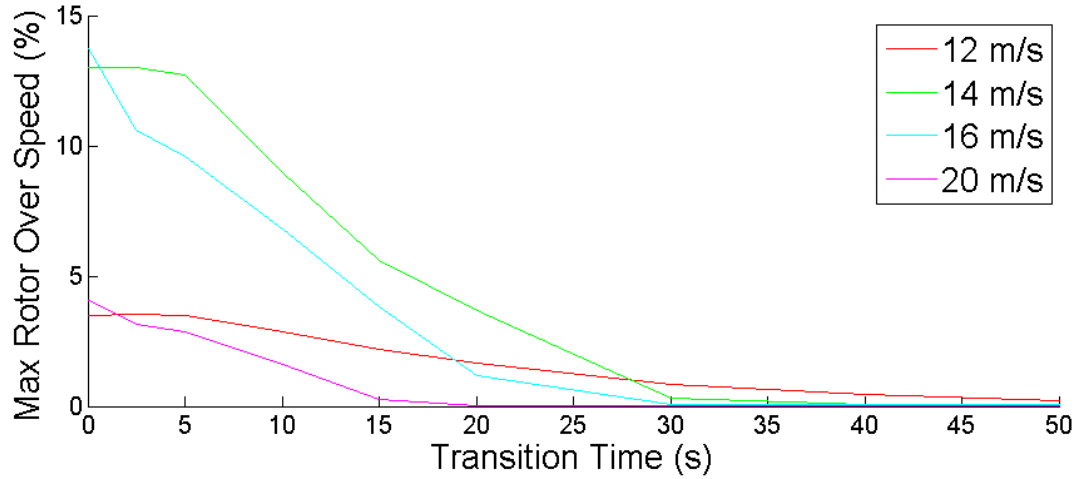
FIGURE 4.16: Effect of input filter settling time on rotor overspeed.

seen above, this filter also gives very good transient behavior when the turbine transitions into and out of derated operation.

4.5   Control System Design

As figure 4.19 illustrates, a plant level controller will monitor the behavior of the upwind turbine and derate the downwind turbine when necessary. To determine when derating is necessary, the plant level controller will monitor the rotor speed of the upwind turbine. If the upwind turbine rotor speed exceeds some pre-defined threshold the plant level controller will interpret that as an extreme gust event and derate the downwind turbine. This threshold should be chosen based on the range of rotor speeds a turbine experiences
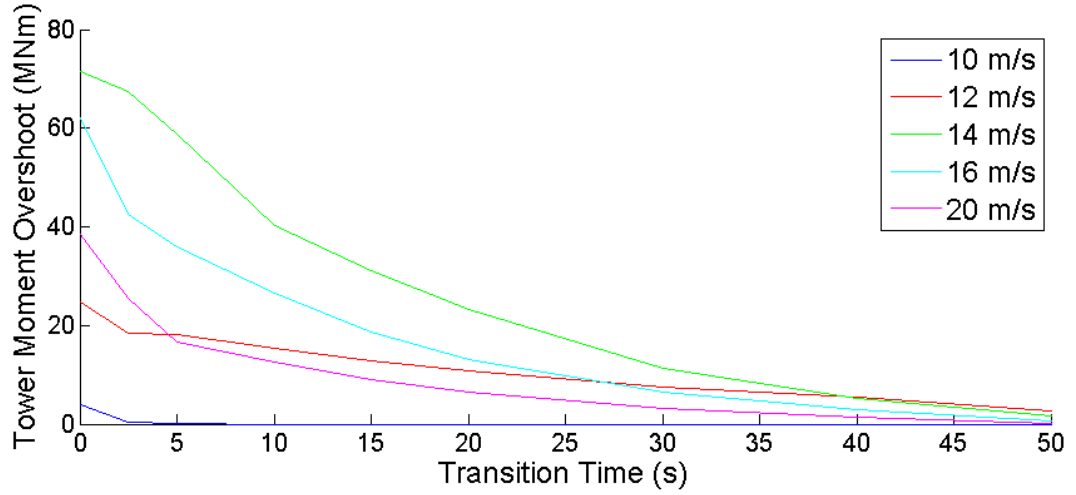
FIGURE 4.17: Effect of input filter settling time on peak tower bending moment.
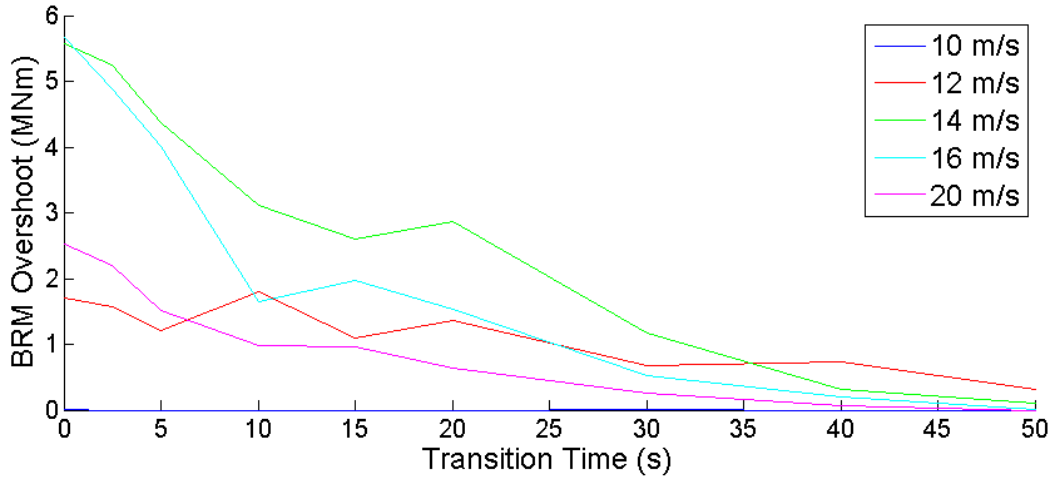
FIGURE 4.18: Effect of input filter settling time on peak blade root moment.

during nominal operation, and how aggressive a plant operator chooses to be with this selective derating strategy. Therefore, in practice this threshold is likely to be site specific.

For the simulations carried out in the following sections the threshold to initiate derating is set to 13.31 RPM (a 10% overshoot). Section 2.2 describes a set of 66 simulations of the NREL 5-MW turbine in turbulent wind. That data set contains 7 hours of simulated turbine operation in wind speeds between 12 m/s and 22 m/s, wind speeds for which the turbine is operating in region 3 control and attempting to track the rated rotro speed of 12.1 RPM. In that 7 hours of data the rotor speed exceeds 5% overshoot only 0.44% of the time and never exceeds 6.76% overshoot. a 10% threshold to initiate derating should be sufficient to identify extreme gust events and roughly splits the difference between what
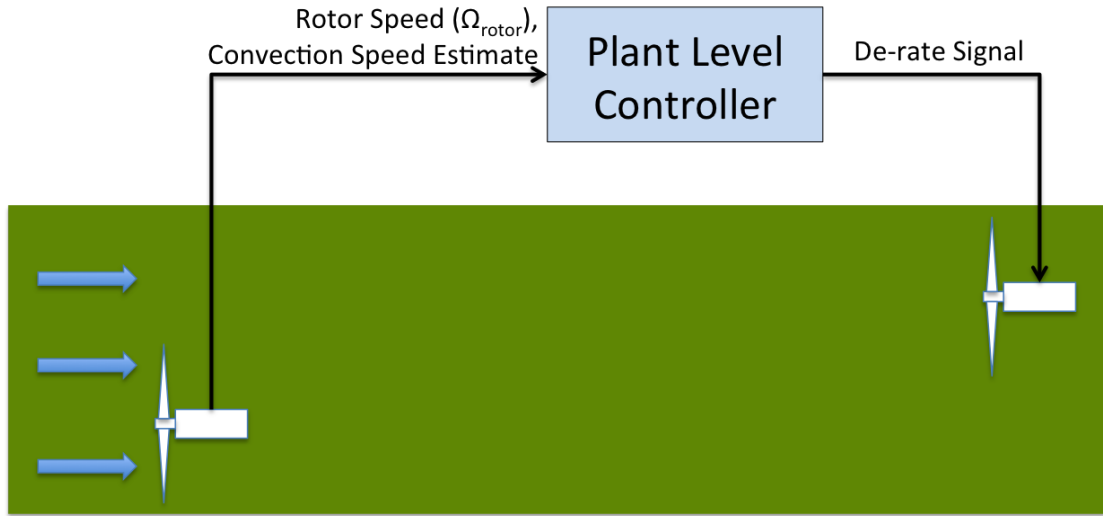
FIGURE 4.19: Control system overview.

the turbine sees during normal operation and a 15% overspeed, which could potentially cause a overspeed shutdown. When derating is initiated, the downwind turbine will be derated by the maximum rotor overspeed obvserved in the extreme gust event minus 5%.

As shown in section 4.3, derating the downwind turbine will reduce the structural loads and rotor overspeed caused by the extreme gust event. As a result the downwind turbine will experience reduced structural damage and avoid a possible overspeed shutdown when the extreme gust arrives. Once the extreme gust has passed the downwind turbine the downwind turbine will be returned to full rated operation. Several methods can be used to determine when the downwind turbine should be derated $(T_{startDerate})$ and when it is safe for the downwind turbine to return to full rated operation $(T_{endDerate})$. Two of those methods are examined in the following paragraphs.

One method of determining when to derate the downwind turbine is to use an estimate of the gust's convection speed. The time it takes for a gust of wind to travel from the upwind turbine to the downwind turbine is given by $t = D/U_{conv}$, where D is the downwind distance between the turbines and the convection speed U_{conv} is the the rate at which wind speed fluctuations propagate downwind. Section 2.4 examined a method for estimating wind speed using blade pitch, rotor speed, generator torque, and known dynamics of the turbine. Section 2.5 examined using that wind speed estimation technique to estimate the convection speed.

Large rotor overspeeds occur when the turbine is operating at or above the rated wind speed. For the NREL 5-MW turbine that means that large overspeeds will occur when

the wind speed is between 12 and 25 m/s. Section 2.5 analyzed 7 hours of simulated turbine operation in those wind conditions. With a 60 second averaging time, the mean error in convection speed estimates was approximately 3.2% and the largest error seen in a convection velocity estimate was approximately 5.6%. To improve this control scheme's robustness to errors in convection velocity estimation we can base our derate timing on a larger error than was seen in those results. If the plant level controller begins and ends the derate signal based on Equations 4.2 and 4.3 then the control system will accomodate extreme wind events traveling up to 20% faster or 20% slower than the convection velocity estimate. t_{Event} is the time at which the upwind turbine experiences an unacceptably large overspeed. Recall that t_{conv} is the estimated time it will take for the gust of wind to travel from the upwind turbine to the downwind turbine and t_s is the time required for the turbine to smoothly transition into derated operation. This system could experience problems if the upwind turbine experienced an overspeed shutdown, as convection velocity estimates would no longer be available.

$$t_{DR_s start} = t_{Event} + 0.8 \times t_{conv} - t_s \tag{4.2}$$

$$t_{DR_e nd} = t_{Event} + 1.2 \times t_{conv} \tag{4.3}$$

Another method of determining when to derate the downwind turbine is to develop worst case scenarios based on the operating conditions of the turbine. For the NREL 5-MW turbine we have determined that large rotor overspeeds will occur when in wind speeds between 12 m/s and 25 m/s. If the downwind turbine is 10 rotor diameters (1260 m) behind the upwind turbine and the convection speed is somewhere between 12 and 25 m/s it would take a gust of wind between 105 and 50.4 seconds to travel from the upwind turbine to the downwind turbine. Therefore, if the turbine is derated from 50.4 seconds to 105 seconds after the upwind turbine experiences an unacceptable overspeed the downwind turbine should be in derated operation when the gust arrives no matter what the wind speed is. To add more safety margin we can base our worst case scenario on an even wider range of convection velocities. If the transition to derated operation is based on a 30 m/s convection time and the transition out of derated operation is based on an 8 m/s wind the derate signal will be based on equations 4.4 and 4.5, where 42 seconds is the time required for a gust traveling 30 m/s to reach the downwind turbine and 157.5 is the time required for a gust traveling 8 m/s to reach the downwind turbine. A similar calculation can be done for other turbines and/or other turbine to turbine spacing. Though this method derates the downwind turbine for longer than is strictly necessary it is simple, robust, and does not require an estimate of the convection velocity.

$$t_{DR_start} = t_{Event} + 42 seconds - t_s \tag{4.4}$$

$$t_{DR_end} = t_{Event} + 157.5 seconds \tag{4.5}$$

Maybe explain how derating signal is processed.??????

4.6 System Performance

The following sections examine the performance of the selective derating feed forward control system. A two turbine system is simulated using FAST using the method described in Section 3.2. The upwind turbine, with a conventional closed loop turbine controller, is simulated first. The dynamic response of that turbine is recorded and post processed to generate feed forward control signals. This post processing simulates the plant level controller. Finally the downwind turbine, with feed forward control, is simulated. By comparing the dynamic behavior of both simulations we can see the effect of the feed forward control system.

4.6.1 Response to IEC Extreme Operating Gust

The first simulation case is a uniform wind field with an extreme operating gust (EOG). The extreme operating gust has been defined according to IEC 61400-1 [36] for an NREL 5-MW turbine operating in 16 m/s wind. This is the same test case used to analyze the performance of feed forward optimal pitch control in Sections 3.4.1 and 3.5.1, however the EOG has been shifted to occur 200 seconds after the start of the simulation, as shown in Figure 4.20. This shift will ensure that transient derating behavior will not overlap with any of the transient turbine startup behavior at the beginning of the simulation.

Figures 4.21 through 4.24 show how feed forward selective derating control affects the rotor speed, tower base fore-aft bending moment, blade root moment, and power generation of the downwind turbine. Table 4.3 quantifies and summarizes several important performance metrics. Two methods were used to time the derating of the downwind turbine. As discussed in Section 4.5, the first method uses an estimate of the gust confection speed to determine when to derate the turbine. The second, more conservative, method derates the downwind turbine over a longer period of time, but does not require an estimate of the convection speed. Both methods have an identical effect on rotor speed and peak structural loads, but they affect power generation differently.
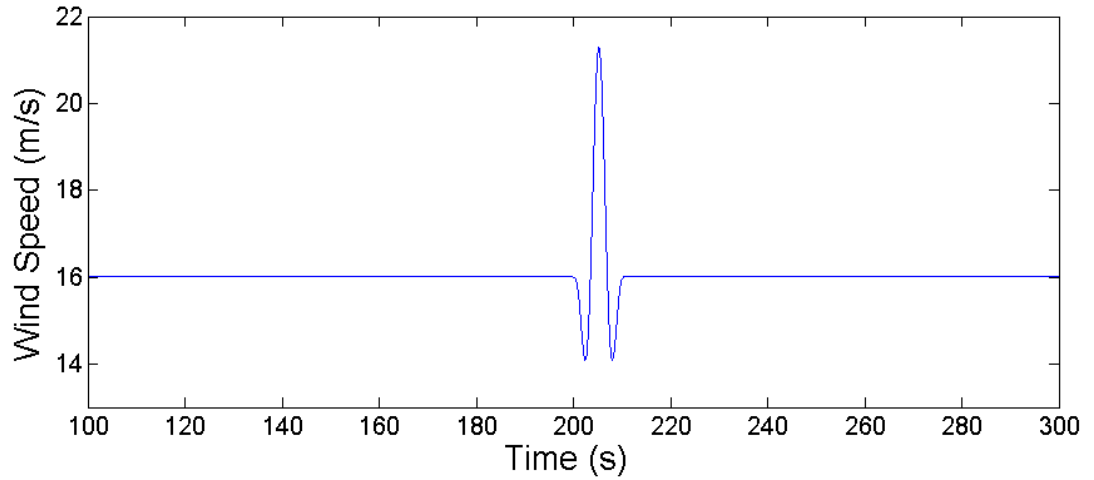
FIGURE 4.20: Extreme operating gust.

Figure 4.21 shows that the upwind turbine experiences an 18.76 % rotor overspeed due to the EOG, potentially enough to cause an emergency shutdown of the turbine, but the feed forward controller reduces the rotor overspeed in the downwind turbine to 4.96%. In Figures 4.22 and 4.23 we see that both the upwind and downwind turbines experience large structural loads due to the EOG, but the loads experienced by the downwind turbine are smaller. The feed forward controller has reduced the maximum tower base fore-aft bending moment by 21.9% and the maximum blade root bending moment by 14.7
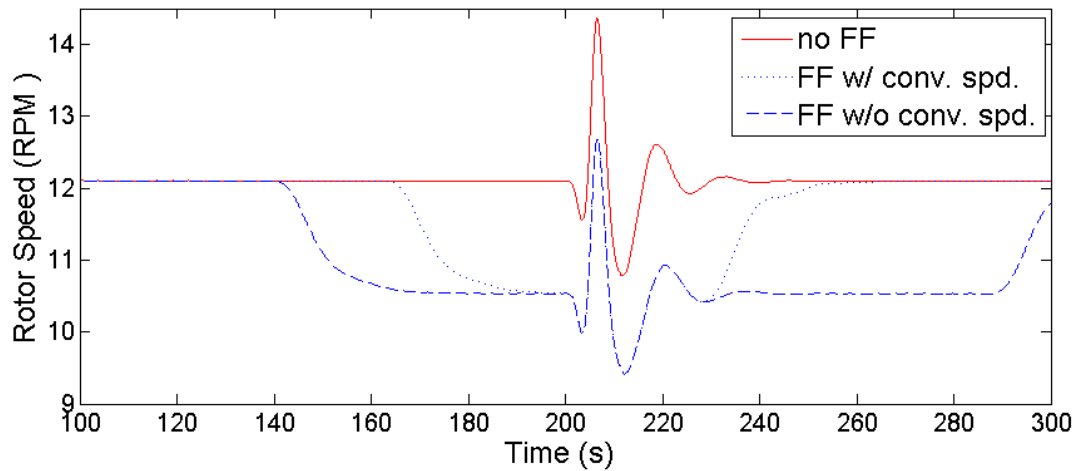
FIGURE 4.21: Rotor speed for turbine subjected to extreme operating gust.

These figures also illustrate that the system is robust to differences the convection speed or errors in convection speed estimates. As discussed in section 3.2, the simulation method used here assumes Taylor's frozen turbulence hypothesis, which implies that the
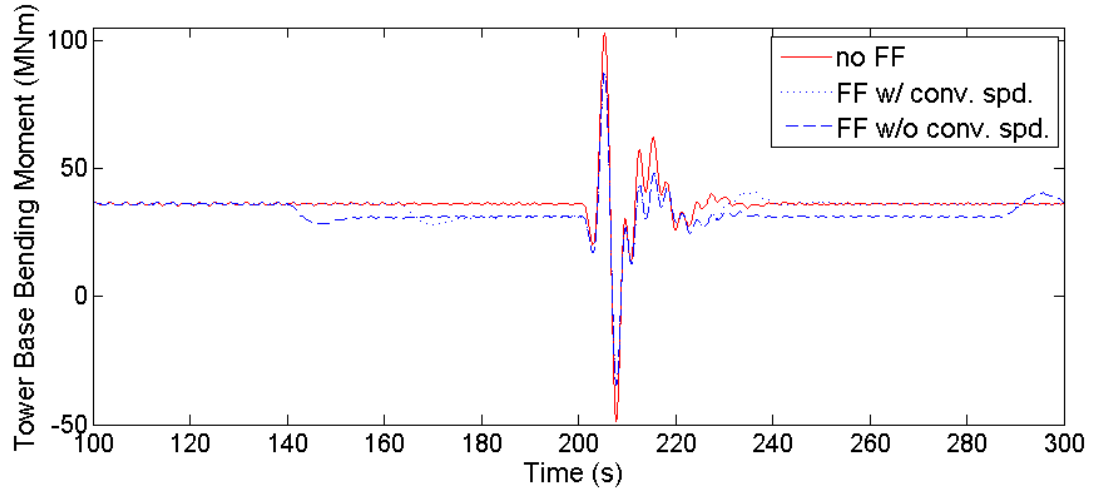
FIGURE 4.22: Tower base fore-aft moment for turbine subjected to extreme operating gust.
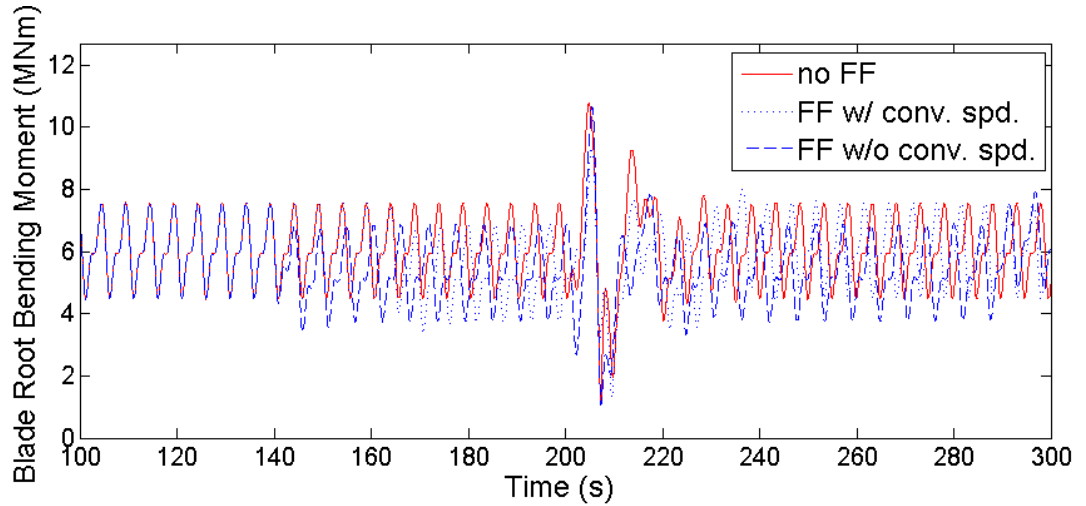
FIGURE 4.23: Blade root bending moment for turbine subjected to extreme operating gust.

true convection speed is equal to the mean wind speed. This assumption causes the EOG to reach the downwind turbine at exactly 200 seconds. However, if the EOG convects faster or slower than the mean wind speed the arrival time will shift. Similarly, if a convection velocity estimate is used to determine when to derate the downwind turbine then an error in the convection velocity estimate will cause that window of derated operation to shift. As we can see from Figures 4.21 through 4.23 small shifts will not affect the performance of the feed forward controller because the downwind turbine will still be in derated operation when the EOG arrives.

Figure 4.23 shows power generation. As expected, derating the downwind turbine results in reduced power generation. When the derate timing is based on a convection velocity

TABLE 4.3: Effect of FF Control on dynamic response to 16 m/s EOG.

| | Max tower base moment | | Max blade root moment | | Max Overspeed | Energy Gen. |
	(MNm)	reduction	(MNm)	reduction	(%)	(kWhr)
No FF Control	102.7	-	10.77	-	18.76	831.8
FF w/ conv. speed	87.46	14.9%	9.43	12.4%	4.96	820.2
FF w/o conv. speed	87.34	15.0%	10.66	1.0%	4.96	805.3

estimate it results in a loss of 11.5KWhr. If energy is sold at 10 cents per kWhr that results in $1.16 of lost revenue. When a convection velocity estimate is not used for derate timing the downwind turbine remains derated longer. This results in a loss of 26.48 kWhr and lost revenue of approximately $2.65. These simulations appear to show that turbines with feed forward selective derating control will generate less energy, however in real world operation this derating strategy may result in a significant increase in energy generation. It is important to note that these simulations do not model emergency rotor overspeed shutdowns. The turbine without feed forward control experiences a rotor overspeed of 18.76%. If this caused a 10 minute emergency shutdown it would result in a loss of approximately 833 kWhr and lost revenue of approximately $83, significantly more than the lost revenue cased by briefly derating the turbine.
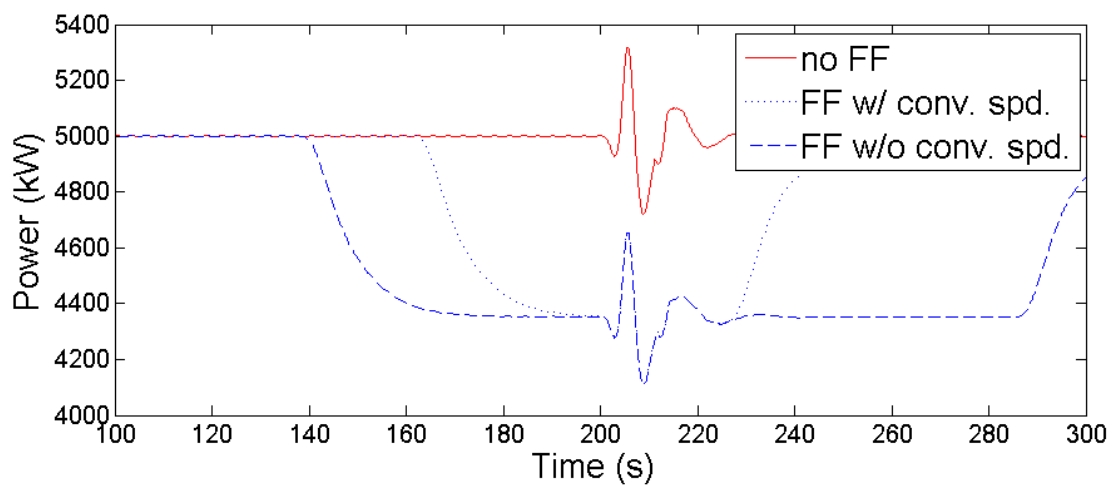
FIGURE 4.24: Power generation for turbine subjected to extreme operating gust.

4.6.2 Response to Turbulent Wind With Large Gust

The Extreme Operating Gust test case provides insight into how selective derating can reduce loading and overspeeds. However, constant wind speeds like those before and after the EOG in the previous section, are rare in the real world. When a turbine experiences a large gust it is most likely part of a turbulent wind field. In this section we examine the effect of selective derating feed forward control on a two turbine system experiencing turbulent wind with a large gust. As discussed in Section 4.5, the NREL 5-MW turbine is vulnerable to large gust induced overspeeds when operating in region 3 control, which occurs in wind speeds between 12 m/s and 25 m/s. As Section 4.3 illustrates, structural loading and overspeeds vary across that range of wind speeds. In an effort to capture these variations, turbulent wind speeds with 3 different mean wind speeds were simulated. Figures 4.25 through 4.29 illustrate the 16 m/s turbulent wind test case, while Tables 4.4 through 4.6 quantify and summarize performance metrics for all test cases. For the sake of space, the 12 m/s and 20 m/s turbulent wind test cases are not illustrated with figures. However, the behavior seen in the 12 m/s and 20 m/s test cases is similar to what is seen in the 16 m/s case.

Figure 4.25 shows the wind speed for 200 seconds of the 16 m/s turbulent test case. As the figure shows, the turbines are subjected turbulent fluctuations in wind speed throughout the simulation with a large gust at 200 seconds. The turbulent fluctuations were generated by TurbSim and are statistically realistic, however these wind speeds are applied uniformly over the whole rotor. Due to the limitations of FAST and TurbSim it was not possible to simulate full field turbulence with a large gust, so the spatial variations in wind speed that would be observed across the rotor in a real turbulent wind field could not be captured in this simulation.
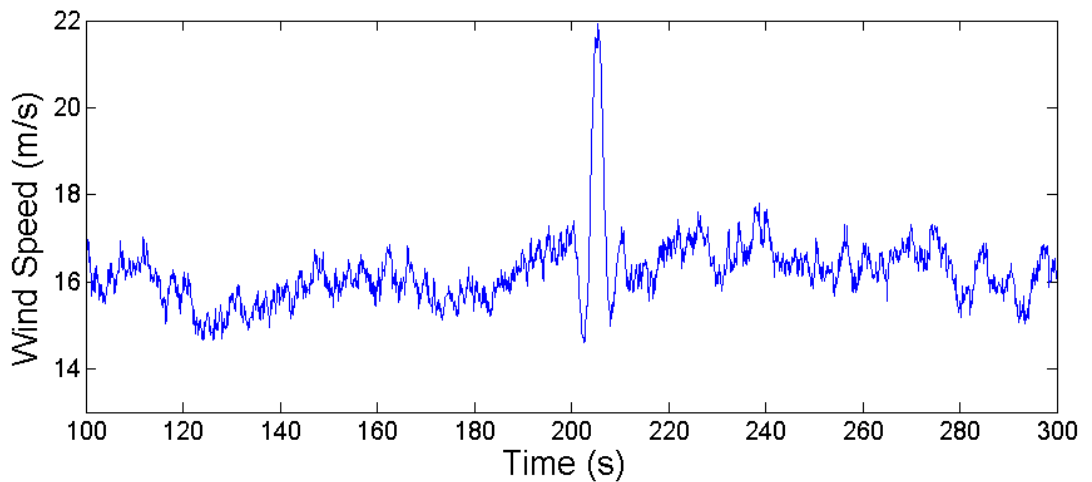
FIGURE 4.25: Turbulent wind with 16 m/s mean wind speed and large gust.

Figures 4.26 through 4.29 show how feed forward selective derating control affects the rotor speed, tower base fore-aft bending moment, blade root moment, and power generation of the downwind turbine for 16 m/s turbulent wind with a large gust. As in Section 4.6.1 two methods were used to time the derating of the downwind turbine.

Figure 4.26 shows that the upwind turbine experiences many small overspeeds throughout the simulation and experiences a large overspeed of 17.77% due to the large gust. This large overspeed could potentially cause an emergency overspeed shutdown of the upwind turbine. Selective derating feed forward control reduces the maximum overspeed experienced by the downwind turbine to approximately 5%, which is in the normal range of operation for this turbine. In Figure 4.27 we see that both the upwind and downwind turbines experience large tower base fore-aft bending moments due to the large gust, but the loads experienced by the downwind turbine are smaller. The feed forward controller has reduced the maximum tower base fore-aft bending moment by approximately 11%. As in the previous section, we see that this system would be robust to changes in the arrival time of the gust.
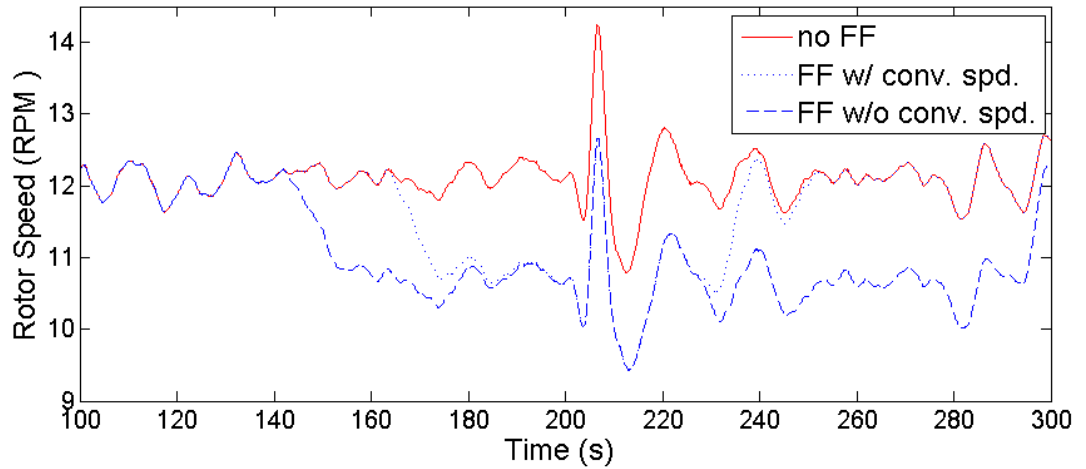
FIGURE 4.26: Rotor speed for turbine subjected to turbulence w/ large gust.

Figure 4.28 shows that derating the downwind turbine for the 16 m/s test case has resulted in a higher peak blade root moment (BRM). Though this result is initially surprising, it can be explained when the factors contributing to the peak load are examined more closely. We can see from Figure 4.28 that BRM has a large cyclical component. These cyclic changes in BRM have a frequency of 12 RPM, which corresponds to the rotational speed of the rotor, and are caused primarily by gravitational loads on the turbine blade. Section 4.3 showed that derating reduces BRM, and we see from Figure 4.28 that derating reduces BRM prior to the arrival of the gust. However, the effect of a large gust on BRM is determined by both how much BRM the gust causes as well as the
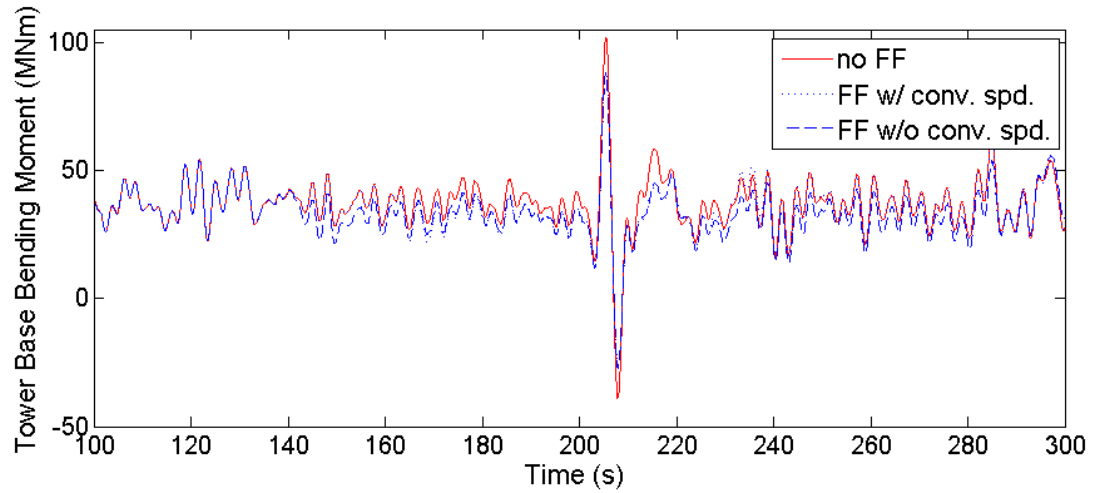
FIGURE 4.27: Tower base fore-aft moment for turbine subjected to turbulence w/ large gust.

timing of the gust and how the gust induced loads interacts with the cyclic gravitational loads. For the upwind turbine, without derating, the gust arrives at an opportune time. A downswing in the cyclic gravitational loading largely cancels out the gust induced BRM and the effect of the gust is almost unnoticeable. For the downwind turbine, the derating process has reduced the rotational speed of the rotor. As a result, the downwind turbine is at a different and less opportune point in it's rotation when the gust arrives. In real world applications the timing of a large gust would be random. Because derating reduces the BRM induced by the gust we would expect derating to reduce peak BRM more often than not. However, as this result illustrates, derating does not always result in reduced peak BRM loads.
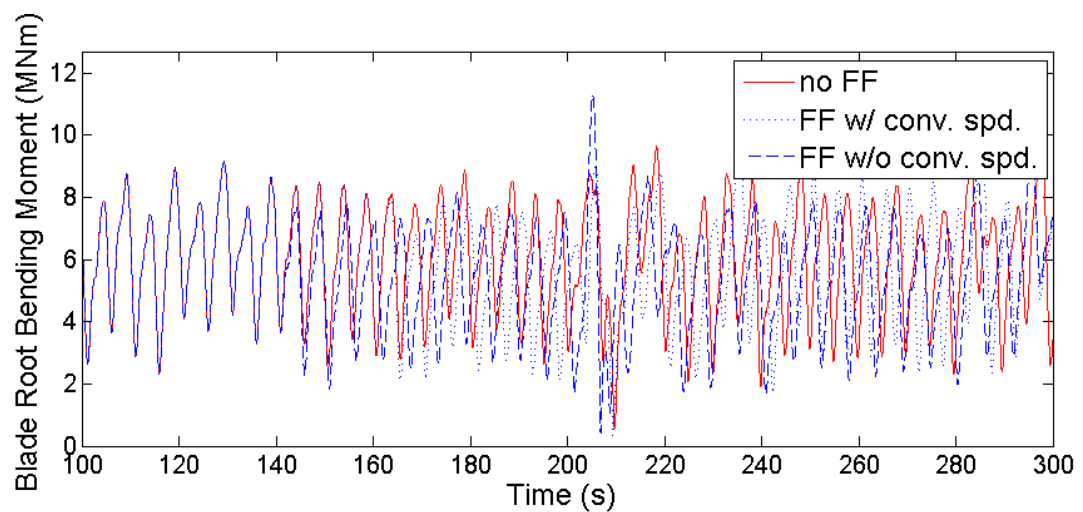
FIGURE 4.28: Blade root bending moment for turbine subjected to turbulence w/ large gust.

Figure 4.29 shows power generation. As expected, derating results in reduced power generation. Derating based on a convection speed estimate results in 10.7 kWhr of lost energy production. The more conservative strategy of derating without a convection speed estimate results in 24.9 kWhr of lost energy production. However, as stated before, these derating strategies are intended to avoid emergency overspeed shut downs. An emergency overspeed shutdown would likely result in a much larger loss of energy.
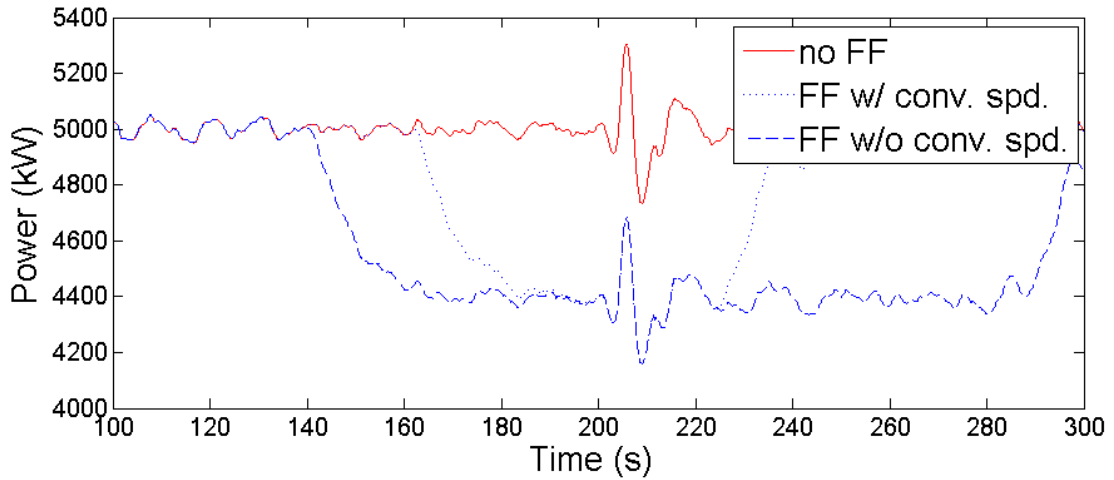
FIGURE 4.29: Power generation for turbine subjected to turbulence w/ large gust.

Tables 4.4 through 4.6 quantify and summarize performance metrics for all three test cases: 12 m/s, 16 m/s, and 20 m/s. In an attempt to capture the overall wear and tear on the tower base and blade root, Damage Equivalent Loads (DEL) are reported instead of peak loads. Though the DEL, overspeed, and energy genration values vary between the test cases, the trends are the same. Selective feed forward derating reduces maximum overspeeds from more than 15%, which could cause an emergency overspeed shut down, to approximately 5%. Tower root bending DELs are significantly reduced for all test cases. Blade root moment DELs are reduced in some test cases, but increased in others. Energy production is reduced by tens of kWhr, which is equivalent to a few dollars of production.

4.7 Conclusions.

This chapter has investigated the benefits and feasibility of derating a downwind turbine based on a feed forward signal from an upwind turbine. A survey of available turbine derating literature was carried out. Three turbine derating strategies from literature were then investigated. It was found that derating a turbine by reducing the rated rotor speed yielded the largest reductions in structural loads and rotor overspeeds. The effect

TABLE 4.4: Effect of FF Control on damage equivalent loads for a large gust in turbulent wind with 12 m/s mean wind speed.

	Tower base DEL		Blade root DEL		Max Overspeed	Energy Gen.
	(MNm)	reduction	(MNm)	reduction	(%)	(kWhr)
No FF Control	78.8	-	6.74	-	15.79	812.1
FF w/ conv. speed	69.2	12.2 %	5.87	12.9%	4.46	800.9
FF w/o conv. speed	67.5	14.3%	5.16	23.2%	4.46	790.98

TABLE 4.5: Effect of FF Control on damage equivalent loads for a large gust in turbulent wind with 16 m/s mean wind speed.

	Tower base DEL		Blade root DEL		Max Overspeed	Energy Gen.
	(MNm)	reduction	(MNm)	reduction	(%)	(kWhr)
No FF Control	75.1	-	5.08	-	17.77	831.8
FF w/ conv. speed	67.2	10.5 %	5.14	-1.2%	5.04	821.1
FF w/o conv. speed	66.3	11.7%	5.44	-7.1%	4.88	806.9

TABLE 4.6: Effect of FF Control on damage equivalent loads for a large gust in turbulent wind with 20 m/s mean wind speed.

	Tower base DEL		Blade root DEL		Max Overspeed	Energy Gen.
	(MNm)	reduction	(MNm)	reduction	(%)	(kWhr)
No FF Control	91.1	-	5.08	-	22.89	831.8
FF w/ conv. speed	77.2	15.3 %	5.06	0.3%	5.04	818.8
FF w/o conv. speed	76.6	15.9%	5.20	-2.4%	5.12	798.5

of turbine derating on dynamic turbine response was then investigated by simulating derated NREL 5-MW turbines subjected to extreme operating gusts (EOGs). It was found that rotor speed, power, blade root bending moments, and tower fore-aft bending moments were all significantly reduced by derating and that the reduction were roughly proportional to the amount of derating. The transition into and out of derated mode was also investigated. It was found that abruptly changing the rating of an NREL 5-MW turbine excited undesirable transient behavior in the turbine. However, the undesirable behavior could be avoided by using a low pass filter. A feed forward selective derating scheme based on these findings was developed. The scheme uses two possible methods to determine when to derate the downwind turbine. The first relies on a wind convection velocity estimate from the upwind turbine. The second, more conservative, method uses the range of wind speeds in which rotor overspeeds are likely to occur.

Once the feed forward selective derating strategy was designed, the performance of that system was tested in a series of FAST simulations. The FAST simulations modeled a two turbine system in several wind conditions, including both IEC extreme operating gusts and turbulent wind with large gusts. The simulation results were promising. The downwind turbine experienced significant reductions in tower fore-aft moments in all simulation cases, as well as reductions in blade root bending moments in some cases. More importantly, the downwind turbine did not experience any rotor overspeeds large enough to trigger an emergency shut down. The downwind turbine experienced reductions in energy generation, however those reductions were much smaller than the reductions in energy generation that would be caused by an emergency overspeed shut down.

Though the simulations carried out in this chapter show promising system performance, more investigation is needed. A real wold implementation of this system would encounter several phenomena that were not captured in these simulation. Due to the limitations of the simulation tools, neither full field turbulence nor the evolution of the wind field over time could be simulated. In addition simulating the system with a different simulation tool could potentially lend validity to the results shown in this chapter. In the following chapters a more sophisticated, though more computationally intensive, wind farm simulation tool will be investigated and used to study the feed forward selective derating scheme developed in this chapter.

Chapter 5

A Comparison of the NREL 5-MW Wake Characteristics Using Both SOWFA and OVERFLOW2

5.1 Main Section 1

AIAA conference paper I wrote with Ray and Case goes here.

5.1.1 Subsection 1

5.1.2 Subsection 2

5.2 Main Section 2

5.3 Experimental results

5.3.1 Comparison of SOWFA and OVERFLOW2 Results

5.3.2 Effects of Near-Wake Grid Resolution

Chapter 6

Analysis of Feed Forward Derating Control Scheme With SOWFA.

6.1 Introduction

Chapter 4 investigated the benefits and feasibility of derating a downwind turbine based on a feed forward signal from an upwind turbine. The feed forward derating control scheme developed in chapter 4 monitors the rotor speed of the upwind turbine for large rotor overspeeds, which are indicative of large wind gusts. When those large rotor overspeeds are detected, the downwind turbine is smoothly transitioned to derated operation until the gust passes. Derating a turbine reduces power generation, but also decreases both structural loads and rotor speed, making that turbine less sensitive to the detrimental effects of a large wind gust. By derating the downwind turbine only when the upwind turbine detects a large wind gust, the downwind turbine gains the benefits of derating (reduced loads and overspeeds) when they are needed most while keeping the cost of derating (reduced energy generation) in check.

The control scheme was evaluated using a series of FAST simulations, which showed promising results (Section 4.6). The control scheme reduced peak structural loads and damage equivalent loads (DEL) while decreasing rotor overspeeds enough to avoid emergency shutdowns of the downwind turbine. The control scheme did reduce electricity generation, but the reduction was small and would likely be much less than the power lost in an emergency turbine shutdown. Though these results are promising, the simulation methodology used to generate them has several noteworthy limitations. First, these simulations did not model emergency turbine shutdowns due to rotor overspeeds.

Second, to simulate this system in FAST we had to assume Taylor's frozen turbulence hypothesis, which provides a very simplistic model of wind speed fluctuations passing through the wind farm. As a result, the simulations did not capture the evolution of the gust as it passes from the upwind turbine to the downwind turbine, it did not capture turbine wake effects, and it did not accurately capture the time it takes for the gust to travel from the upwind turbine to the downwind turbine. In this chapter we will evaluate the control scheme developed in Chapter 4 using a simulation tool that does not have these limitations.

As discussed in Chapter 5, the Simulator fOr Wind Farm Applications (SOWFA) is wind farm simulation tool. SOWFA uses FAST to model the dynamics of one or more turbines, a Large Eddy Simulation (LES) to model atmospheric airflow, and actuator line models to enable interaction of the LES and FAST models. Because SOWFA models atmospheric airflow, we can use it to design a simulation that will capture the evolution of a gust over time, wake effects, and the time it takes a gust to reach the downwind turbine. We can also add control logic that will capture the effects of emergency turbine shutdowns due to rotor overspeed. In Chapter 5 SOWFA simulations of the NREL 5MW rotor were compared to Reynolds Averaged Navier Stokes (RANS) simulaions of the same rotor and were found to yield similar results. In addition, several SOWFA simulation parameters were varied to investigate the tradeoffs between simulation accuracy and computational cost. Because of the work documented in Chapter 5 we have confidence in the accuracy of SOWFA simulations and a good understanding of how to achieve accurate results at an acceptable computational cost.

Sections 6.2 through 6.5 describe much of the background work that had to be done before SOWFA simulations of the feed forward selective derating scheme could be carried out. They discuss topics such as implementation of the turbine controller, tuning and validation of the SOWFA turbine model, modeling gusts in SOWFA, as well as choosing an appropriate LES grid resolution and computational domain. Section 6.6 presents the first simulation case, in which the downwind turbine is directly behind the upwind turbine and in it's wake. Section 6.7 presents the second simulation case, in which the turbines are offset slightly so that the downwind turbine isn't in the wake of the upwind turbine. Section 6.8 summarizes this chapter and it's findings.

6.2   Controller Implementation

The simulations carried out in Chapter 4 use Simulink and Matlab to model control systems. Individual turbine control, such as determining the appropriate blade pitch and generator torque, is modeled in Simulink. Plant level control, such as monitoring

the upwind turbine and determining when to derate the downwind turbine, is modeled in Matlab scripts. This method has several bennefits. First, Simulink and Matlab are user friendly programming languages. They include a large number of pre-programmed functions and subsystems that make controller implementation easier. Second, these Simulink and Matlab controllers are not part of the FAST executable file. Therefore, changing the controller does not require recompiling FAST. This can save a lot of time and effort, especially when a new control system is being developed, tested, and tuned.

Unfortunately, the same controller implementation can not be used for SOWFA simulations. Though SOWFA does use FAST to model turbine dynamics, it uses a modified version of FAST that is compiled for Linux operating systems and does not have the ability to interface with Simulink. To overcome this limitation the Simulink controller developed in Chapter 4 is re-written as a set of fortran subroutines and inserted into the SOWFA/FAST source code. FAST and SOWFA are then recompiled to implement the turbine control system developed in chapter 4.

Fortran subroutines PitchCntrl() and UserVSCont() implement the collective pitch and generator torque controll. Subroutine updateControlParameters() implements a low pass filter on generator speed and scales control parameters to transition the turbine into and out of derated operation. Subroutine UserHSSBr() models a brake that can be used to park the rotor at the end of an emergency shutdown. All four subroutines are in file UserSubs.f90. Module EAControl(), in FAST_Mods.f90, stores variables that are accessed by multiple control subroutines. FAST_IO.f90 has been modified so information that a turbine would recieve from a plant level controller, such as when to derate the turbine, can be read in as part of the input file primary.fst. The source code containing this controller implementation is available in the github repository https://github.com/ewandersonUCDavis/SOWFA_openFAST_EA.git.

The simulations carried out in Chapter 4 did not model emergency turbine shutdowns due to rotor overspeeds. However, these events are important. Energency shutdowns reduce power generation and can dramatically affect a turbine's wake. To ensure those effects are captured in our SOWFA simulations, emergency shutdown functionality was added to the turbine controller. The NREL 5MW turbine specification does not describe an emergency shutdown protocol[2], so an emergency shutdown protocol was implemented based on the "aerodynamic shutdown" process described by Pedersen and Steineche [52]. If the turbine experiences a rotor overspeed in excess of 15% an emergency shutdown is initiated. The emergency shutdown protocol overrides the pitch and generator torque controllers. Generator torque is turned off and the turbine blades are collectively pitched to 90° at a rate of 8° per second. The pitched blades induce aerodynamic braking, which rapidly slows the turbine rotor. When the rotor is almost

completely stopped a high speed shaft brake is initiated to ensure the rotor comes to a complete stop and remains stationary.

Plant level control can not be modeled in SOWFA at this time. Though NREL did develop a version of SOWFA capable of modeling plant level control [53, 54] it was never released publicly and is currently unavailable. For the simulations carried out in this chapter plant level control will be implemented outside of SOWFA. This is accomplished by running each simulation twice. First the simulation is run without plant level control. The results of the first simulation provide a performance baseline and allow plant level control signals to be generated offline. The second simulation is run with plant level control. Plant level control signals (when to derate the downwind turbine and by how much) are fed to the downwind turbine through the input file primary.fst. Results from the second simulation can be compared to results from the first simulation to determine how the plant level controller affects system performance.

6.3   Computational Domain and Grid Resolution

The LES computational domain used in this chapter is 5040 meters × 2520 meters × 2520 meters. As in chapter 5 this rectangular grid is initially composed of 32 m × 32 m × 32m cells, but portions of the domain are refined to decrease cell size near the turbine rotors and their wakes. Two configurations will be simulated, as illustrated in figure 6.1. In the first configuration the upwind turbine will be 10 rotor diameters (1260 meters) downstream of the center of the inlet while the downwind turbine is 10 rotor diameters further downstream. In this configuration the downwind turbine will be in the wake of the upwind turbine. The second configuration is similar, but each turbine is offset horizontally by 0.75 rotor diameter so the downwind turbine is not in the wake of the upwind turbine.

Choosing a grid resolution is a compromise. A fine grid captures flow behavior that coarse grids doesn't capture. However, using a fine grid has a higher computational cost than a coarse grid, requiring more cores and/or more time to run a simulation. One way to balance simulation detail and computational cost is to make the grid resolution finer in the areas you are most interested in (such as near the turbine rotor) and coarser in areas that are of less interest (such as far from the turbine). Another way is to make the grid resolution as fine as it needs to be, but not making it any finer.

For simulations in Section 5.3.1 (referencing a chapter 5 section that hasn't been inserted yet) a grid resolution of 1 meter was used near the turbine rotor. This near-rotor grid was not very large, extending only 1 rotor diameter upstream, 6 rotor diameters downstream,

Configuration #1: Turbine in Wake Test Case

Configuration #2: Offset Turbines Test Case

10 Rotor Diameters (1260 m)

1.5 Rotor
Diameters
(252 m)
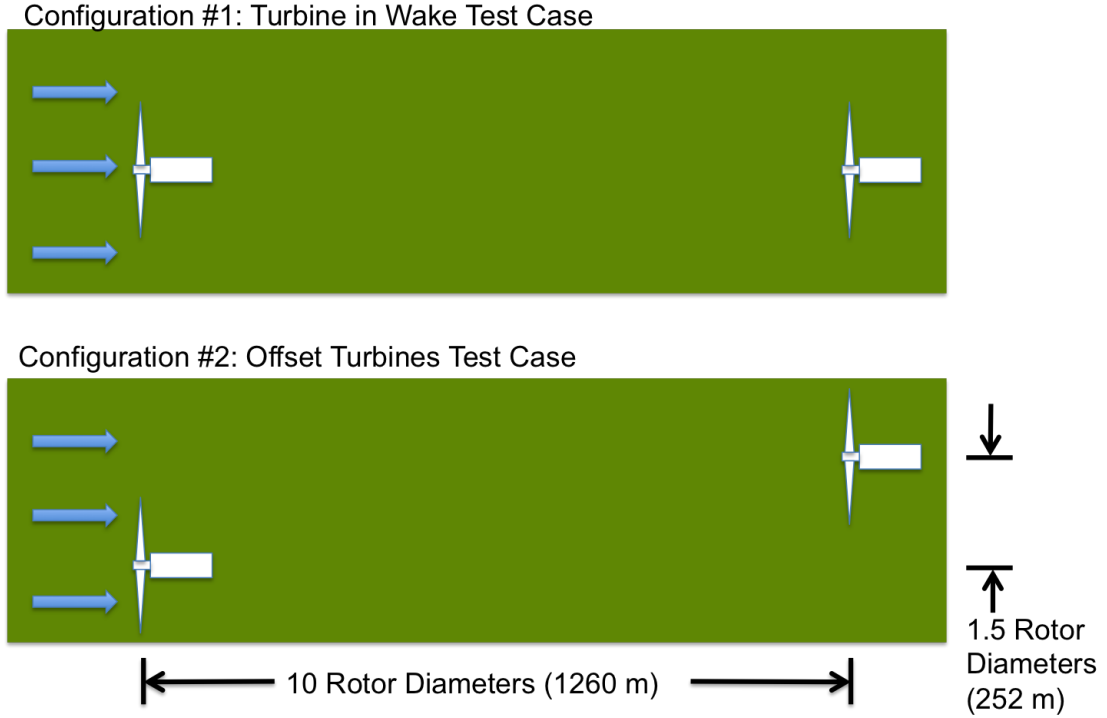
FIGURE 6.1: Configurations for SOWFA simulations of feed forward derating control.

and 1.4 rotor diameters radially, which is approximately 0.04% of the simulation domain volume. However, this near-rotor grid contains approximately 11 million cells, which is about 57% of the cells in the simulation domain. A 1 m × 1 m × 1 m grid large enough to encompass the two turbine systems shown in figure 6.1 would have a prohibitively large number of cells and have a prohibitively high computational cost.

To make the computational cost more manageable a 2 meter near-rotor grid resolution will be used for simulations in this chapter. Though simulation results will be less detailed, we still have high confidence in the accuracy of the results. As Section 5.3.2 shows, even a near-rotor grid resolution of 4 meters yielded good agreement for power generation, rotor thrust, wake vorticity, and momentum deficit.

6.4   Tuning and Validation of SOWFA Turbine Model

An actuator line model couples SOWFA's LES based atmosphere model to SOWFA's FAST based turbine dynamics model. To get accurate turbine performance from SOWFA, the actuator line model must be tuned. A series of simulations revealed that an actuator line model with 62 elements per blade and a Gausian projection width of 7.5 meters yields good agreement between SOWFA and FAST simulations. These actuator line

parameters comply with the best practices recommended by Churchfield, Lee, and Moriarty [55] as well as those recommended by Troldborg [56]. It is worth noting that the Gausian projection width chosen here is different than the one chosen for SOWFA simulations in Chapter 5. This difference is partially due to the use of a 2 meter near-rotor grid resolution, but it is also caused by a difference in tuning requirements. The SOWFA simulations carried out in Chapter 5 did not model turbine control, so the actuator line was only tuned to produce good agreement on turbine loads and power generation. The Gausian projection width chosen here produces good agreement on controller behavior as well as loading and power generation.

To illustrate the close agreement between SOWFA and FAST simulations a simple test case from chapter 4 was simulated in SOWFA. In that test case the turbine is subjected to a constant 16 m/s wind. At 100 seconds the turbine is derated by 20%. At 200 seconds the turbine is returned to full rated operation. Figures 6.2 through 6.6 show FAST and SOWFA simulation results for this test case. We see in the figures that FAST and SOWFA produce nearly identical results for rotor speed, power, and blade root bending moments. There is also good agreement on blade pitch and tower base bending moment. The blade pitch predicted by SOWFA is typically within 1% of the blade pitch predicted by FAST, but does briefly exceed 1% when the turbine is returning to full rated operation. The maximum discrepancy is almost 4% and occurs at a simulation time of 210 second. SOWFA predicts more high frequency oscillations in tower base bending moment than FAST. However, there is close agreement on the magnitudes of the predicted loads. If we disregard the high frequency components of the SOWFA results the tower base bending loads are typically within 1.5% of the loads predicted y FAST. However, there are larger differences while the turbine is transitioning from derated operation to full rated operation.
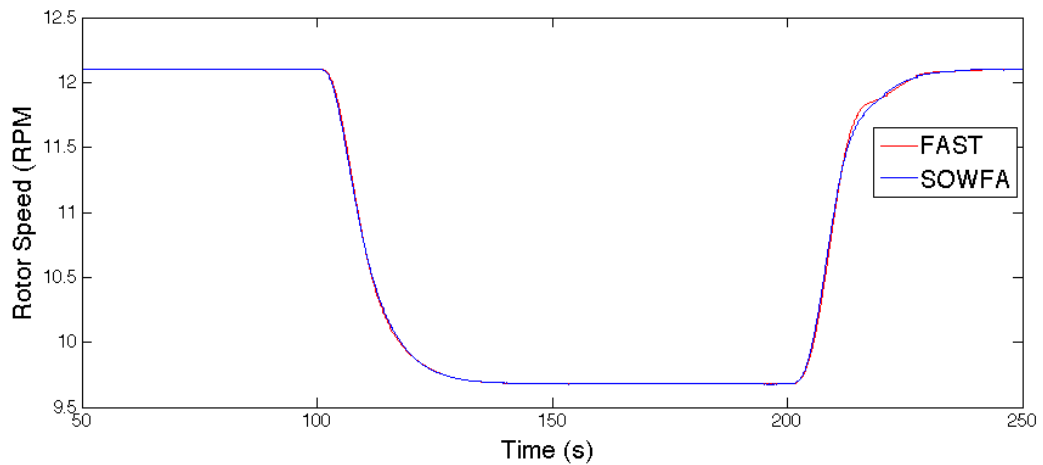

FIGURE 6.2: Comparison of rotor speed predicted by FAST and SOWFA.
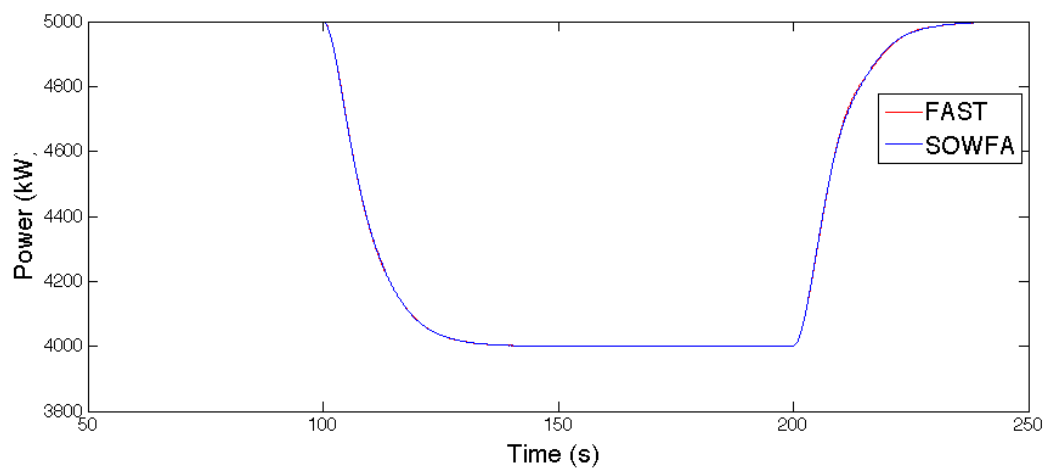
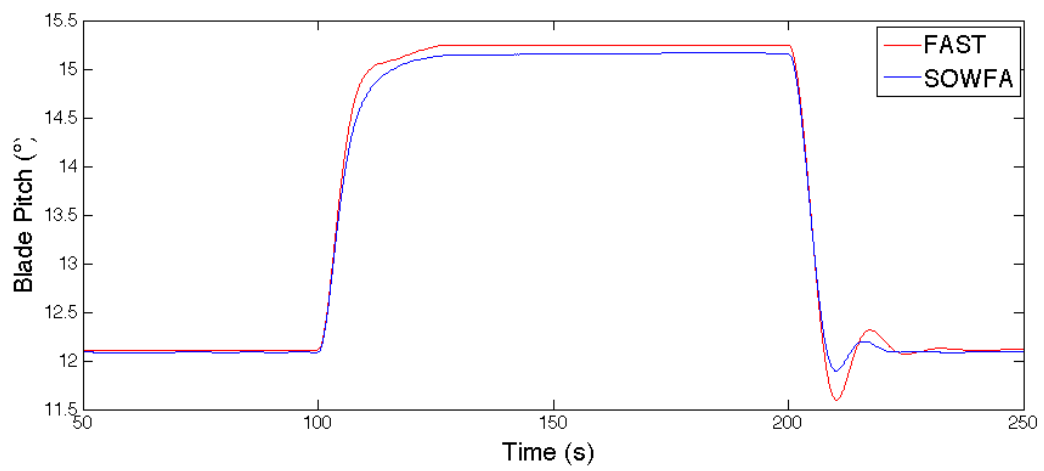FIGURE 6.3: Comparison of power predicted by FAST and SOWFA.

FIGURE 6.4: Comparison of blade pitch predicted by FAST and SOWFA.
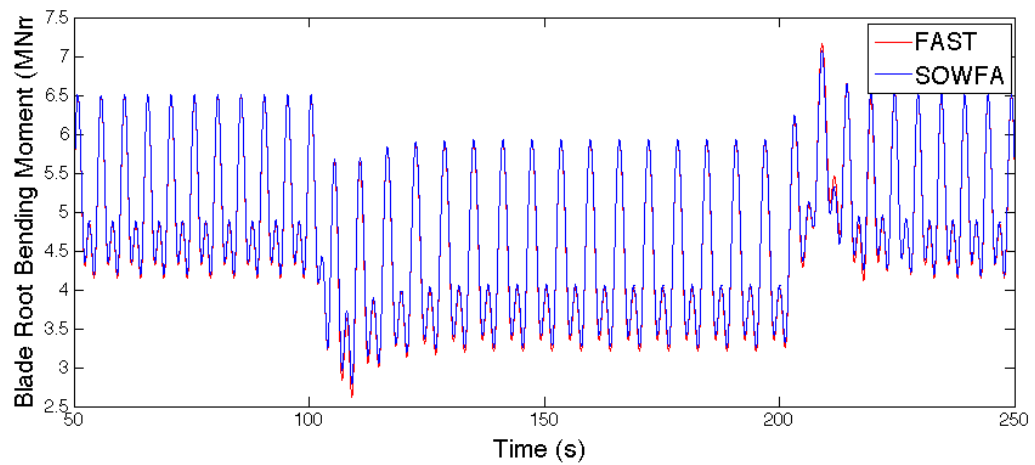
FIGURE 6.5: Comparison of blade blade root bending moment predicted by FAST and SOWFA.
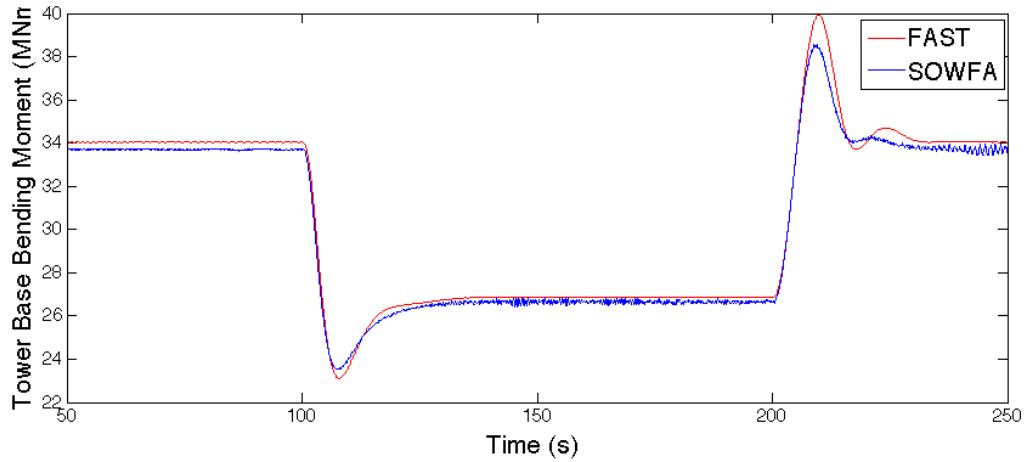
FIGURE 6.6: Comparison of tower base bending moment predicted by FAST and SOWFA.

6.5 Gust Modeling in SOWFA

For the FAST simulations in Chapter 4 gusts are modeled by simply increasing the incoming wind speed. However, this method does not work in SOWFA. SOWFA models airflow as an incompressible fluid in a finite computational domain. Increasing the wind speed across the inlet would cause an increase in the amount of air flowing into the computational domain. Because the fluid is incompressible and constrained, conservation of mass dictates that an increase in the amount of air flowing into the domain be immediately matched by an increase in the amount of air flowing out of the domain and an increase in the amount of air flowing from the input to the output. Therefore, increasing the wind speed across the inlet of the computational domain causes an instantaneous increase in wind speed throughout the computational domain.

To model a gust propagating through a wind farm we must be more subtle. This is done by increasing wind speed across part of the inlet, while decreasing wind speed elsewhere in the inlet. As long as the total amount of air flowing into the domain remains the same, the flow far downstream of the inlet will not be affected. Using this method, the gust is localized near the inlet initially then propagates through the computational domain over time.

In SOWFA, the user can specify a time varying velocity profile across the inlet by applying a TimeVaryingMappedFixedValue boundary condition. For this boundary condition, the user specifies a list of locations on the inlet plane, then specifying velocities at those points for several simulation times. SOWFA interpolates between the supplied data to determine the velocity profile across the inlet for all time steps in the simulation.

Several inlet velocity profiles were investigated in a series of preliminary SOWFA simulations. The inlet profile was found to have a large effect on how the gust initially appears in the simulation domain and how it behaves as it propagates through the domain. Inlet profiles that confine the gust to a small portion of the inlet were found to give the most control over gust behavior. When the gust covers a large portion of the inlet profile, SOWFA smooths out the effect of the gust. This smoothing effect turns rapid velocity changes at the inlet into more gradual velocity changes within the simulation domain. In the following sections we use inlet profiles that confine the gust to a small portion of the inlet. On the remainder of the inlet, the velocity remains constant.

In chapter 4 the turbines were subjected to a hat shaped Extreme Operating Gust as defined in section 6.3.2.2 of IEC61400-1[36]. Preliminary SOWFA simulations found that it is not possible to simulate a hat shaped gust that will propagate through the SOWFA simulations domain. A hat shaped fluctuation of the inlet velocity begins as a hat shaped gust near the inlet. However, the gust decreased in magnitude and changed shape as it moved through the simulation domain. Instead, simulations in the following sections will model an Extreme Coherent Gust similar to the one defined in section 6.3.2.5 of IEC61400-1.

Figure 6.7 illustrates the difference between an Extreme Operating Gust (EOG) and an Extreme Coherent Gust (ECG). The EOG is a brief fluctuation in wind speed, while the ECG is a sustained increase. IEC1400-1 defines the ECG as a 15 m/s increase in wind speed described by equation 6.1. For simulations in this chapter, the 15 m/s ECG magnitude specified by IEC1400-1 is interpreted to be a maximum coherent gust magnitude, not a required magnitude. If a 15 m/s coherent gust is possible then smaller magnitude coherent gusts are also possible. Coherent gusts were found to propagate through the SOWFA simulation domain with only small changes to the magnitude and shape of the gust, as illustrated in figure 6.8

$$U_{gust} = \begin{cases} 0 & for & t < t_{gust} \\ 7.5(1 - cos(\pi t/10))m/s & for & t_{gust} \leq t < (t_{gust} + 10) \\ 15m/s & for & \leq (t_{gust} + 10) \end{cases} \qquad (6.1)$$
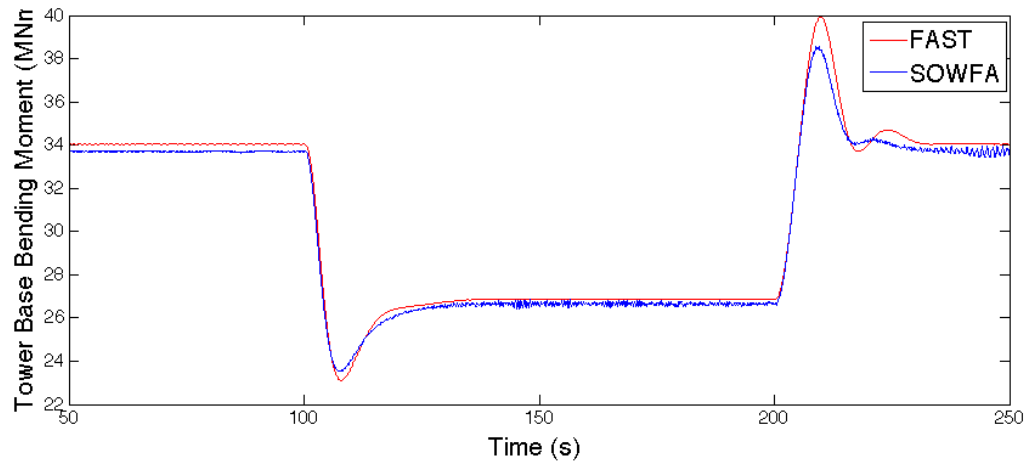
FIGURE 6.7: Velocity profiles for EOG and ECG.
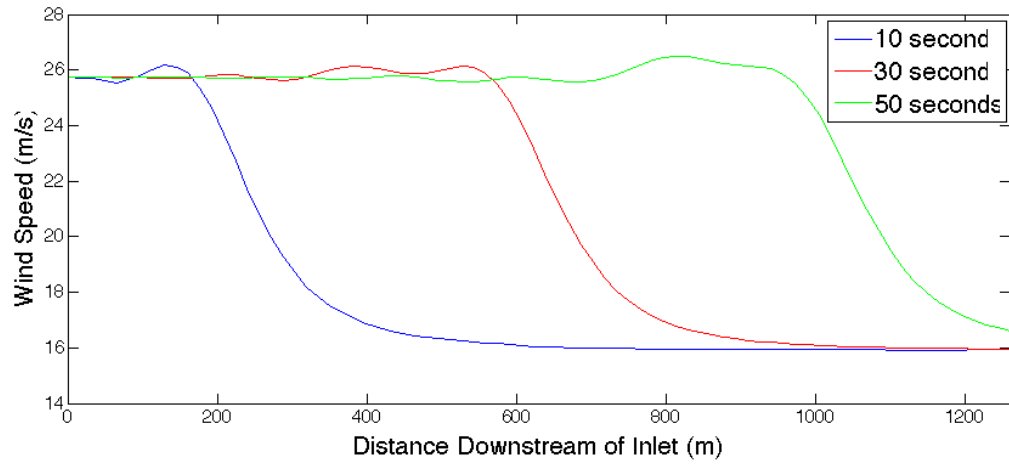
FIGURE 6.8: Center line velocity as ECG propagates through computational domain.

6.6 Turbine in Wake Test Case

6.7 Offset Turbines Test Case

6.8 Conclusions

Appendix A

FAST simulation input files

This section will include typical FAST input files used to generate the set of simulations generated in chapter 2.

Appendix B

Damage Equivalent Load (DEL) Calculation

Damage equivalent loads are calculated by MLife, A fatigue analysis tool developed by NREL [57, 58]. MLife automates the damage analysis techniques outlined in Annex G of IEC 61400-1 [36]. The load history of a component, like those shown in Figures **??** and **??**, can be thought of as a series of load cycles. Each of those load cycles has some mean load and cyclic loading range. If damage accumulates linearly and independently for each cycle, as proposed by Palmgren [59] and Miner[60], then the total damage from all cycles will be given by:

$$D_{fatigue} = \sum_i \frac{1}{N_{fatigue,i}}$$ (B.1)

where $N_{fatigue,i}$ denotes the number of cycles to failure for the ith loading cycle. For example, if the ith loading cycle would have to be repeated 10,000 times to drive a new component ($D_{fatigue} = 0$) to failure ($D_{fatigue} = 1$) then $N_{fatigue,i} = 10,000$ and the damage accumulated due to the ith loading cycle would be 0.0001. For a given loading cycle $N_{fatigue,i}$ is estimated by:

$$N_{fatigue,i} = \left(\frac{L_{ultimate} - L_{mean}}{\frac{1}{2} L_{range,i}} \right)^m$$ (B.2)

where $L_{ultimate}$ is the ultimate design load of the component, L_{mean} is the mean load over the component's load history, $L_{range,i}$ is the ith cycles range, and m is the Wöhler exponent. It can be seen in equation B.2 that larger loads cause more damage. Increasing

the load cycle range or the mean load lead to smaller values of $N_{fatigue,i}$, which means more damage per cycle.

The Wöhler exponent is a property of the component under consideration, but it is highly dependent on the material the component is made from. For damage equivalent load calculations in this dissertation m was assumed to be 10 for steel components (tower) and 4 for fiberglass components (blades). These are the values of m that Stewart, Lackner, Haid, Matha, Jonkman, and Robertson used to perform fatigue analysis of the NREL 5 MW turbine in [61].

Because the NREL 5MW turbine is a fictional turbine ultimate loads ($L_{ultimate}$) are not available for it's components. This presents a problem when attempting to calculate accurate fatigue damage ($D_{fatigue}$) estimates. However, this problem can be circumvented if we use the component load history to calculate a damage equivalent load instead of using it to calculate fatigue damage.

The damage equivalent load (DEL) is a constant amplitude fatigue load that occurs at a fixed frequency and produces the same damage as the actual load history of the component. The damage caused by the DEL is:

$$D_{fatigue} = \frac{n_{equivalent}}{N_{equivalent}} \tag{B.3}$$

$$N_{equivalent} = \left(\frac{L_{ultimate} - L_{mean}}{\frac{1}{2}DEL} \right) \tag{B.4}$$

where $N_{equivalent}$ is the number of cycles to failure for the damage equivalent load, and $n_{equivalent}$ is the number of damage equivalent loading cycles the component is subjected to. $n_{equivalent}$ is chosen by the analyst. All DEL calculations in this dissertation have used $n_{equivalent} = 1$. In other words, the complex load history of the components under consideration have been converted to single loading cycles that cause equivalent damage. Setting $n_{equivalent} = 1$ and combining equations B.1 and B.3 yields:

$$\sum \frac{1}{N_{fatigue,i}} = \frac{1}{N_{equivalent}} \tag{B.5}$$

Substituting in equations B.2 and B.4 then solving for DEL gives:

$$DEL = \left(\sum_i (L_{range,i})^m \right)^{\frac{1}{m}} \tag{B.6}$$

We see from equation B.6 that the ultimate load of the component is not required to calculate the damage equivalent load. the DEL does quantify the amount of damage done to a component, but it is a useful tool for comaring the relative damage done by two time histories. A higher DEL indicates more damage. In this dissertation DEL is used to compare various control strategies to see if they reduce or increase the damage experienced by the turbine.

A few notes on the Goodman correction: The DEL calculations carried out in this dissertation, as outlined above, do not include the Goodman correction. When the Goodman correction is used, equation B.2 becomes:

$$N_{fatigue,i} = \left(\frac{L_{ultimate} - L_{mean,i}}{\frac{1}{2} L_{range,i}} \right)^m \tag{B.7}$$

where $L_{mean,i}$ is the mean load for the ith loading cycle, not the mean load of the load history. Using the Goodman correction leads to more accurate estimates of fatigue damage. However, when the goodman correction is used, the equation for DEL is not independent of the ultimate load:

$$DEL = \left(\sum_i \left(L_{range,i} \left(\frac{L_{ultimate} - L_{mean}}{L_{ultimate} - L_{mean,i}} \right) \right)^m \right)^{\frac{1}{m}} \tag{B.8}$$

Since accurate estimates of $L_{ultimate}$ were not available for NREL 5 MW components, the Goodman correction was not used for DEL calculations in this dissertation.

Bibliography

[1] Steve Sawyer and Klaus Rave. Global wind report–annual market update 2012. *GWEC, Global Wind Energy Council*, 2012.

[2] J.M. Jonkman, S. Butterfield, W. Musial, and G. Scott. Definition of a 5-mw reference wind turbine for offshore system development. Technical report, National Renewable Energy Laboratory, 2009.

[3] Jonathan Berg, Dale Berg, and Jon White. Fabrication, integration and initial testing of a smart rotor. In *Proceedings of the 50th AIAA Aerospace Sciences Meeting, Nashville, Tennessee*, 2012.

[4] David Schlipf, Ervin Bossanyi, Carlo Enrico Carcangiu, Tim Fischer, Timo Maul, and Michele Rossetti. Lidar assisted collective pitch control. Technical report, ProjectUpwind, 2011.

[5] B.J.Jonkman and M. Buhl. Turbsim user's guide. Technical report, National Renewable Energy Laboratory, 2012.

[6] 2013.

[7] E Williams, J Hensley, and E Salerno. Awea us wind industry annual market report year ending 2012. *AWEA, Washington, DC*, 2012.

[8] Renewables 2011 global status report. Technical report, REN21, 2011.

[9] T. Burton, N. Jenkins, D. Sharpe, and E. Bossanyi. *Wind Energy Handbook, Second Edition.* John Wiley and Sons, 2011.

[10] Torben Juul Larsen, Helge A Madsen, and Kenneth Thomsen. Active load reduction using individual pitch, based on local blade flow measurements. *Wind Energy*, 8 (1):67–80, 2005.

[11] EA Bossanyi. Developments in individual blade pitch control. In *Proceedings of "the Science of Making Torque from Wind" Conference*, pages 486–497, 2004.

[12] CP Van Dam, Dale E Berg, and Scott J Johnson. Active load control techniques for wind turbines. Technical report, Sandia National Laboratories, 2008.

[13] *GE Energy 1.5 MW Wind Turbine Brochure*, 2009.

[14] A. Manjock. Evaluation report, design codes fast and adams for load calculation of onshore wind turbines. *, Germanischer Lloyd WindEnergie GmbH, 2005.

[15] K. Z. Østergaard, P. Brath, and J. Stoustrup. Estimation of effective wind speed. *Journal of Physics: Conference Series 75*, 2007.

[16] EL Van der Hooft and TG Van Engelen. Estimated wind speed feed forward control for wind turbine operation optimisation. In *Proceedings of European Wind Energy Conference in London, UK*, 2004.

[17] David Schlipf. Lidar assisted control of wind turbines. *Struttgart Wind Energy. Universitat Stuttgart*, 2014.

[18] AD Platt and ML Buhl Jr. Wt _ perf user guide for version 3. 05. 00. Technical report, National Renewable Energy Laboratory, 2012.

[19] Geoffrey Ingram Taylor. The spectrum of turbulence. In *Proceedings of the Royal Society of London A: Mathematical, Physical and Engineering Sciences*, volume 164, pages 476–490. The Royal Society, 1938.

[20] David JC Dennis and Timothy B Nickels. On the limitations of taylor's hypothesis in constructing long structures in a turbulent boundary layer. *Journal of Fluid Mechanics*, 614:197–206, 2008.

[21] VW Goldschmidt, MF Young, and ES Ott. Turbulent convective velocities (broadband and wavenumber dependent) in a plane jet. *Journal of Fluid Mechanics*, 105: 327–345, 1981.

[22] Juan C Del Alamo and Javier Jiménez. Estimation of turbulent convection velocities and corrections to taylor's approximation. *Journal of Fluid Mechanics*, 640:5–26, 2009.

[23] Callum Atkinson, Nicolas Alexander Buchmann, and Julio Soria. An experimental investigation of turbulent convection velocities in a turbulent boundary layer. *Flow, Turbulence and Combustion*, 94(1):79–95, 2015.

[24] Isaac Van der Hoven. Power spectrum of horizontal wind speed in the frequency range from 0.0007 to 900 cycles per hour. *Journal of Meteorology*, 14(2):160–164, 1957.

[25] Chad W Higgins, Martin Froidevaux, Valentin Simeonov, Nikki Vercauteren, Caitlin Barry, and Marc B Parlange. The effect of scale on the applicability of taylor's frozen turbulence hypothesis in the atmospheric boundary layer. *Boundary-layer meteorology*, 143(2):379–391, 2012.

[26] David Schlipf, Tim Fischer, Carlo Enrico Carcangiu, Michele Rossetti, and Ervin Bossanyi. Load analysis of look-ahead collective pitch control using lidar. In *Proceedings of the 10th German Wind Energy Conference DEWEK*, 2010.

[27] Ahmet Arda Ozdemir, Peter Seiler, and Gary J Balas. Benefits of preview wind information for region 2 wind turbine control. In *51st AIAA Aerospace Sciences Meeting including the New Horizons Forum and Aerospace Exposition*, page 317, 2013.

[28] Fiona Dunne, Lucy Y Pao, Alan D Wright, Bonnie Jonkman, Neil Kelley, and Eric Simley. Adding feedforward blade pitch control for load mitigation in wind turbines: Non-causal series expansion, preview control, and optimized fir filter methods. In *Proc. 49th AIAA Aerospace Sciences Meeting, Orlando, FL*, 2011.

[29] David Schlipf and Martin Kühn. Prospects of a collective pitch control by means of predictive disturbance compensation assisted by wind speed measurements. In *Proceedings of the 9th German Wind Energy Conference DEWEK 2008*, 2008.

[30] David Schlipf, Stefan Kapp, Jan Anger, Oliver Bischoff, Martin Hofsäß, Andreas Rettenmeier, and Martin Kühn. Prospects of optimization of energy production by lidar assisted control of wind turbines. In *EWEA 2011 conference proceedings*, 2011.

[31] David Schlipf, Dominik Johannes Schlipf, and Martin Kühn. Nonlinear model predictive control of wind turbines using lidar. *Wind Energy*, 16(7):1107–1129, 2013.

[32] Andrew Scholbrock, Paul Fleming, Lee Fingersh, Alan Wright, David Schlipf, Florian Haizmann, Fred Belen, et al. Field testing lidar based feed-forward controls on the nrel controls advanced research turbine. In *51th AIAA Aerospace Sciences Meeting Including the New Horizons Forum and Aerospace Exposition*, 2013.

[33] Jason M Jonkman and Marshall L Buhl Jr. Fast user's guide. *National Renewable Energy Laboratory, Golden, CO, Technical Report No. NREL/EL-500-38230*, 2005.

[34] Jason Jonkman. Nrel national wind technology center forum: Blade pitch control. https://wind.nrel.gov/forum/wind/viewtopic.php?f=30&t=1048, 2014.

[35] Fiona Dunne, David Schlipf, Lucy Y Pao, Alan D Wright, Bonnie Jonkman, Neil Kelley, and Eric Simley. *Comparison of two independent lidar-based pitch control designs.* National Renewable Energy Laboratory, 2012.

[36] International Electrotechnical Commission et al. Wind turbine—part 1: Design requirements, iec 61400-1, ed. 3. *International Electrotechnical Commission, Geneva, Switzerland,* 2005.

[37] Ameet S Deshpande and Rhonda R Peters. Wind turbine controller design considerations for improved wind farm level curtailment tracking. In *2012 IEEE Power and Energy Society General Meeting,* 2012.

[38] Sari Fink, C Mudd, K Porter, and Brett Morgenstern. Wind energy curtailment case studies. *NREL subcontract report, NREL/SR-550,* 46716, 2009.

[39] Jarmo Aho, Andrew Buckspan, Jason Laks, Paul Fleming, Yunho Jeong, Fiona Dunne, Matthew Churchfield, Lucy Pao, and Kenneth Johnson. A tutorial of wind turbine control for supporting grid frequency through active power control. In *American Control Conference (ACC), 2012,* pages 3120–3131. IEEE, 2012.

[40] Jacob Aho, Andrew Buckspan, Lucy Pao, Paul Fleming, et al. An active power control system for wind turbines capable of primary and secondary frequency control for supporting grid reliability. In *Proc. 51st AIAA Aerospace Sciences Meeting Including the New Horizons Forum and Aerospace Exposition,* 2013.

[41] Benjamin Biegel, Daria Madjidian, Vedrana Spudic, Anders Rantzer, and Jakob Stoustrup. Distributed low-complexity controller for wind power plant in derated operation. In *Control Applications (CCA), 2013 IEEE International Conference on,* pages 146–151. IEEE, 2013.

[42] Phillip W Richards, D Todd Griffith, and Dewey H Hodges. Operating strategies and design recommendations for mitigating local damage effects in offshore turbine blades. Technical report, Sandia National Laboratories (SNL-NM), Albuquerque, NM (United States), 2014.

[43] Daniel Todd Griffith. Structural health and prognostics management for offshore wind plants; final report of sandia r&d activities. Technical report, Sandia National Laboratories (SNL-NM), Albuquerque, NM (United States), 2015.

[44] Mate Jelavić, Vlaho Petrović, Mario Barišić, and Ivana Ivanović. Wind turbine control beyond the cut-out wind speed. In *Annual Conference and Exhibition of European Wind Energy Association (EWEA2013),* 2013.

[45] Vlaho Petrović and Carlo Luigi Bottasso. Wind turbine optimal control during storms. In *Journal of Physics: Conference Series*, volume 524, page 012052. IOP Publishing, 2014.

[46] Vlaho Petrović and Carlo Luigi Bottasso. Wind turbine envelope riding. In *33rd Wind Energy Symposium-AIAA SciTech 2015*, 2015.

[47] I Carlén. Some simple concepts for dynamic wind sector management of wind farms. Technical report, Teknikgruppen report TG, 2010.

[48] Susan A Frost, Kai Goebel, and Léo Obrecht. Integrating structural health management with contingency control for wind turbines. *IJPHM Special Issue on Wind Turbine PHM (Color)*, page 11, 2013.

[49] David Eldridge and Peter Gregg. Ge wind services powerup platform. Technical report, General Electric, 2013.

[50] Vestas power plus. Brochure, 2015.

[51] Stephen Steen. The impacts of uprating and derating on turbine reliability. Online seminar: http://www.slideshare.net/Sentientscience/the-impacts-of-uprating-and-derating-on-turbine-reliability.

[52] Andreas Søndergaard Pedersen and Christian Sigge Steiniche. Safe operation and emergency shutdown of wind turbines. *Aalborg University*, 2012.

[53] Paul Fleming, Pieter Gebraad, Jan-Willem van Wingerden, Sang Lee, Matt Churchfield, Andrew Scholbrock, John Michalakes, Kathryn Johnson, and Pat Moriarty. The sowfa super-controller: A high-fidelity tool for evaluating wind plant control approaches. In *Proceedings of the EWEA Annual Meeting, Vienna, Austria*, 2013.

[54] Paul Fleming, Pieter Gebraad, Matt Churchfield, Sang Lee, Kathryn Johnson, John Michalakes, Jan-Willem van Wingerden, and Patrick Moriarty. Sowfa+ super controller user's manual. *National Renewable Energy Laboratory, Golden, CO*, 2013.

[55] MJ Churchfield, S Lee, and P Moriarty. Overview of the simulator for offshore wind farm application (sowfa) national renewable energy laboratory. *Golden, CO, USA*, 3, 2012.

[56] Niels Troldborg. Actuator line modeling of wind turbine wakes. 2009.

[57] G Hayman. Mlife theory manual for version 1.00. *National Renewable Energy Laboratory, Golden, CO*, 2012.

[58] GJ Hayman and ML Buhl Jr. Mlife users guide for version 1.00. *National Renewable Energy Laboratory, Golden, CO*, 2012.

[59] Arvid Palmgren. Die lebensdauer von kugellagern. *Zeitschrift des Vereins Deutscher Ingenieure*, 68(14):339–341, 1924.

[60] Milton A Miner. Cumulative damage in fatigue. *Journal of applied mechanics*, 12 (3):159–164, 1945.

[61] G Stewart, M Lackner, L Haid, D Matha, J Jonkman, and A Robertson. Assessing fatigue and ultimate load uncertainty in floating offshore wind turbines due to varying simulation length. *Safety, Reliability, Risk and Life-Cycle Performance of Structures and Infrastructures*, page 239, 2013.